CATALYTIC PROPERTIES OF SOME METALLOSILICATE MOLECULAR SIEVES

A THESIS

SUBMITTED TO THE

UNIVERSITY OF POONA

FOR THE DEGREE OF

DOCTOR OF PHILOSOPHY

(IN CHEMISTRY)

by

ANUJ RAJ

CATALYSIS DIVISION

NATIONAL CHEMICAL LABORATORY

PUNE - 411 008, INDIA

OCTOBER 1993

----- *TO MY BELOVED PARENTS & BROTHER*

CERTIFICATE

Certified that the work incorporated in the thesis **"Catalytic Properties of Some Metallosilicate Molecular Sieves"** submitted by Mr. Anuj Raj, for the degree of Doctor of Philosophy, was carried out by the candidate under my supervision in the National Chemical Laboratory, Pune, India. Such material as has been obtained from other sources has been duly acknowledged in the thesis.

(P. RATNASAMY)

(Research Guide)

ACKNOWLEDGEMENTS

I wish to express my deep sense of gratitude to Dr. P. Ratnasamy, Deputy Director, National Chemical Laboratory, Pune for his invaluable guidance and encouragement throughout the course of this investigation.

I am indebted to Dr. S. Sivasanker and Dr. Rajiv Kumar for their stimulating discussions and constant professional and personal help rendered during the course of the present investigation. I am equally obliged to Dr. A.P. Singh for his able support and help. Without their help, it would not have been possible for me to complete my research work successfully.

I am thankful to Dr. A.V. Ramaswamy for his encouragement and support. I take this oppurtunity to thank Dr. R.F. Shinde for his help.

I am grateful to Dr. S.K. Date, Dr.(Mrs.) Veda Ramaswamy, Dr. R. Vetrivel, Dr. Sujit B. Kumar and Dr. K. Ramesh Reddy for their help during the present study.

I am also thankful to the scientific and supporting staff of the Catalysis Division and my numerous friends and relatives for their wholehearted help in many ways.

My special thanks are due to my parents for their incessant encouragement and support. I am also thankful my brother and sister-in-law for their moral support. No thanks are enough to acknowledge their efforts.

Finally, my thanks are due to Council of Scientific and Industrial Research, New Delhi, for the award of a fellowship and the director, National Chemical Laboratory, Pune for permitting me to submit this work in the form of thesis.

ANUJ RAJ

Chapter 1

GENERAL INTRODUCTION

Contents...

1.1 DEFINITION

Molecular sieves are porous solids with pores of molecular dimensions, 0.3-2 nm in diameter *[1-3]*. Zeolites are crystalline aluminosilicate molecular sieves, with rigid three dimensional framework formed by corner sharing of all four oxygens of the $[SiO_4]^{4-}$ and $[AlO_4]^{5-}$ tetrahedra in such a way that two aluminiums are not adjacent *[2-5]*. The crystallographic unit cell of a zeolite may be represented as :

$$M_{x/n}\,[(AlO_2)_x\,(SiO_2)_y]\,Z\,H_2O$$

Where M is the charge compensating cation having valency n, generally an element from group I or II or an organic cation. The ratio of y/x can be one to infinity. Z represents the number of water molecules, which are reversibly adsorbed in the zeolite pores.

Recently, the definition of zeolites has been extended to encompass a larger class of molecular sieves. Zeolites are now defined as any three dimensional structure with tetrahedral atoms (T-atoms) joined with oxygen bridges with a framework density < 21 T-atoms per 1000 $Å^3$ *[6]*. Apart from the silica based materials, they now include aluminium phosphates, beryllophosphates and clathrasils. The silica based zeolites can be subdivided into pure silica and metallosililcate zeolites (Fig.1.1).

1.2 NOMENCLATURE

The International Zeolite Association Structure Commission and IUPAC have assigned structural codes to the known synthetic and natural zeolites *[6,7]*. Designations consisting of three capital letters have been used to identify structure types. These codes have generally been derived from the names of the type of minerals they are derived from or their names as given by their parent inventors. These codes define the

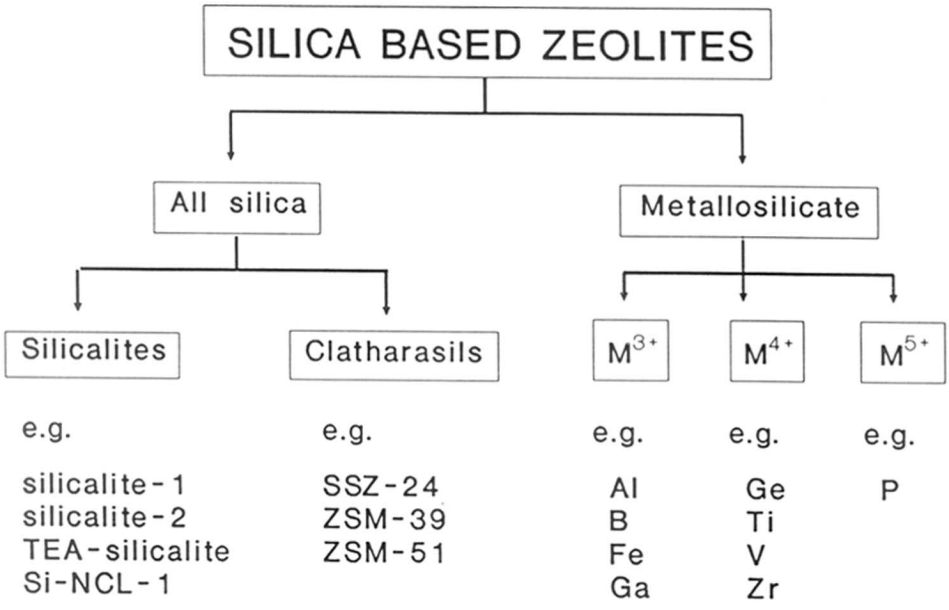

Fig. 1.1 Classification of silica based zeolites

particular class of molecular sieves possessing the symmetry and are independent of the composition and cell dimensions. 85 such codes have been given so far *[6,7]*. The computerized information research tool software "ZEOSYN" *[8]* has listed all the known zeolites with their properties.

1.3 SYNTHESIS OF METALLOSILICATE MOLECULAR SIEVES

A conventional synthesis procedure designed for aluminosilicates involves the hydrothermal crystallization of basic alkali metal aluminosilicate gel (at a certain temperature) under autogeneous pressures *[4]*. Using fluoride as mineralizing agent, a method has been developed where the crystallization takes place in neutral to acidic medium *[9]*. The synthesis of other metallosilicates can be achieved by direct synthesis through addition of metal ions in gel *[10,11]* as well as post synthesis methods *[12,13]*. Liquid phase post synthesis incorporation of Fe, Si and Ti into framework of various zeolite has been reported using ammonium salts of the corresponding metal hexafluorides ((NH_4MF_6) *[12]*. In vapor phase methods the zeolite is first dealuminated by acid treatment or hydrothermal treatment to form silanol nests. These nests are then healed with the vapor of a volatile compound of metal to be replaced *[13]*. Complete replacement of Al by these methods is not known. However, the addition of metal ions in the gel leads to synthesis of Al free analogs. Though the literature covers the synthesis of many metallosilicates (Al, B, Be, Cr, Fe, Ga, Ge, P, Sn, Ti, V etc.), only a few metallosilicates (viz. Al, B, Ga, Fe and Ti) are well characterized.

When the metal salt solution is added during gel preparation for direct hydrothermal synthesis of metallosilicates, the metal ion may occupy one or more or all of the following locations in the crystalline solid.

- lattice framework positions
- surface defect sites (Si-O-M)

- cation exchange sites
- Finely dispersed oxide clusters inside/ outside the pores
- Bulk oxides on the external surface

To achieve successful incorporation of metal ions in the zeolite framework, during crystallization by direct hydrothermal syntheses, it is necessary to form a good metallosilicate gel. Since the final metallosilicate gel is basic (pH 9-13), much depends on the solubility of the metal oxide /hydroxide formed (Fig. 1.2). Based on solubility of the oxide/ hydroxide of the metal ion in the basic medium, the metallosilicate synthesis can be divided into two classes: (i) Metal ion forming soluble oxide in basic medium, where the dissolution of metal oxide, if formed, helps in the formation of metallosilicate species, a prerequisite for the metal ion incorporation in the zeolitic framework, and (ii) insoluble/sparingly soluble metal oxides in basic medium; Such metal ions are susceptible to form precipitates of metal oxide/hydroxide thereby hindering the formation of metallosilicate gel and the incorporation of metal ions in the zeolite lattice. The sequence of addition in these cases is very important and the formation of metal oxide must be prevented by a careful and calculated sequence of addition of reactants. For example in the case of ferrisilicates, this is achieved by carefully adding basic silicate solution to acidified Fe^{3+} salt solution. Once the white or pale lemon colored ferrisilicate gel is formed the desired pH may be adjusted by adding alkali followed by the template *[2,10,11]* without the precipitation of metal oxide/hydroxide.

1.4 PHYSICO-CHEMICAL CHARACTERIZATION

The characterization of zeolites requires many instrumental and chemical techniques *[14]* :

- Powder X-ray diffraction
- Adsorption properties
- Thermal properties (DTA/TG)

Hydrothermal synthesis in basic (OH^-) medium

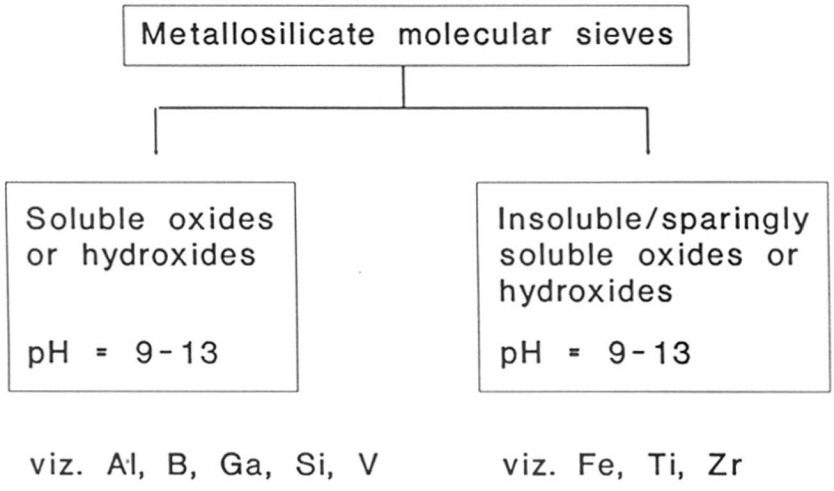

Fig.1.2 Classification of metallosilicates based on the solubility of the oxides or hydroxides.

- Infra-red spectroscopy
- MAS-NMR spectroscopy
- ESR spectroscopy
- UV-VIS spectroscopy
- Mössbauer spectroscopy
- Extended X-ray Absorption Fine Structure spectroscopy
- X-ray Absorption Near Edge Spectroscopy
- X-ray Photoelectron Spectroscopy or Electron spectroscopy for Chemical analysis
- Ion-exchange capacities
- Catalytic properties

Some of the above mentioned techniques alongwith the relevant information provided by them are discussed below :

1.4.1 Powder X-ray Diffraction

Powder X-ray diffraction (PXD) is the single most important technique used in the study of zeolites. It is used in (i) the identification of the crystalline phase/ phases (fingerprinting) (ii) calculation of the unit cell parameters and (iii) to find out the degree of crystallinity. Isomorphous substitution in the zeolite in lattice is accompanied by the change in unit cell parameter, where this technique is handy. A substance is assumed to be pure when the X-ray signature matches exactly in the number and relative intensities with the reported one *[6-8]*.

High energy X-ray can further be used to decipher the structure of a zeolite after appropriate refinement. Modern methods (viz. autoindexing, position sensor detectors) and softwares such as Reitveld refinement are becoming popular with growing computational facilities.

1.4.2 Infra-red Spectroscopy

Infra-red spectroscopy is a sensitive technique for the investigation of structural features of zeolites, isomorphous substitution, acidic properties and nature of adsorbate-zeolite interaction *[15-17]*. The lattice vibrations of the zeolites in the infra-red spectrum are observed in the range of 300 -1300 cm^{-1}. These vibrations can be classified into two groups, (i) internal vibrations of the TO_4 units or structure insensitive vibrations and (ii) vibrations due to external linkages of the TO_4 units or structure sensitive vibrations *[15,16]*. The major infra-red band assignments are as follows :

Structure insensitive vibrations	
Asymmetric stretching	1250 - 950 cm^{-1}
Symmetric stretching	720 - 650 cm^{-1}
T - O bond	420 - 500 cm^{-1}
Structure sensitive vibrations	
Asymmetric stretching	1050 -1150 cm^{-1}
Symmetric stretching	750 - 820 cm^{-1}
Double ring	650 - 500 cm^{-1}
Pore opening	300 - 420 cm^{-1}

Systematic studies of the framework vibrations of zeolites A, X, Y, ZK-5 and Omega have been reported *[16]*. For some structure sensitive bands a linear relation between the band intensity and the number of lattice aluminum atoms is reported *[16]*. Isomorphous substitution shifts both symmetric and asymmetric framework vibrations. The substitution of lighter elements such as B shifts the framework vibrations to higher wave numbers *[17]*, while the incorporation of heavier metal ions such as Fe, Ga and

Ti shift to lower wave numbers *[18]*. In the case of titanium and vanadium silicates an additional asymmetric stretching vibration at around 960 cm^{-1} was reported. It was attributed to Si-O-M (M = Ti, V) linkages *[19-21]*.

IR spectroscopy is an efficient technique to study both the Brönsted and Lewis acidity and basicity using probe molecules such as ammonia, pyridine, benzene, carbon monoxide, pyrrole, CO_2, *etc. [22-25]*.

1.4.3 Mössbauer spectroscopy

Mössbauer spectroscopy is based on the recoilless emission of γ-rays from a nucleus in excited state and its subsequent resonant fluorescence, by a nucleus of the same isotope in ground state *[26-28]*. Resonance absorption is achieved by super-imposing a Doppler velocity on the source which gives rise to γ-rays with variable range of frequencies. Mössbauer spectrum is primarily reflected in (1) the chemical isomer shift, (δ) (2) the quadrupole splitting (Δ) and (3) the magnetic splitting.

(1) Chemical isomer shift (δ)*[26]*: The chemical isomer shift is a consequence of the electric monopole (Coulomb) interaction between the nuclear charge distribution over a finite volume and the electronic charge density over this volume. The shift arises because of the difference in the nuclear volume in the ground and the excited states.

(2) Quadrupole splitting (Δ) *[26]* : At times a sample containing all the atoms in the same state of chemical bonding can display two lines in the Mössbauer spectrum. This is due to the phenomenon of quadrupole moment of the excited nucleus. The quadrupole splitting data can provide information concerning the nature of the chemical bonding and crystal lattice.

(3) Hyperfine interactions *[27]*: The energy levels of the nucleus split in presence of an externally applied or an internal field (formed by magnetic ordering of the spins). A hyperfine interaction, thus results in a spectrum which has many transitions in it.

The parameters such as the isomer shift, the quadrupole splitting and the magnetic hyperfine splitting, which can be extracted from Mössbauer spectroscopy provide a wealth of information about the chemical state of certain atoms (e.g. Fe) in the given sample.

Mössbauer spectroscopy has been used to study the Fe(II) and Fe(III) ion exchanged in the zeolites and iron-containing molecular sieves *[29-32]*. The use of Mössbauer spectroscopy for catalyst characterization has been reviewed by Jones *[28]* and Berry *[27,33]*. It has been reported that the Fe^{3+} introduced in the cationic position has an isomer shifts of +0.35 mm/sec with respect to the iron metal and a quadrupole splitting of 0.77 mm/sec *[38]*. Fe(II) introduced in the cationic position has an isomer shift of 1.41 mm/sec with respect to the iron metal and a quadrupole splitting of 2.56 mm/sec. Meagher *et al.* have assigned an IS ~ 0.2 - 0.3 mm/sec for iron (III) in tetrahedral lattice sites of ZSM-5 *[34]*. The quadrupole splitting is not observed for perfectly placed lattice iron. Based on the literature the isomer shift range for different types of iron can be assigned as follows :

Isomer shift (mm/sec)	State of iron
0.2-0.3	tetrahedral Fe^{3+}
0.3-0.5	octahedral Fe^{3+}
0.5-0.7	tetrahedral Fe^{2+}
0.7-1.2	octahedral Fe^{2+}

In-situ Mössbauer spectroscopy has been used to characterize samples under evacuation and hydrogen reduction both on doped and ferrisilicate samples *[32,35]*.

1.4.4 Magnetic Properties

Magnetic properties of materials can be classified into five types: diamagnetism, paramagnetism, ferromagnetism, antiferromagnetism and ferrimagnetism. The measurement of the materials at various temperatures and at various field strengths (of the externally applied magnetic field) can be used to determine the magnetic behavior of the sample under investigation. Lewis and Wilkins have discussed in detail the procedure involved in making such measurements *[37]*.

The Faraday method is the most popular method used to obtain the magnetic susceptibility data. In the Faraday method a small amount of the sample is maintained in a region of constant magnetic gradient and the force acting on it is measured by Cahn elctrobalance. The measured force is a direct measure of the magnetic susceptibility. The absolute value of the magnetic susceptibility is determined by calibration of the system with a standard sample having known magnetic susceptibility, e.g. $Hg[Co(CNS)_4]$.

Nair has made a detailed study of the magnetic properties of [Fe]-ZSM-5 *[38]*. Both as-synthesized and calcined form of materials showed a magnetic moment range of 5.5-5.8 BM. This has also been recommended by Kumar and Ratnasamy *[39]*. The presence of extralattice iron increases the value to > 6 BM. A strong temperature dependence is observed in hydrothermally treated samples of Fe-MFI containing significant amount of extra lattice iron *[38]*.

1.4.5 Electron Paramagnetic Resonance

EPR spectroscopy is the resonance absorption of the electromagnetic (microwave) radiation by magnetically split spin states of unpaired electrons. The electron undergoes a transition to excited state by the absorption of microwave energy when it is matched with the splitting caused by the field. EPR is very sensitive technique to analyze

different paramagnetic species even in a dilute system *[40]*. The splitting of the magnetic levels can give information regarding the symmetry around the metal (M^{n+}) ion. This technique has been applied to know the isomorphous substitution of metal ions in the zeolite (g ~ 4.3 corresponds to rhombically distorted iron which is incorporated in the molecular sieve lattice) *[41]*.

EPR spectroscopy has been used to identify different coordinations and oxidation state around a paramagnetic ion. If the iron atoms are in perfect tetrahedral or octahedral coordination only one signal is observed at g = 2.0. As the distortion increases the signal moves towards to the down field region and can have g values 2 to 6. When the symmetry is lowered the signal corresponds to orthorhombic symmetry as is observed at g = 4.3 (perfect orthorhombic g = 4.27). Apart from the g = 4.3 for framework Fe, Ratnasamy *et al. [42]* observed peaks at 2.0, 2.3, 5.3. The g = 5.3 signal was assigned to extra lattice iron species, however the location of such species is not reported. The signal at g = 2.3 is assigned to the iron oxide/hydroxide phase *[43,41]*.

EPR of vanadium zeolites is used extensively as a proof for atomically dispersed vanadium which gives rise to a hyperfine spectrum split into 8 component peaks (I = 7/2 ; 2nI+1 states). ESR spectrum has been observed for Ti after reduction at 673K in CO *[44]*.

1.5 ACIDITY AND BASICITY IN ZEOLITES

A pure silicate framework is neutral. When Si is replaced with trivalent ions like Al, Fe, Ga etc., it leads to an anionic framework which is neutralized by cations. When this charge compensating cation is replaced by protons through ion-exchange, the number of Al-(OH)-Si, Fe-(OH)-Si etc. species in zeolites is equal to the number of Brönsted acid sites. Brönsted acidity is induced in a zeolite by exchanging the

charge compensating ions by H^+. The strength of these acid sites is found to vary with (i) zeolite structure, (ii) Si/Al ratio, at least upto the value of 10, and (iii) isomorphously substituted metal ions in the zeolite framework *[22,45,49]*.

Lewis acid sites arise at the defect sites where trigonal Al is present either in the framework or at charge compensating ions *[45]*. The Lewis acidity can also be formed by high temperature (>500) dehydroxylation of the Si(OH)Al (i.e. Brönsted) sites.

When extraframework Al^{3+} ions are associated with acidic aluminium sites they produce 'superacid sites' which are responsible for the higher cracking activities in the dealuminated zeolites *[50]*. Barthomeuf *et al.* have also proposed an efficiency coefficient which is equivalent to the activity coefficients in liquid *[51]*. This concept takes into account the whole spectrum of acid sites contributing as a whole to the acidity of the zeolite.

The basic properties of zeolites in catalysis and adsorption have also been reported *[52,53-55]*. Like acid sites, basic sites may be of the Brönsted (basic OH groups) or Lewis (framework oxygen atoms) type. The extent of charge on the oxygen determines their basic strength.

Most of the zeolites contain mainly Lewis basicity. The number of potential basic sites are equal to the number of oxygen atoms in the framework. The framework oxygen atoms are less mobile than the protons. Barthomeuf *et al.* and Hathaway *et al.* have studied the basicity of zeolites using in-situ adsorption of pyrrole *[52,56]*. They have shown that the actual basic strength of a zeolite depends not only on the chemical composition but also on the structural environment of the framework oxygen. Kaliaguine *et al.* proposed a model for the adsorption of pyrrole on alkali exchanged zeolite based on the in-situ infra-red studies *[55]*.

Zeolites act as Brönsted acid sites through donation of the protons to the substrate resulting in the formation of carbenium ion *[55,56,57]*. On the other hand, basic sites are of Lewis type (Fig. 1.3 I) they are formed by the ionization and charge delocalization at the nearest oxygen.

When tetravalent metal ions like Ti^{4+}, V^{4+}, Zr^{4+} etc. are incorporated in the silicate network, the resulting metallosilicates are charge neutral and hence do not possess any charge compensating cations. Many models are proposed to explain the reactivity of these metal ions (Fig. 1.3 II, III) *[59]*. Not much is known about the active centers. However, Kaliaguine *et al.* have proposed a highly constrained site for the titanium (Fig. 1.3 IV) based on the bond distances obtained from the EXAFS data *[60]*.

The acidity and/or basicity can be determined through many techniques *[24,45,47]* :

- spectroscopic techniques : IR, UV-VIS, NMR, ESR, XPS
- calorimetric methods
- chromatographic methods
- titration methods
- test reaction

1.6 MOLECULAR SELECTIVITY IN ZEOLITES

Due to the unique molecular dimensions of the pores, zeolites can 'sense' molecules based on their size. The term 'shape selectivity' was assigned to such a phenomenon *[65]*. The concept of shape selectivity was first demonstrated some 35 years back by the selective conversion of n-paraffins over 5A molecular sieves. Since then it has been used widely in the field of catalysis.

Based on the diffusion constraints Csicsery *[66]* has proposed three types of shape selectivities:

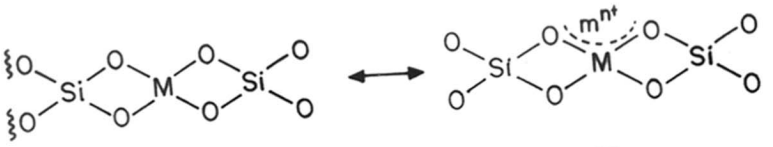

I II

M = Al, Ga, Fe

$m^{n+} = H^+, Na^+, K^+$

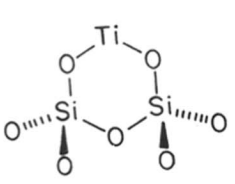

III

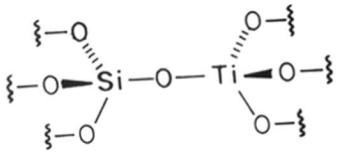

IV

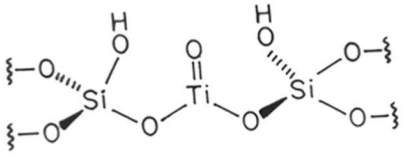

V

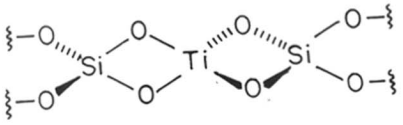

VI

Fig. 1.3 Possible structures for the active of some metallosilicates.

• *Reactant selectivity*

When only one/some of the reactant molecules in the reaction mixture is/are small enough to diffuse through the zeolite pores and is/are thus converted to products. Such type of selectivity is used to crack linear molecules and save branched chain alkanes which are more useful in petrochemical industry.

• *Product selectivity*

This is a consequence of the products that can be formed within the pores or cavities, diffuse faster leaving behind bulkier molecules which are either converted to less bulky molecules that can diffuse out or eventually deactivate the catalyst

• *Restricted transition state selectivity*

This depends upon size and shape of the transition state complex vis-á- vis required void space available in the cavities of the zeolite. The products which result from less bulky transition states are preferentially produced.

On the other hand, the chemical nature of the active sites viz. Strength of the acid sites and electronic as well as thermodynamic effects also found to influence the overall selectivity in certain reactions *[47]*. Chen *[62]* has suggested that the application of shape selective catalysis can be applied to catalysis provided the acidity and acid strengths are well understood.

Hölderich demonstrated through a series of catalytic reactions that shape selectivity does not always guide the reaction path in zeolites but electronic as well as thermo-dynamic effects dominate over the diffusionally controlled shape selectivity *[68]*.

In hydroisomerization of n-alkanes *[69]* it was found that selectivity for branched alkanes increased while the isomerization to cracking ratio decreased with the acidity of the zeolite.

Recently, the role of chemical nature in directing the selectivities in zeolites has been interpreted by Corma on the basis of Pearson's concept of hard and soft acids and bases and the Perturbation theory *[66]*. According to this the energy levels of HOMO and LUMO orbitals play an important role in determining the path of the reaction.

Taking the above factors into consideration the selectivity in zeolites can be divided into :

[A] Geometrically Induced Selectivity (GIS)

(i) Reactant selectivity

(ii) Product selectivity

(iii) Restricted transition-State selectivity

[B] Chemically Induced Selectivity (CIS)

(i) acidity (strength/density) related selectivity

(ii) electronic and hardness/softness of the acid sites dependent selectivity

In the literature numerous examples for geometrically induced selectivity (GIS) *[61,68]* as well as chemically induced selectivity (CIS), *[61,66,67]* are well documented.

1.7 CATALYTIC PROPERTIES

Zeolites have advantages over conventional heterogeneous catalysts in many applications, involving acid, acid-base, base, oxidation, reduction and polyfunctional catalysis. Though zeolites have many definite advantages, they have some disadvantages too. This has recently been reviewed by Perot and Guisnet *[76]*. The major disadvantages are the deactivation by irreversible adsorption of secondary products and the restriction of pore size to the bulkier molecules.

1.7.1 Isomerization Reactions and rearrangements

Two types of aliphatic isomerizations are found, one in which the carbon skeletal rearrangements are observed and other, in which carbon skeleton remains unchanged and only the functional group migrates. The latter type include double bond isomerizations over acidic and basic zeolites *[70-72]*. Regioselective isomerization of 1-butene to isobutene is known *[73]*. Skeletal isomerization of alkanes takes place under mild conditions over strongly acidic zeolites. The isomerization of alkanes over Pt doped zeolites enhances the RON of gasoline thus is important for petroleum industry *[74-76]*. Apart from being used in industry, the hydroisomerization of n-C_{10} alkane is also is used to characterize the pore structure and void volume of the zeolites, the refined constrained index *[77]*. Catalytic dewaxing by isomerization of long chain alkanes is suggested as a prospective field for improving the flow properties of the gasoline *[73]*. Aldehyde to ketone rearrangement are known to occur selectively over mildly acidic iron zeolites *[78]*. The selectivity for ketone increases with the decrease in the acidic strength. Pinacol rearrangement, epoxide rearrangement are other commonly known reactions of this type *[79]*.

Isomerization of substituted aromatics, alkylaromatic like *m*-xylene is isomerized with high selectivity to *p*-xylene *[80]*. It is also used as a test reaction for acidity and shape selectivity. The selective isomerizations known to occur over zeolites are isomerization of dichlorobenzene, chlorotoluenes, alkylanilines, substituted heteroaromatics *[80-82]*.

1.7.2 Electrophilic aromatic reactions

Alkylation of aromatics with alcohols or alkenes is one of industrially useful reaction over zeolites. The gas phase alkylation of the aromatic nucleus which can orient in o- or p- position is coupled with molecular seiving properties to achieve para

selective alkylation. Similarly naphthalene shows high selectivity to 2-alkyl product and biphenyl to 4,4' dialkyl biphenyl isomers over certain zeolites, viz. ZSM-12, dealuminated mordenite etc. *[83,84]*.

Aromatic halogenations with bromine and chlorine known to be feasible over zeolites *[87-89]*. Whereas, conventional Lewis acid catalysts lead to lower para isomer in products, the zeolites restrict the ratio in favour of para products. Moreover, they also avoids the formation of bulkier halogenated product (e.g. trichloro or tetrachloro benzene isomers) through geometrically induced shape selectivity.

1.7.3 Oxidations

The oxidation using zeolites has been reported by many workers . In recent times most of the oxidation catalysis in literature involves the use of titanium and vanadium silicate molecular sieves. TS-1 and TS-2 molecular sieves are reported to catalyze in alkane oxidations with high selectivities to hydrogen peroxide *[90-93]*. While these cannot oxidize the primary carbon atom, vanadium silicates can activate even primary carbon atom (from n-hexane to 1-hexanol/al) *[94]*. Oxidation of phenol to dihydroxybenzenes was first commercialized by ENICHEM group using titanium silicate catalyst. Gas phase oxidation of benzene to phenol is reported to be catalyzed by H-[Fe]-ZSM-5 in the presence of N_2O *[95]*. V-NCL-1, a large pore vanadium silicate molecular sieve is reported recently. It is also capable of hydroxylating larger molecules like naphthalene, xylenes, trimethylbenzenes *[96,97]*. It can also oxidize the side chain of alkylaromatics to yield benzyl alcohols and benzaldehyde. *[98]*.

1.8 SCOPE OF THE THESIS

The incorporation of various metal ions (such as Fe^{3+}, Ga^{3+}, Ti^{4+}, V^{4+} etc.) substituting Al^{3+} and/or Si^{4+} in a number of zeolite frameworks is now well established. The availability of these isomorphously substituted metallosilicate molecular sieves provides an opportunity to study the shape selective properties and deactivation behavior in catalytic reactions as a function of their chemical nature. This may help to understand whether the geometric features (pore structure, crystal morphology etc.) of a particular zeolite and/or its chemical composition is controlling its overall catalytic behavior.

Since, the zeolites are generally synthesized at high pH under hydrothermal conditions, the synthesis of some metallosilicates of those metal ions which form insoluble oxides or hydroxides in basic medium requires very rigid procedures and sequence of adding reactants so that the formation of insoluble metal oxide/ hydroxide is avoided prior to the formation of metallosilicate gel. However by using a suitable complexing agent, the instantaneous formation of insoluble metal hydroxide/ oxide, is avoided and the sequence of addition of reactants is no longer a limiting step for the incorporation of metal ions in the framework.

Chapter II describes the synthesis and characterization of Al, Ga and/or Fe silicate analogs of ZSM-11 (MEL), EU-1 (EUO), ZSM-48 and beta (BEA) used during the course of this study. Various spectroscopic (IR, ESR, Mössbauer, MAS NMR, XRD), magnetic susceptibility, scanning electron microscopy and ion exchange techniques have been utilized.

Chapter III describes the catalytic reactions of the metallosilicates, in chlorination of toluene, *m*-xylene isomerization and alkylation of xylenes and toluene. The effect of temperature, space velocity and time-on-stream are studied. The results have been correlated to the acidity and shape selective properties of the zeolites.

Chapter IV describes the use of complexing agents in the synthesis of titanium- and ferri-silicate molecular sieves. Techniques such as XRD, IR, UV-VIS, TG-DTA, Mössbauer, ESR and XPS have been used to characterize these materials. Further, the titanium silicates were tested in the catalytic reactions such as alkane oxidation and aromatic hydroxylation.

Chapter V describes the stability of ferriBeta to reduction. The reduction was carried out in H_2 and under vacuum. The changes were monitored using in-situ Mössbauer spectroscopy and the results were correlated to the catalytic activity, ion-exchange capacity and XRD d spacing.

1.9 REFERENCES

1. McBain, *"The sorption of gases and vapors by solids"*, Rutledge, London, 1932.
2. R. Szostak, *"Molecular Sieves : principles of synthesis and identification"*, Van Nostrand Reinhold, New York, 1989.
3. J.V. Smith, *Zeolites*, **4**, 309 (1984).
4. D.W. Breck ,*"Zeolite Molecular Sieves"*, Wiley, New York, 1974.
5. R.M. Barrer, *"Hydrothermal Chemistry of Zeolites"*, Academic Press, New York, 1982.
6. a) W.M. Meir and D.H. Olson, *"Atlas of Zeolite Structure Types"* (2nd ed.) Butterworths, London, 1987; b) *Zeolites* **12**, 14 (1992).
7. R. von Balmoos, *"Collection of Simulated XRD Powder Patterns for Zeolites"*, Butterworths, 1984.
8. D.N. Iyer, T. Selvam and R. Vetrivel, *Appl. Catal.*, (communicated).
9. J.L. Guth, H. Kessler, J.M. Higel, J.M. Lamberlin, J. Patarin, A. Seive J.M. Chezeau and R. Wey, *ACS Symposium Ser.* **398**, Washington D.C., 1989 p.176.
10. P. Ratnasamy and R. Kumar, *Catal. Lett.*, (in press)
11. P. Ratnasamy and R. Kumar, *Catal. Today* **9**, 329 (1990).
12. G.W. Skeels and E.M. Flanigen, *ACS Symposium Ser.* **398**, Washington D.C. 1989 p.420
13. A. Carati, S. Contarini, R. Millini and G. Bellussi, *Pro. Mat. Res. Soc.*, Extended Abstract (EA 24), 1990.
14. J.H.C. Van Hooff and J.W. Roelofsen, *Stud. Surf. Sci. Catal.* **58**, 242 (1991).
15. E.M. Flanigen, H. Khatami and H.A. Szymanski, *ACS Symposium Ser.* **101**, Washington D.C., 1971 p.201.
16. E.M. Flanigen, *ACS Symposium Ser.* **171**, Washington D.C., 1976 p.80.
17. J.W. Ward, *ACS Symposium Ser.*, **171**, Washington D.C., 1976 p.
18. N.A. Kutz, *"Heterogeneous Catalysis-II"*, Ed. B.L. Shapiro *et al.*, 1984 p.121.
19. R. Szostak and T.L. Thomas, *J. Catal.* **101**, 549 (1986).
20. B. Notari, *Stud. Surf. Sci. Catal.* **37**, 413 (1988).

21. J. Kornatowski, M. Sychev, V. Goncharuk and W.H. Baur, *Stud. Surf. Sci. Catal.* **65**, 581 (1992).

22. P.R. Hari Prasad Rao, A.V. Ramaswamy and P. Ratnasamy, *J. Catal.* **137**, 225 (1992).

23. M.R. Boccuti, K.M. Rao, A. Zecchina, G. Leofanti, G. Petrini, *Stud. Surf. Sci. Catal.* **48**, 133 (1989).

24. H.G. Karge, *Stud. Surf. Sci. Catal.* **65**, 133 (1992).

25. V.A. Maroni, K.A. Martin and S.A. Johnson, *ACS Symposium Ser.* **368**, 1987 p.

26. F.J. Berry, *Stud. Surf. Sci. Catal.* **57A**, 299 (1991).

27. N.N. Greenwood and T.C. Gibb, *"Application of Mössbauer Spectroscopy"*, Chapman and Hall, London, 1971.

28. W. Jones, *"Characterization of Catalyst"*, Eds. J.M. Thomas and R.M. Lambert, John Wiley, New York, 19 p.114.

29. M. Petrera, A. Gennaro, P. Gherardi, G. Gubitosa and N. Pernicone, *JCS Faraday Trans. I* **80**, 709 (1984).

30. D.G. Rethwisch and J.A. Dumesic, *J. Phys. Chem.* **90**, 1863 (1981).

31. B. Wichterlowa, *Zeolites* **1**, 181 (1981).

32. W.N. Deglass, R.L. Garten and M. Boudart, *J. Phys. Chem.* **73**, 2970 (1969).

33. F.J. Berry, *"Mössbauer Spectroscopy Applied to Inorganic Chemistry"* Vol 1, Plenum Press, 1984 p.323.

34. A. Meagher, V. Nair and R. Szostak, *Zeolites* **8**, 3 (1988).

35 K. Lazar, G. Borbely and H. Beyer, *Zeolites* **11**, 214 (1991).

36. a.L.N. Mulay and T. Pannaparayil, *ACS Symp. Ser.* **288**, Washington D.C., 1985 p. 498.
b.R. Schimdt, M.D. Amiridis, J.A. Dumesic, L. M. Zelewski and W.S. Milman, *J. Phys. Chem.* **96**, 8142 (1992).

37. J. Lewis and R.G. Wilkins, *"Modern Coordination Chemistry"*, Interscience, New York, 1960.

38. V. Nair, *Ph.D. Thesis*, Georgia Institute of Technology, Georgia, USA, 1987.

39. R. Kumar and P. Ratnasamy, *Stud. Surf. Sci. Catal* **60**, 43 (1990)

40. J.E. Wertz and J.R. Bolton, *"Electron Spin Resonance Elementary Theory and Practical Applications"*, McGraw Hill, New York, 1972.

41. N.P. Evmiridis, *Inorg. Chem.* **25**, 4362 (1986).

42. P. Ratnasamy, R.B. Borade, S. Sivasanker, V.P. Shiralkar and S.G. Hegde, *Acta Phys. Chem.* **31**, 137 (1985).

43. B.D. McNicol and G.T. Pott, *J. Catal.* **25**, 223 (1975).

44. A. Tuel, J. Diab, P. Gelin, M. Dufaux, J.F. Dutel and Y. Ben Taarit, *J. Mol. Catal.* **63**, 95 (1990).

45. D. Barthomeuf, *Stud. Surf. Sci. Catal.* **37**, 157 (1992).

46. C.T.W. Chu and C.W. Chang, *J. Phy. Chem.* **89**, 1569 (1985).

47. a.J.C. Vedrine, *"Guidelines to Mastering the Properties of Molecular Sieves"* NATO Ser. **221**: Physics B, Eds. D. Barthomeuf, E.G. Derouane, and W. Hölderich, Plenum Press, New York, 1990 p.121.
b.L. Lerchert, *React. Kinet. Catal. Lett.* **46**, 153 (1992).

48. J.W. Ward, *Adv. Chem Ser.* **101**, 380 (1970).

49. J.W. Ward, *J. Catal.* **16**, 173 (1970).

50. C. Mirodatos and D. Barthomeuf, *J. Chem. Soc. Chem. Commun.*, p.39 (1981).

51. D. Barthomeuf, *Mater. Chem. Phy.* **17**, 49 (1987).

52. a.D. Barthomeuf *J. Phys. Chem.* **88**, 42 (1984).
b.D. Barthomeuf and A. de Mallman, *Stud. Surf. Sci. Catal.* **37**, 365 (1987).

53. Y. Okamoto, M. Ogawa, A. Maezawa and T. Imanaka, *J.Catal.* **112**, 427 (1988).

54. K. Tanabe in *"Solid acids and bases"*, Academic Press, New York, 1970.

55a. M. Huang, and S. Kaliaguine, *J. Chem. Soc., Faraday Trans.* **88**, 751 (1992).

b. M. Huang and S. Kaliaguine, *Stud. Surf. Sci. Catal.* **73**, 291, (1992).

56. I.E. Hathaway and M.E. Davis, *J. Catal.* **116**, 263 (1989).

57. P.A. Jacobs, "*Carboniogenic Activity of Zeolites*", Elsevier, Amsterdam, 1977.

58. V.B. Kazansky, *Acc. Chem. Res.*, **24**, 379 (1991).

59. G. Bellussi, A. Carati, M. Clerici, G. Maddinelli, R. Millini, *J. Catal.* **133**, 220 (1992).

60. D. Trong on, A. Bittar, S. Kaliaguine and L. Bonnevoit, *Catal. Lett.*, **16**, 85 (1992).

61. S.M. Csicsery, *Zeolites* **4**, 220 (1984).

62. N.Y. Chen *ACS Symp. Ser.* **368**, Washington D.C., 1988 p.468.

63. F. Fajula, M. Lambert, F. Figureas, *Stud. Surf. Sci. Catal.* **46**, 61 (1989).

64. N.S. Chang, C.C. Chen, S.J. Chu, P.J. Chen and T.K. Chuang, *Stud. Surf. Sci. Catal.* **46**, 223 (1989).

65. W. Höelderich, *"Guidelines to Mastering the Properties of Molecular Sieves" NATO Ser.*, **221**: Physics B, Eds. D. Barthomeuf, E.G. Derouane, and W. Hölderich, Plenum Press, New York, 1990 p.319.

66. A. Corma, *"Guidelines to Mastering the Properties of Molecular Sieves" NATO Ser.*, **221**: Physics B, Eds. D. Barthomeuf, E.G. Derouane, and W. Hölderich, Plenum Press, New York, 1990 p.299.

67. P.B. Weiz, in *Stud. Surf. Sci. Catal.* **7A**, 3 (1980).

68. P.B. Weiz, V.J. Frilette, R.W. Maatman and E.B. Mower, *J. Catal.* **1**, 307 (1962).

69. G. Perot and M. Guisnet, *J. Mol. Catal.* **61**, 173 (1990).

70. K. Tanabe, M. Misono, Y. Ono and H. Hattori, *Stud. Surf. Sci. Catal.* **51**, 215 (1989).

71. L.R. Martens, P.J. Grobet, W.J.Vermeiren and P.A. Jacobs, *Stud. Surf. Sci. Catal.* **28**, 935 (1986).

72. R. Fischer, W. Höelderich, W.D. Mross and H.M. Weitz, Eur. Pat. 0167 021, (1986).

73. J. Weitkamp, *Stud. Surf. Sci. Catal.* **65**, 32 (1992).

74. M. Stoeker, R. Hemmersbach, H. Raeder and J.K. Grepsted, *Appl. Catal.* **25**, 223 (1986).

75. Li-Jen Leu. Liang-Yuan Hou, Ben-Chang Kang, Chiuping Li, Swu-Tzy Wu and Jung-Chung Wu, *Appl. Catal.* **69**, 49 (1991).

76. M. Guisnet and N.S. Gnep, *Appl. Catal. A* **89** 1 (1993).

77. J.A. Martens, M. Tielen, P.A. Jacobs and J. Weitkamp, *Zeolites* **4**, 98 (1984).

78. W. Höelderich, F. Merger, W.D. Mrosz and R. Firscher, Eur. Pat., 0162 387, (1985).

79. P.B. Venuto and P.S. Landis , *Adv. Catal.* **18**, 259 (1968).

80. A. Paul, Anuj Raj and A.P. Singh, *Appl. Catal.* (communicated).

81. K. Iwayama, Y. Imeda and K. Iwayama, Jap. Pat. 6 393 738 (1984).

82. V. Dettemeyer, K. Eichler, K. Kühlein, E.J. Leupold and H. Litterer, *Angew. Chem. Intl. Ed.* **26**, 468 (1987).

83. M. Neuber and J. Weitkamp, *Stud. Surf. Sci. Catal.* **49A**, 545 (1989).

84. E.M. Flanigen, WO Pat. 9103443 (1991).

85. I. Nicolan, and A. Agnilo, US Pat. 4 652 683 (1987).

86. A. Corma, M.J. Climent, H. Garcia and J. Primo, *Appl. Catal.* **49**, 109 (1989).

87. Th. M. Wortel, D. Oudijin, C.J. Vleugel, D.P. Roelofsen and H. Van Bekkum, *J. Catal.* **60**, 110 (1979)

88. Y. Higuchi and T. Suzuki, Eur. Pat. 112 722 (1984).

89. T. Miyake, K. Sekizawa, T. Hironaka, M. Nakano, S. Fuji and T. Tsutsumi, *Stud. Surf. Sci. Catal.* **28**, 147 (1986).

90. A. Tuel, S.M. Khouzami, Y. Ben Taarit, and C. Naccache, *J. Mol. Catal.* **68**, 46 (1991).

91. T. Tatsumi, M. Nakamura, K. Yuasa and H. Tominga, *Catal. Lett.* **10**, 259 (1991).

92. D.R.C. Huybrechts, P.C. Buskens and P.A. Jacobs, *J. Mol. Catal.* **11**, 129 (1991). abid, *Nature* **345**, 240 (1990)

93. A. Thangaraj, R. Kumar, P. Ratnasamy, *Appl. Catal.* **51**, L1 (1990).

94. P.R.H.P. Rao and A.V. Ramaswamy, *J. Chem. Soc. Chem. Commun.*, p.1245 (1992).

95. G.I. Panov, G.A. Sheveleva, A.S. Karitonov, V.N. Romannikov and A.V. Vostrikova, *Appl. Catal.A* **82**, 31 (1992).

96. K. Ramesh Reddy, A.V. Ramaswamy and P. Ratnasamy, *J. Chem. Soc. Chem. Commun.*, p.1613, 1992. *J. Catal.* **143**, 275 (1993).

97. A.V. Ramaswamy and S. Sivasanker, *Catal. Lett.*, (communicated)

98. J.C. Oudejans, F.J. van der Gaag and H. van Bekkum, *Proc. 6th Intl. Zeolite Conf.*, Reno, Butterworth, p. 536, 1984.

99. C.A. Tolman and N. Herron, *Catal. Today* **3**, 235 (1988).

Chapter 2

SYNTHESIS AND CHARACTERIZATION

2.1 INTRODUCTION

In this chapter, the synthesis and characterization of metallosilicate analogs of ZSM-11, EU-1, ZSM-48 and Beta are described.

2.2 EXPERIMENTAL

2.2.1 Synthesis of metallosilicates

The materials used for the synthesis of metallosilicate analogs of ZSM-11, ZSM-48, EU-1 and Beta are listed in Table 2.1. A diagrammatic representation of the autoclave used for the synthesis of these zeolites is given in Fig. 2.1. The autoclaves were cleaned with dilute HF (10% aqueous) and polished with carbon brushes prior to their use. The typical synthesis procedures of various molecular sieves are given below :

ZSM-11

[Fe]-ZSM-11 *[1]* was synthesized by adding a solution of 1.90 g of ferric nitrate in 30 g water to 45 g of tetraethylorthosilicate (TEOS) under stirring till a homogeneous solution was obtained. Then 28.5 g of tetrabutyl ammonium hydroxide (40% aqueous) in 34 g water was added very slowly to avoid the precipitation of brown colored iron oxides/hydroxides. Finally 14 g H_2O was added and the pale lemon colored gel thus obtained was autoclaved and the crystallization was carried out at 443 K for 4 days under rotation at 60 rpm.

For synthesizing the [Al]- and [Ga]- analogs the following procedure was used *[2-4]* : 45 g TEOS was hydrolyzed with a solution of 28.5 g TBAOH (40% aqueous) in 34 g water followed by the addition of respective M(III) (M = Al or Ga) nitrate solution in 30 g water. The gel thus formed was stirred for 20 min before adding 14

Table 2.1 Specifications of reactants used in the synthesis of metallosilicate zeolites.

	Reagent & Source	Chemical formula	purity
1.	Fumed Silica, S-5005, Sigma	SiO_2	99.8%
2.	Tetraethylorthosilicate, TEOS, Aldrich	$Si(OC_2H_5)_4$	98%
3.	Ferric nitrate, BDH	$Fe(NO_3)_3.9H_2O$	98%
4.	Ferric sulphate, BDH	$Fe_2(SO_4)_2.5H_2O$	98
5.	Aluminium nitrate, BDH	$Al(NO_3)_3.9H_2O$	98%
6.	Gallium nitrate, Aldrich	$Ga(NO_3)_3$	>99%
7.	Tetrabutyl ammonium hydroxide, Aldrich	$(C_4H_9)_4NOH$	40% aqueous
8.	Tetraethyl ammonium hydroxide, Aldrich	$(C_2H_5)_4NOH$	40% aqueous
9.	Hexamethonium bromide monohydrate,[Hexamethylene bis(trimethyl ammonium) dibromide], diquat-6, Aldrich	$[Br(CH_3)_3N\text{-}(CH_2)_3]_2.H_2O$	98%

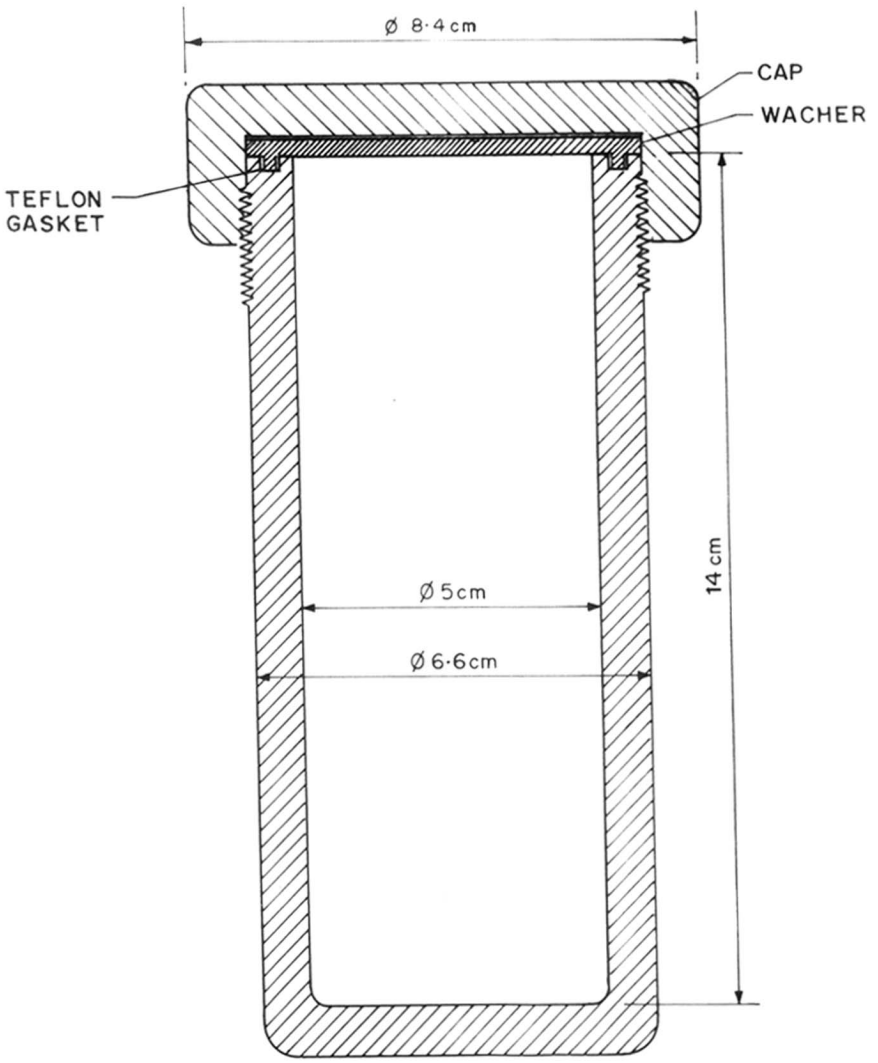

Fig. 2.1 Stainless steel autoclave with Teflon gasket for hydrothermal synthesis

g water. The resultant gel was stirred for another hour and then autoclaved at 443 K for 5 days under rotation at 60 rpm. 1.77 g aluminium nitrate and 1.19 g gallium nitrate were used in the synthesis of the corresponding metallosilicates.

ZSM-48

A typical synthesis of [Fe]-ZSM-48 *[5]* consisted of adding 21.22 g TEOS to a solution of 0.54 g ferric nitrate in 30 g water with stirring. This mixture was stirred for 45 min before adding to it a solution of 1.6 g hexamethonium bromide in 20 g water. Finally, a solution comprising of 0.42 g NaOH in 20 g water was added to the above mixture under vigorous stirring. The resulting white gel was further stirred for 1 h and crystallized at 438±2 K under rotation (60 rpm) for 5 days. A similar procedure was adopted for the synthesis of [Al]-ZSM-48 except that aluminium nitrate (0.5 g) was used instead of the ferric nitrate.

EU-1

The ferrisilicate analog of zeolite EU-1 was synthesized according to the reported procedure *[6,7]*. However, a typical synthesis consisted of slowly adding a solution of 43 g sodium silicate in 49 g water to another solution comprising 1.80 g ferric nitrate and 2.5 g H_2SO_4 (96%) in 45 g H_2O. To the above off-white gel, a solution of 7.6 g hexamethonium bromide in 20 g water was added under stirring. The resultant white gel was stirred for 30 min before autoclaving. The crystallization was carried out under agitation (60 rpm) at 433 K for 7 days. The hydrothermal synthesis of the aluminosilicate analog was carried out by replacing ferric nitrate by aluminium nitrate (1.67 g) *[8]*.

Beta

The synthesis of [Fe]-Beta *[9]* was carried out by adding a mixture of 0.62 g sodium hydroxide, 0.46 g potassium hydroxide and 74 g tetraethyl ammonium hydroxide to 24 g fumed silica. The resultant mixture was stirred for 4 h to obtain a clear solution. This silicate solution was added very slowly to a solution of 3.74 g ferric sulfate in 40 g water. The grey colored gel thus obtained was stirred for another 1 h and then crystallized at 413K for 15 days. [Al]- analog *[10]* was also synthesized in the same way by using aluminium sulphate (2.32 g) instead of ferric sulphate.

The as-synthesized zeolites (C/N form) containing organic template were carefully calcined (especially in the case of ferrisilicate molecular sieves). The calcination for the removal of template was carried out at 753 K (heating rate 2 K min^{-1}) first in a flow of dry nitrogen (3 lit h^{-1}) for 8 hours and then in a flow of dry air (6 lit h^{-1}) for additional 8 hours. The sample after calcination contained the alkali cations used in the synthesis at the exchangeable sites and was thus called as Na/K form depending on the alkali cation.

The template-free (Na/K form) samples were subjected to ammonium exchange treatment. 5 g of sample was slurried in 250 ml of 1 M ammonium nitrate solution. The pH of this solution was maintained around 7-8 by adding a few drops of 25% ammonium hydroxide solution. This mixture was stirred at 353 K for 2 h and the procedure was repeated twice to ensure complete exchange. The ammonium form of zeolites (NH_4-form) were then calcined at 753 K (applying the same procedure used to remove organic template, mentioned above) to give the proton form (H-form).

2.2.2 Characterization

2.2.2.1 Ion-exchange capacities

Ion-exchange capacity measurements were performed by treating the H-form of the zeolite (1 g) with 10 g 1M KNO_3 (+ few drops of dilute KOH to maintain the pH at ~ 8) and then stirring for 2 h, washing thoroughly and drying to obtain the K-form of the zeolite. The K-form of the zeolite was analyzed by chemical analysis procedure which gave the ion-exchange capacity (K^+/MO_2^- molar ratio, M = Al, Ga or Fe).

2.2.2.2 Chemical analysis

A known weight of the zeolite sample was taken in a platinum crucible with lid, and ignited for 1 h. The crucible was transferred to a desiccator and cooled. The anhydrous weight of the sample was noted. This residue was dissolved in 15 ml aqueous hydrofluoric acid (40%) after adding a few drops of concentrated sulfuric acid (96%) and evaporated. This procedure was repeated to ensure that all the SiO_2 is evaporated as H_2SiF_6. The remaining sample was again ignited and the weight was taken after cooling in a desiccator. The difference in weight of the residue and the original weight gave the weight of SiO_2 in the sample. The residue was fused with potassium pyrosulphate till a clear liquid was formed. To the solid obtained after cooling 2-3 drops of HCl were added and then dissolved in a known volume of water. This solution was analyzed in an atomic absorption spectrometer (model Hitachi Z-8000) for Fe, Na, Al, Ga, K.

2.2.2.3 Powder X-ray diffraction (PXD)

The samples at each stage during the study were analyzed by PXD for qualitative and quantitative phase identification. The PXD patterns were recorded using a Rigaku D MAX III VC diffractometer using Ni filtered CuKα radiation (λ = 1.5404 Å). The

integrated area of the PXD peaks in the 2 θ range between 18-25° were used to determine the relative crystallinity of the metallosilicate analogs of particular type of the zeolite topology. The samples exhibiting maximum area was taken as a reference sample. Unit cell calculations were made by indexing the peaks with known h,k,l, values and refining them using PDP11 and HOCT softwares.

2.2.2.4 Infrared spectroscopy

The infrared spectra were recorded through a FTIR spectrometer (Perkin Elmer series 1600) in the range of 450-1300 cm^{-1} wavenumbers using nujol mull technique. 20 mg of the sample was taken and powdered and mulled with nujol to form a homogeneous mixture. This was applied on KBr plates before recording the spectrum.

2.2.2.5 ESR spectroscopy

ESR spectra of ferrisilicate samples were recorded (Brüker ER 200D) at 9.7 MHz (X Band) with a rectangular cavity (ST8424). Frequency modulation was carried out at 100 KHz (intensity at 1.25 GPP) and a time constant of 10^3 msec was used. The hf power was chosen small enough to prevent signal saturation. The spectra was scanned both at room temperature and at liquid N_2 temperature. A constant weight (0.1 g) of the sample was used to record the spectra.

2.2.2.6 Magnetic susceptibility

Magnetic susceptibility measurements were made at room temperature using a Faraday balance (Cahn-Ventron, Ceritos, CA, USA). The magnetic moments of the samples were calculated using standard procedures. The formula for the calculation of the magnetic moment of the zeolites, especially for ferrisilicates is derived below *[11]*:

Molecular sieves have large structures for which molecular weights are not a well defined parameter. For ferrisilicate molecular sieves, since only the iron acts as the magnetic center and contributes to the magnetic susceptibility of the material the molar susceptibility can be defined with respect to moles of iron present in the material. Therefore, for ferrisilicates, molar susceptibility was calculated as follows

$$\chi_M = \frac{\text{gram magnetic susceptibility}, \chi_g}{\text{moles of iron in the sample } (M_{Fe})}$$

$$\text{where}, \chi_g = \frac{\text{magnetic susceptibility}}{\text{sample weight, g}}$$

$$M_{Fe} = \frac{Z}{100 \times 55.8}$$

Where, Z is the wt% of iron in the ferrisilicate sample.

$$\chi_M = \frac{\chi_g \times 55.8 \times 100}{Z}$$

The magnetic moment μ can then be given by

$$\mu = 2.83\sqrt{(\chi_M \times T)}$$

where T is temperature in Kelvin

2.2.2.7 Mössbauer spectroscopy

Mössbauer spectra were recorded on an Austin Science Associates Mössbauer spectrometer. The velocity drive was controlled by S-600 spectrometer controller and the data were collected in 1024 channels on a multichannel analyzer (Canberra series 95) in a multiscalar mode (constant acceleration). Spectra were fitted by Lorentzian

curves and the reported isomer shift values are relative to metallic iron. 400-600 mg of the sample was pressed into a wafer for recording the spectra. The spectra were fitted by a least square fitting program.

2.2.2.8 Scanning electron microscopy

The morphology of the zeolite samples used during the study was examined using a Jeol JSM 5200 scanning electron microscope. The sample was dusted on alumina and coated with a thin film of gold to prevent surface charging and to protect the zeolite material from thermal damage by the electron beam. In all the analyses a uniform thickness of about 0.1 mm was maintained.

2.3 RESULTS AND DISCUSSION

2.3.1 Synthesis

The synthesis of metallosilicate (Al-, Ga- or Fe-) analogs of ZSM-11, EU-1, ZSM-48 and Beta was carried out in basic medium under hydrothermal conditions *[1-9]*. The sequence of addition of reactants may not affect the incorporation of Al^{3+} and Ga^{3+} in the framework of zeolites due to the solubility of their oxides in highly alkaline medium. However, in the case of ferrisilicate molecular sieves, formation of insoluble and stable Fe_2O_3 retards the incorporation of Fe^{3+} in the framework of molecular sieves *[12]*. To avoid a basic environment around Fe^{3+} before the formation of ferrisilicate gel, the basic sodium silicate was added slowly to the acidic ferric salt solution *[13]*. This way of addition facilitates the initial formation of white/yellow colored ferrisilicate gel. Once the ferrisilicate gel is formed, the desired template is added followed by the addition of alkali (if any). Alternatively, when TEOS is used as the silica source, the ester is hydrolysed with the acidic ferric nitrate to form a

ferrisilicate (as in the case of ZSM-11 and ZSM-48). The basic template is then added very slowly to obtain a ferrisilicate gel *[12,13]*. The molar gel composition and other gel parameters are given in Table 2.2.

2.3.2 Characterization

All the catalysts (H-form) were potassium exchanged and analyzed using atomic absorption spectrometry. The chemical analysis provided, the final Si/M (M= Al, Ga or Fe) molar ratios (Table 2.3) as well as the molar ion-exchange capacities (K^+/MO_2^-). The tetrahedrally coordinated M^{3+} ions in the framework positions give rise to ion-exchange sites and generate equivalent Brönsted acid sites in the H-form of zeolite *[9,14]*. The high value of ion-exchange of metallosilicates (Table 2.3) indicate that most of the metal ions were present in the lattice. The white/off-white color of the sample in the case of ferrisilicate analogs further suggest the absence of condensed iron oxide phase. The latter imparts a brown color to the sample, when present.

The powder X-ray diffraction patterns of (Fig. 2.2-2.5) of all the metallosilicates were similar to those of the zeolite analogs reported in the literature *[1,4,7,15-18]*. The PXD patterns of these molecular sieves show the absence of any other crystalline impurity phase.

The adsorption capacities (at p/p_o 0.5 and T = 298K) of metallosilicate molecular sieves for n-hexane and cylcohexane are given in Table 2.3. The metallosilicates exhibit adsorption capacities comparable to those reported in the literature *[19,20]* indicating the absence of any appreciable amount of amorphous material in our samples.

The crystals of Al, Ga and Fe silicate analogs of ZSM-11 possessed oval or spindle like morphology. The average crystal sizes were between 0.5-1.2μm range (Table 2.3) *[20]*. The crystals of EU-1 Zeolite were ball shaped having an average

Table 2.2 : Molar gel composition and synthesis parameters of different metallosilicate molecular sieves.

Zeolite	Si/M	Si/Na	Si/R[1]	OH/Si	H_2O/Si	Gel pH	Yield[2] %
Al-ZSM-11	46.0	0.0	4.5	0.15	31.0	11.95	85
Ga-ZSM-11	45.8	0.0	4.5	0.15	31.0	11.80	73
Fe-ZSM-11	46.5	0.0	4.5	0.15	31.0	11.93	77
Al-EU-1	44.7	1.6	10.0	0.29	39.4	12.38	69
Fe-EU-1	44.7	1.6	10.0	0.29	39.4	12.23	67
Al-ZSM-48	76.5	9.7	24.0	0.06	38.0	12.16	93
Fe-ZSM-48	76.5	9.7	24.0	0.06	38.0	11.90	89
Al-Beta	31.7	17.7	2.0	0.22	20.0	12.52	61
Fe-Beta	26.0	17.7	2.0	0.22	20.0	12.15	65

[1]R is the template used as given in the synthesis procedure

[2]Yield of the solid crystalline product

TABLE 2.3 : Physico-chemical properties of different metallosilicates

Zeolite	Si/M	K^+/MO_2^-	average crystal size, μm	Magnetic moment μ,BM	Adsorption[a]	
					n-Hx	c-Hx
Al-ZSM-11	37	0.90	0.6	-	11.4	5.9
Ga-ZSM-11	39	0.86	0.9	-	11.0	5.6
Fe-ZSM-11	40	0.84	1.1	5.6	11.3	5.2
Fe-ZSM-11 (silylated)[b]	nd	nd	nd	nd	10.8	4.9
Al-EU-1	35	0.86	2.5	-	8.0	5.0
Fe-EU-1	37	0.76	2.0	5.8	11.1	5.7
Al-ZSM-48	64	0.90	2.5	-	6.8	4.5
Fe-ZSM-48	69	0.86	3.0	5.4	7.8	4.0
Al-Beta	21	0.89	0.4	-	16.5	19.2
Fe-Beta	26	0.85	0.7	5.8	16.7	19.2

[a] : At T = 298 K; P/P_o = 0.5 (Cahn balance); n-Hx = n-hexane; c-Hx = cyclohexane

[b] : 2.5 wt% silylated H-Fe-ZSM-11, silylation was carried out using TEOS.

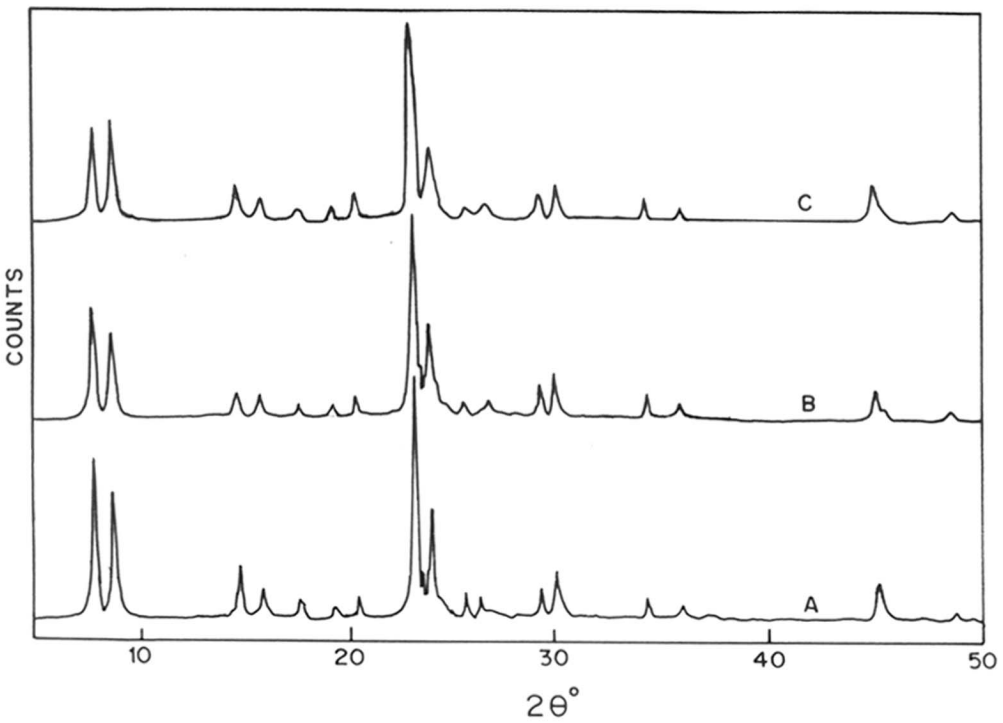

Fig. 2.2 Powder X-ray diffraction patterns of metallosilicates of ZSM-11 A:H-[Al]-ZSM-11; B: H-[Ga]-ZSM-11; C: H-[Fe]-ZSM-11.

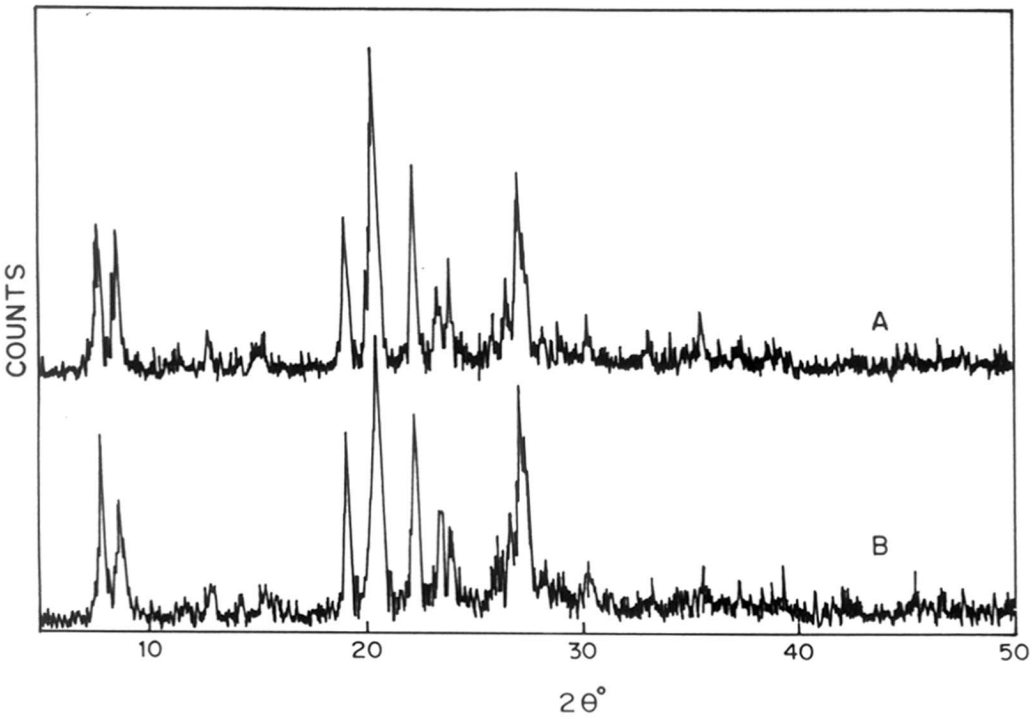

Fig. 2.3 Powder X-ray diffraction patterns of metallosilicates of EU-1
A:H-[Al]-EU-1; B: H-[Fe]-EU-1.

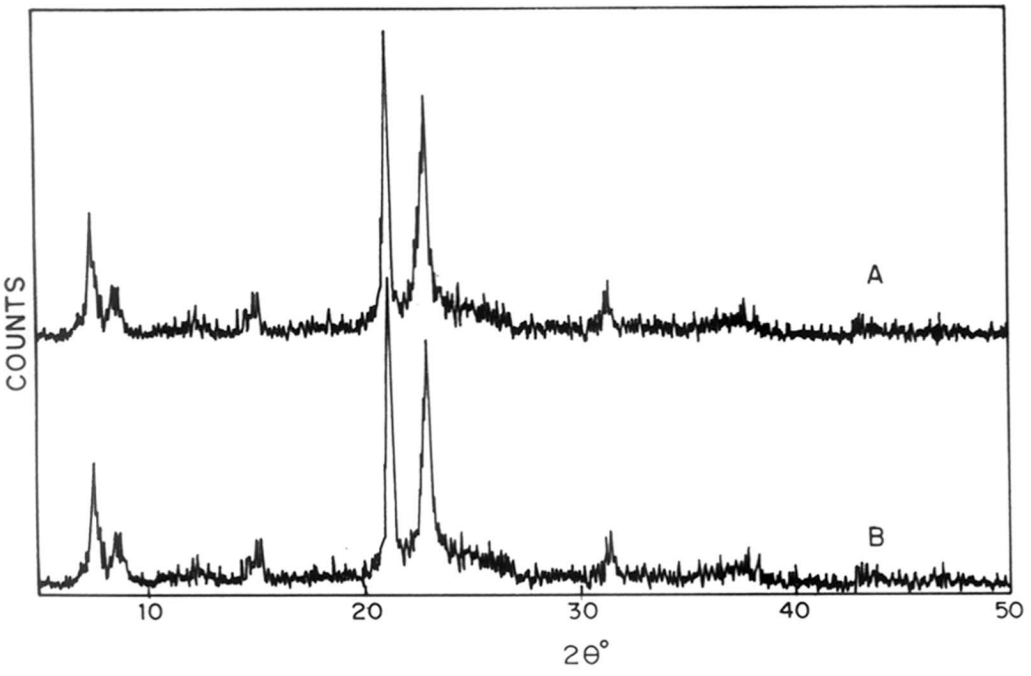

Fig. 2.4 Powder X-ray diffraction patterns of metallosilicates of ZSM-48. A:H-[Al]-ZSM-48; B: H-[Fe]-ZSM-48.

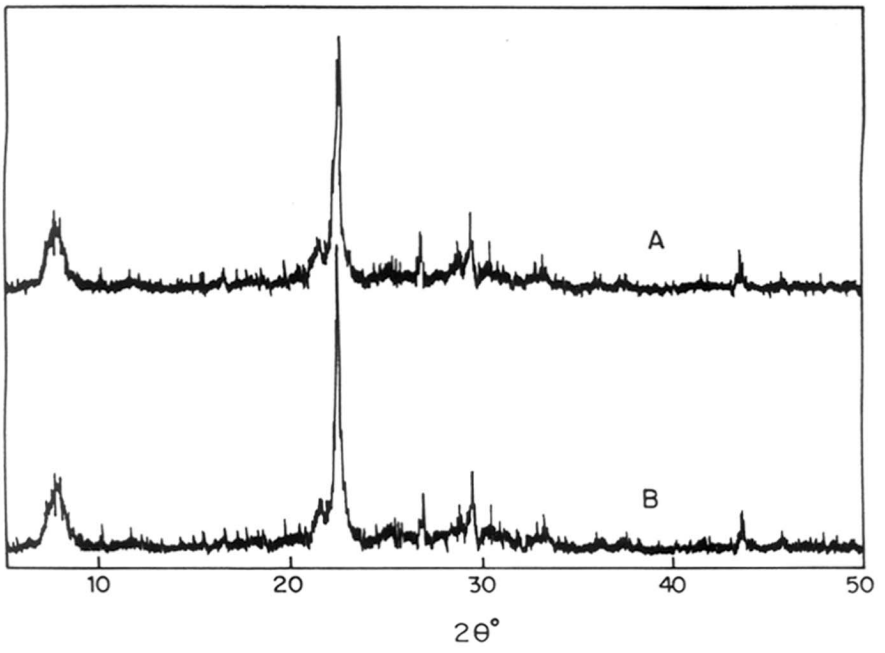

Fig. 2.5 Powder X-ray diffraction patterns of Beta
A: H-[Al]-Beta; B: H-[Fe]-Beta.

crystal sizes of 1.5 and 2.5 μm for Al-and Fe- analogs, respectively *[8]*. Needle shaped crystals were observed for ZSM-48 analogs with average crystal sizes 2.5 (Al) and 3.0 (Fe) *[17]*. Zeolite Beta (Al- and Fe-) exhibited cuboid crystallites of 0.5-0.8 μm.

The magnetic moments of the H-form of the zeolites at 297 K are given in Table 2.3. If the ferric ions are well dispersed in a diamagnetic matrix, they are expected to have a magnetic moment (spin only value) of 5.9 BM. The presence of condensed iron oxide phases increases the magnetic moment to > 6.0 BM. The values obtained in here for ferrisilicates are in the range of 5.6-5.9 BM indicating the absence of condensed iron oxide phases and magnetic clusters.

The ESR spectra of the H-form of the ferrisilicate analogs of ZSM-11 (Fig 2.6), EU-1 (Fig 2.7) and ZSM-48 (Fig 2.9) and Beta (Fig 2.10) are characteristic of iron in the framework of zeolites. The variation of spectra with temperature is also compared in the respective figures.

^{57}Fe Mössbauer spectrum of Fe-ZSM-11 and Fe-EU-1 are presented in Fig.2.10 (detailed Mössbauer studies of Fe-Beta will be presented in Chapter 5). They show a broad lorentzian line with large line widths Γ = 1.5 to 1.7 mm/sec. The somewhat broad linewidths indicate that iron ions are distributed in sites having only slightly different chemical environments. The isomer shifts δ for ZSM-11 and EU-1 were 0.25 and 0.27 mm/sec, respectively and QS = 0 mm/sec (see Table 2.4) are indicative of tetrahedrally coordinated Fe^{3+} species *[1,7,12]*.

The temperature dependent ESR spectra of various zeolites (Fig 2.8 through 2.11) show that on decreasing the temperature of the materials to 77K, the intensity of the peak at 4.3 (vis-á-vis at g = 2.0) increased considerably indicating the presence of Fe(III) as a matrix element intimately associated with the molecular sieve structure, as expected for Fe(III) in the tetrahedral framework sites. Similar, results were obtained by Ball *et al. [21]* on ferrisilicate ZSM-5.

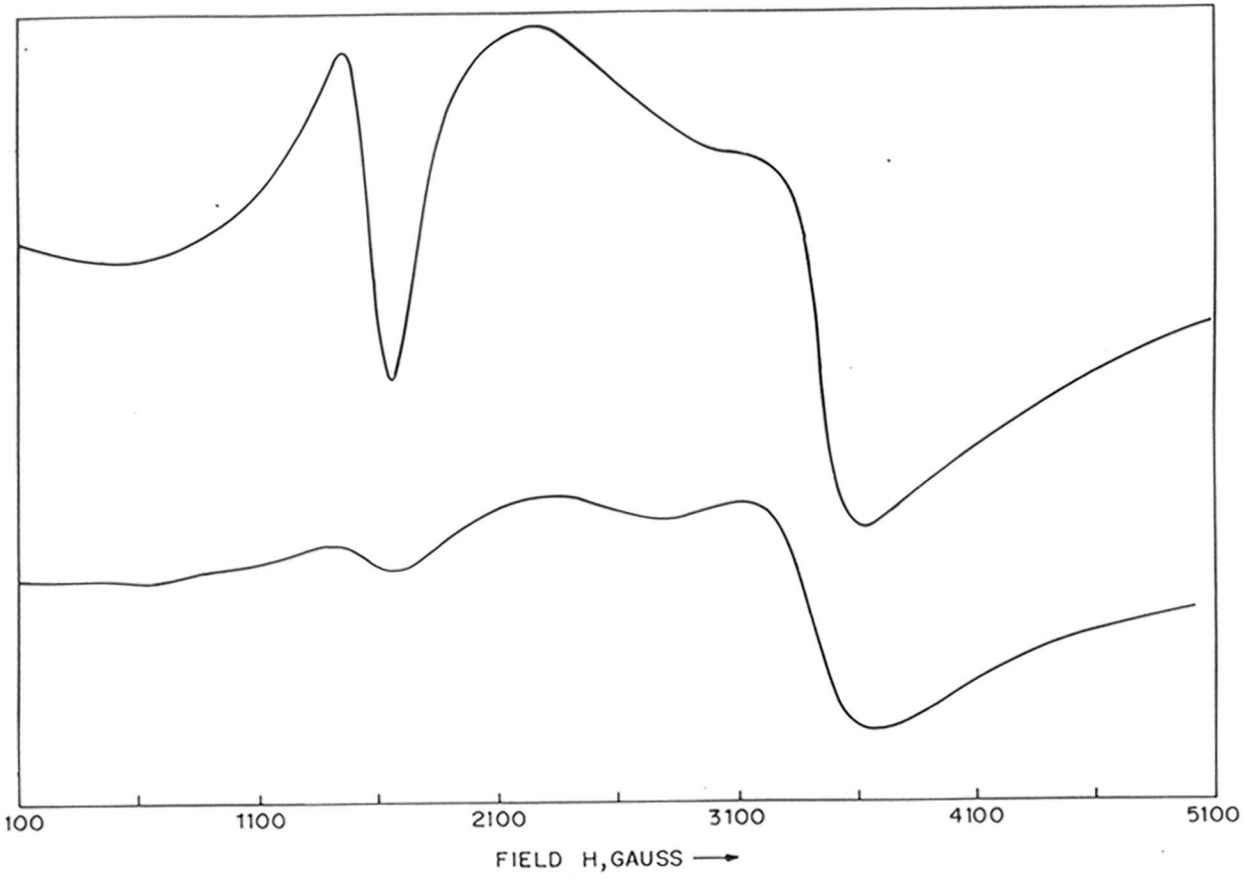

Fig. 2.6 Electron spin resonance spectrum of sample Fe-ZSM-11 A: 297 K B: 97 K.

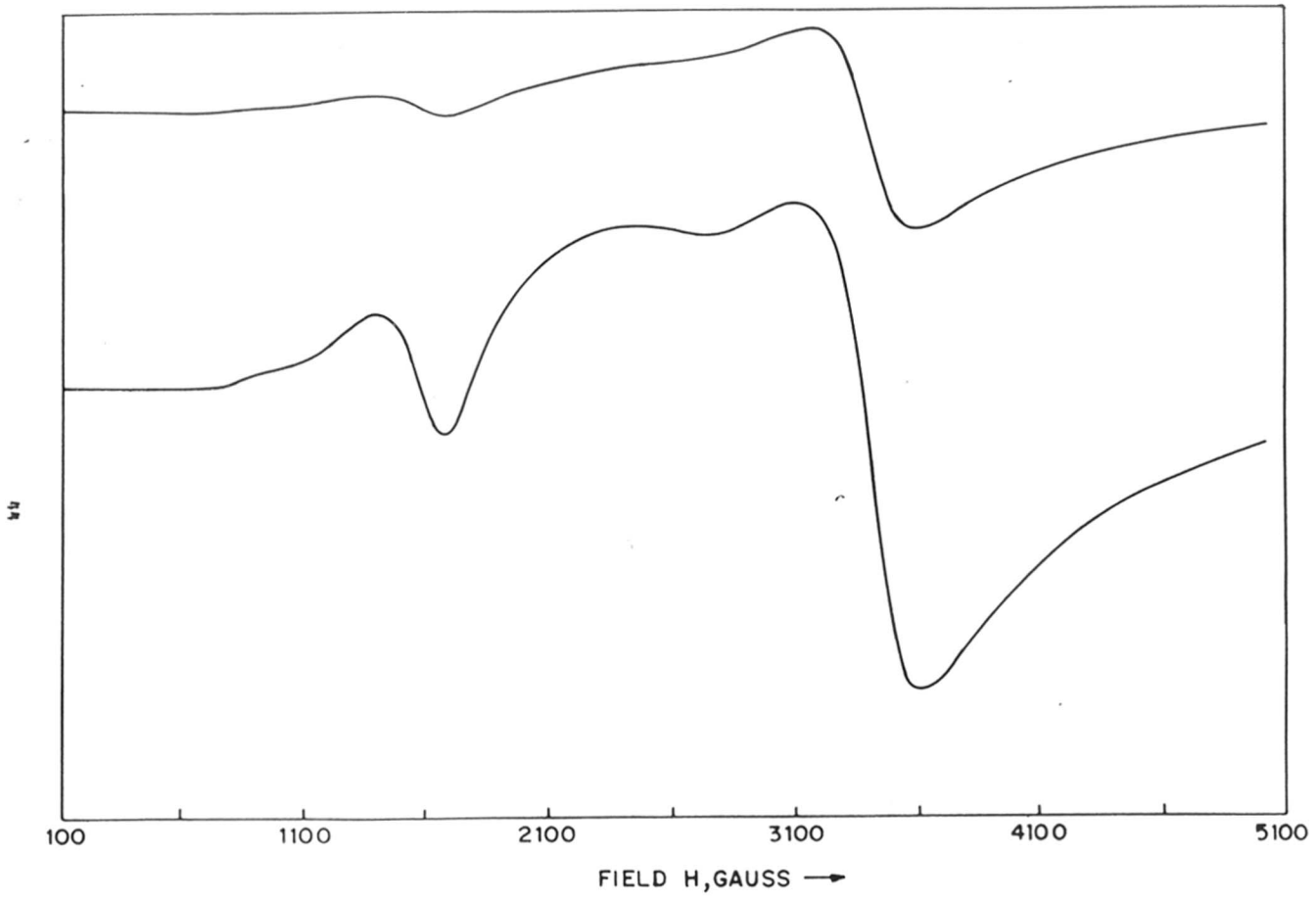

Fig. 2.7 Electron spin resonance spectrum of sample Fe-EU-1 A: 297 K B: 97 K.

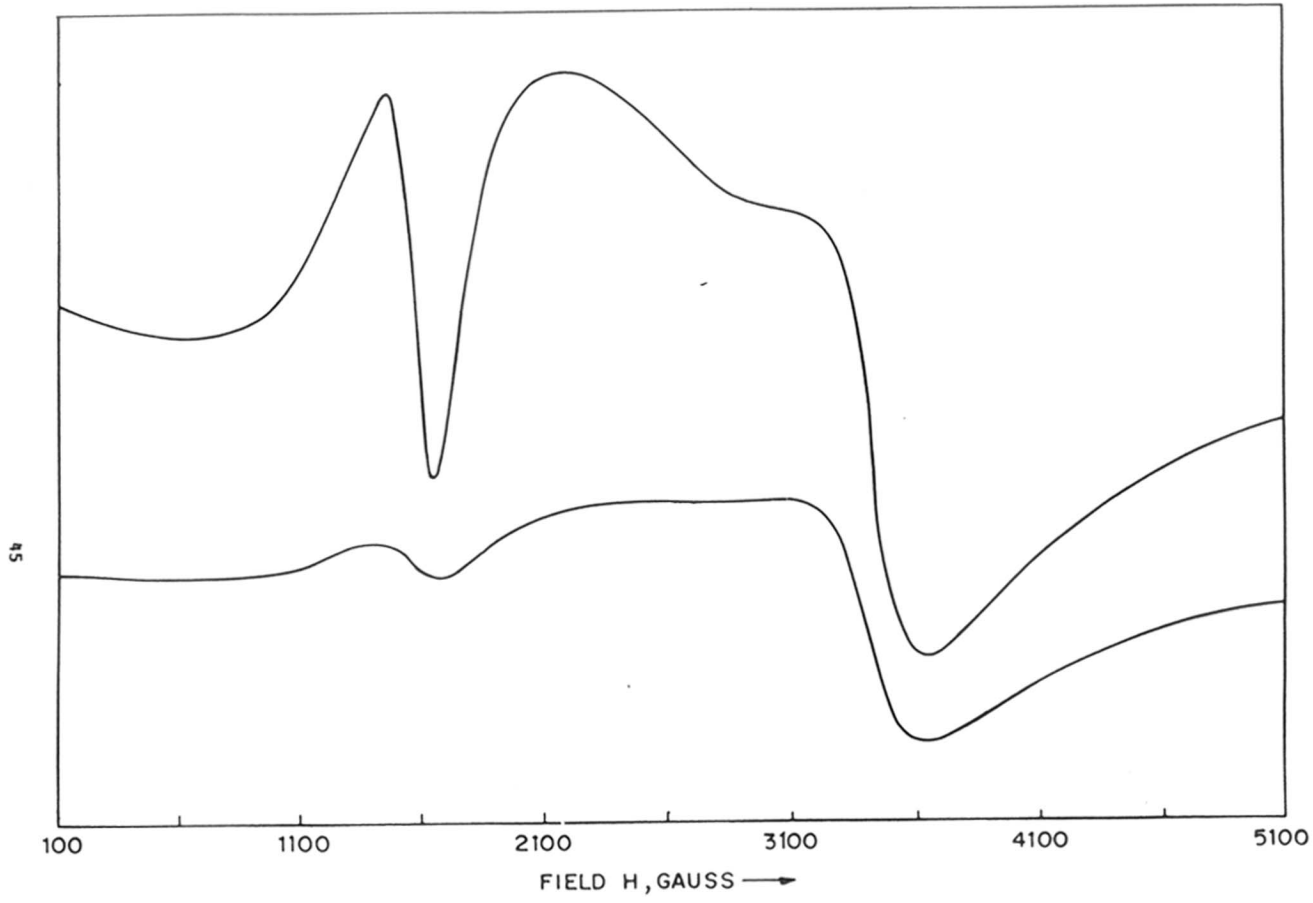

Fig. 2.8 Electron spin resonance spectrum of sample Fe-ZSM-48 A: 297 K B: 97 K.

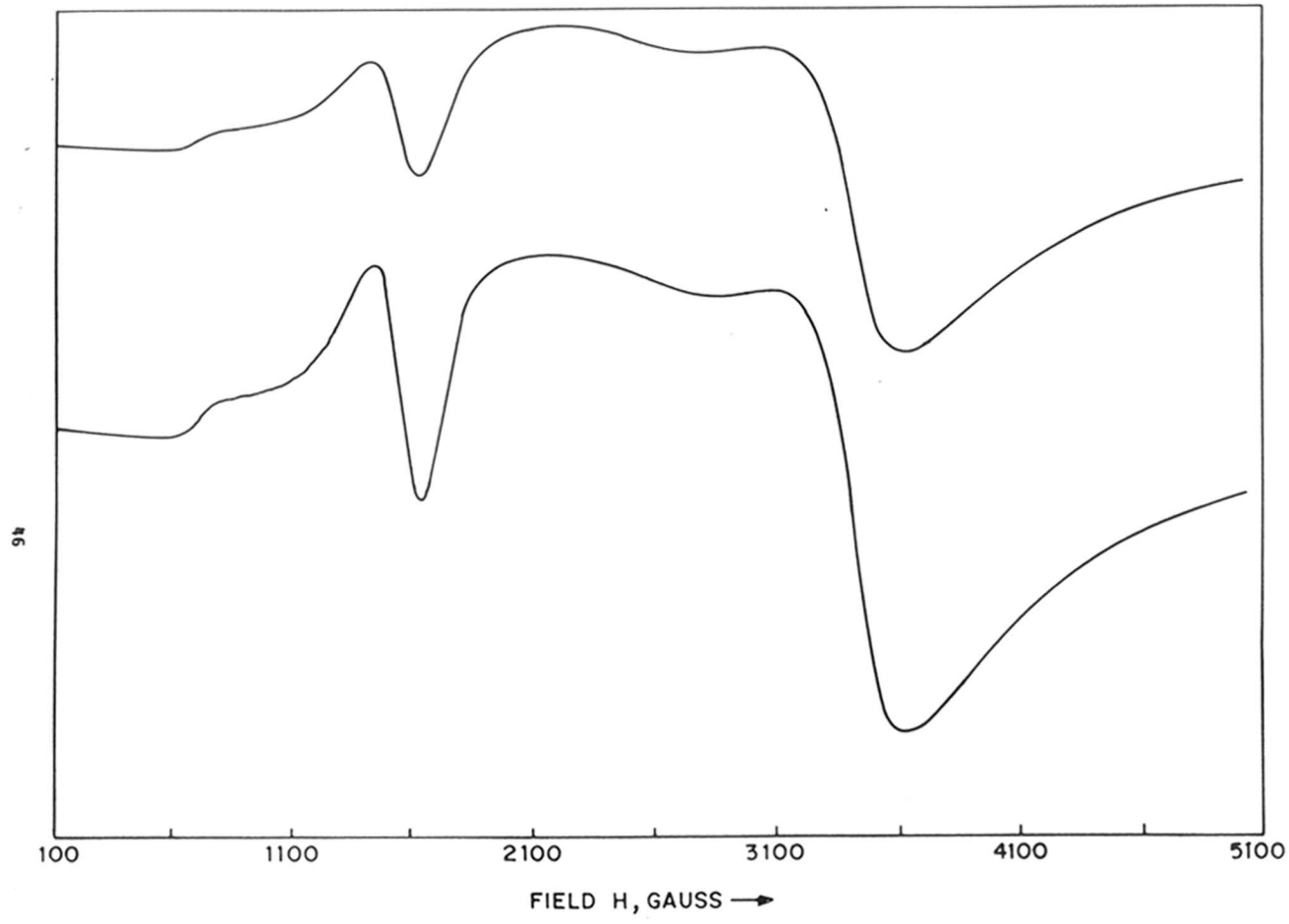

Fig. 2.9 Electron spin resonance spectrum of sample Fe-Beta A: 297 K B: 97 K.

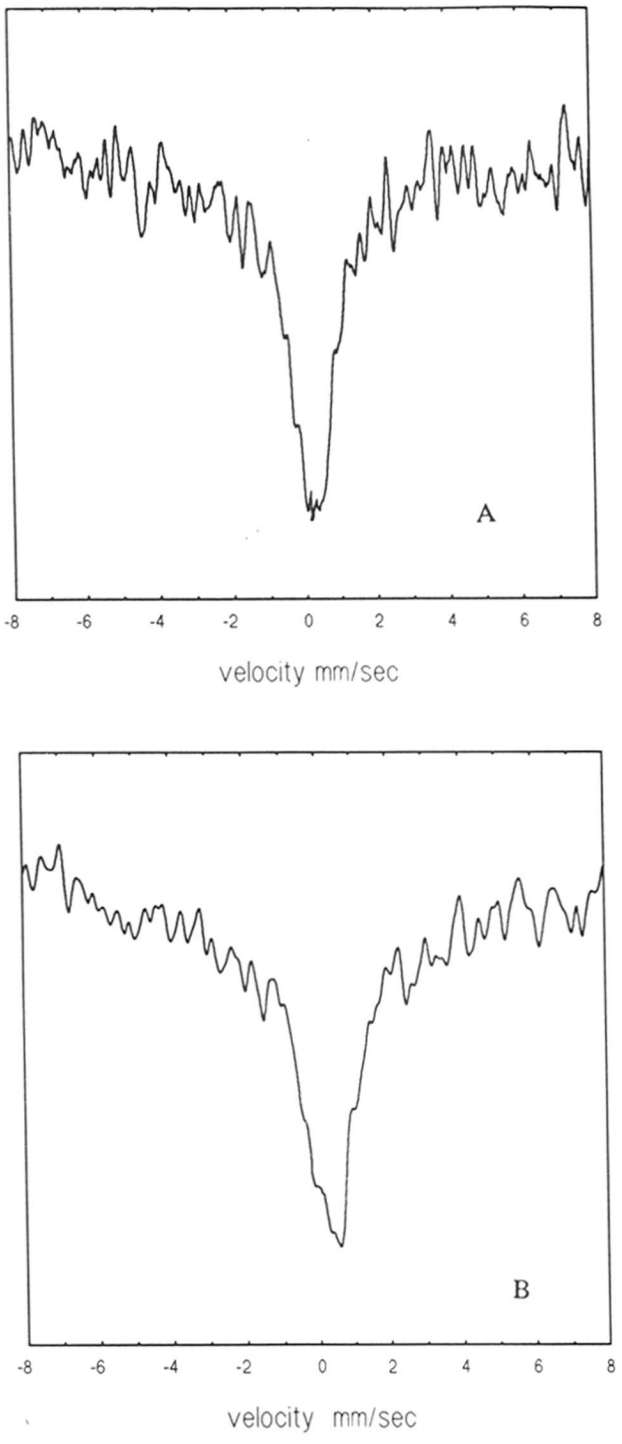

Fig. 2.10 Mossbauer of spectra of Fe-ZSM-11 (A) and Fe-EU-1 (B) samples.

Table 2.4 : Fitting Parameters for Mössbauer spectra

Sample	Coordination State	Mössbauer parameters		Relative Intensity (%)
		IS	QS	
H-Fe-ZSM-11	Td	0.25	0	85
	Oh	0.29	0.85	15
H-Fe-EU-1	Td	0.27	0	75
	Oh	0.32	0.90	25
H-Fe-ZSM-48	Td	0.21	0	100

For Mössbauer parameters of Fe-Beta see chapter 5, Table 5.1.

^{27}Ai MAS NMR spectrum of Al-analog of zeolites, ZSM-11, EU-1, ZSM-48 and Beta displayed a single line at δ = 52.55 ppm with reference to aluminium nitrate solution (δ = 0 ppm). The presence of a peak atδ = 50-56 ppm is attributed to tetrahedral Al^{3+} ions in zeolitic framework *[22]*. The presence of gallium in framework was indicated by a peak at δ = 150 ppm with reference to $Ga(NO_3)_3$ solution (δ = 0) by ^{71}Ga MAS NMR spectra. However, peak for octahedral extraframework species was not observed in Ga- analogs.

2.4 REFERENCES

1. J.S. Reddy, K.R. Reddy and R. Kumar, Zeolites, **11**, 553 (1991).

2. Anuj Raj, J.S. Reddy and R. Kumar, *Proc. 9th Intl. Zeolite Conf.*, Montreal, 1991, Butterworth-Heinmann, USA 1993, p.551.

3. Anuj Raj, K.R. Reddy, J.S. Reddy and R. Kumar, *Stud. Surf. Sci. Catal.* **75B**, 1715 (1993).

4. J.S. Reddy, K.R. Reddy and R. Kumar, *Proc. 10th National Symp. Catal. and 4th INDO-SOVIET Seminar Catal.*, Narosa Publishing house, New Delhi,1991, p.575.

5. K.R. Reddy, Anuj Raj and R. Kumar, Appl. Catal. (submitted).

6. A. Thangaraj and R. Kumar, in *Recent Research Reports, 8th Intl. Zeolite Conf.*, Amsterdam, 1989, p. 53

7. R. Kumar, Anuj Raj, S.K. Date, E. Bill and A. Trautwein, *Appl. Catal.* (submitted)

8. G.N. Rao, P.N. Joshi, A.N. Kotasthane and P.Ratnasamy, *Zeolites* **9**, 483 (1989).

9. Anuj Raj, K. Lázár and S. Sivasanker, *J. Catal.* (1993). (Accepted)

10. M.A. Camblor and J. Péréz Parienté, *Zeolites* **11**, 202 (1991).

11. V. Nair, *Ph.D Thesis*, Georgia Institute of Technology, USA, p.143.

12. P. Ratnasamy and R. Kumar, *Catal. Today* **9**, 341 (1991).

13. R. Szostak and T.L. Thomas, *J. Catal.* **100**, 555 (1984).

14. R. Szostak, V. Nair and T.L. Thomas, *J. Chem. Soc. Perkin Trans. I* **83**, 487 (1987).

15. P.A. Jacobs and J.A. Martens, *Stud. Surf. Sci. Catal.* **33**, 177 (1987).

16. J.L. Casci, T.V. Whittam and B.M. Lowe, *Proc. 6th Intl. Zeolite Conf.*, Reno 1983, Butterworths, London, 1984, p.894.

17. J.L. Schlenker, W.J. Rohrbaugh, P. Chu, E.W. Valyocsik and G.T. Kokotailo, *Zeolites*, **5**, 355 (1985).

18. J.M. Newsam, M.M.J. Treacy, W.T. Koetsier and C.B. De Gruyter, *Proc. R. Soc. London*, **A420**, 375, (1988).

19. G.N. Rao, P.N. Joshi, A.N. Kotasthane and V.P. Shiralkar, *J. Phys. Chem.* **94**, 8589 (1990)

20. J.S. Reddy, *Ph. D. Thesis*, University of Poona, Pune, India, 1990 p.130.

21. W.J. Ball, J. Dwyer, A.A. Garforth and W.J. Smith, *Stud. Surf. Sci. Catal.* **28**, 137 (1986).

22. J. Klinowski, *"Progress NMR Spectroscopy"* **16**, 237 (1984).

Chapter 3

CATALYTIC REACTIONS

3.1 INTRODUCTION

The modification of chemical properties of zeolites through framework isomorphous substitution of Al^{3+} by Fe^{3+} *[1-4]*, a transition metal ion, is a significant development in the domain of molecular sieves. Although, the details of the synthesis and characterization of ferrisilicate analogs of a number of medium and large pore zeolites have been well documented *[3,4]*, the information about their catalytic properties, particularly in shape selective aromatic hydrocarbon reactions, is not so well documented. Recently, the detailed catalytic properties of [M]-ZSM-5 (M = Al or Fe) *[5]* and [M]-ZSM-11 (M = Al, Ga or Fe) *[6,7]* in C_7-C_9 aromatic reactions were reported.

In this chapter, following reactions will be discussed. They are namely :

Methylation of toluene

Isomerization of m-xylene,

Methylation of *m*-xylene

Chlorination of toluene

Three medium pore zeolites viz. ZSM-11, EU-1 and ZSM-48 and their Al-, Fe- and/or Ga- analogs were used as catalyst to illustrate the effect of isomorphous substitution on their shape selective properties. These zeolites were selected on the basis of their unique structural features. ZSM-11 has a three dimensional 10-membered ring with intersecting channels *[8]*, EU-1 has unidimensional non-intersecting 10-membered ring channels with large, deep side pockets *[9]*, while, ZSM-48 consists of non-intersecting, unidimensional 10 membered ring pores *[10]*. Hence, the present study is also expected to show the effect, if any, of chemical modification by framework

incorporation of Fe instead of Al, on the shape selectivity. It also compares how shape selectivity varies among the structures, particularly among medium pore zeolites mentioned above.

The alkylation of toluene to give xylene isomers, especially *p*-xylene, in high yields has been studied in detail by many workers over Al-zeolites *[11-24]*. High paraselectivities have been reported for the formation of xylene isomers over Mg [11-17], P *[11-14,16,17]* or B *[12,16,17]* oxides incorporated in ZSM-5 zeolites. Whereas, Kaeding *et al.* have proposed a diffusion limited mechanism for *p*-xylene selectivity *[11]*. Paparatto *et al.* have assigned it to blocking of the external non-selective sites which further isomerize *p*-xylene *[25a]*. Kim *et al. [25]* have proposed that the higher alkylation activity is due to the suppression of isomerization activity over these (modified) catalysts. Young *et al.* observed that the rate of alkylation (K_a) was about three times the rate of isomerization of *p*-xylene and 7-15 times the rate of isomerization (K_i) of *m*-and *o*- xylene *[14]*. Modification of zeolites by doping external surface alters both pore size as well as chemical properties *[16]*.

m-xylene isomerization apart from being an industrial process for *p*-xylene is also a test reaction for zeolites *[26-27]*. It is used to characterize the site density, acid strength, size and shape of the channels through relative rates of isomerization and transalkylation reactions, *p/o* xylene ratio and the distribution among trimethylbenzene isomers *[28]*. Isomerization of *m*-xylene was carried out over metallosilicates of ZSM-11, EU-1 and ZSM-48.

Very little is reported about the selective methylation of xylene isomers to 1,2,4 trimethylbenzene (1,2,4 TMB). Namba *et al. [29]* have reported very high selectivity (>99%) for the 1,2,4 isomer in the TMB fraction during methylation of individual xylene isomers over H-ZSM-5 zeolite. Desimone *[30]* has claimed that a crystalline borosilicate molecular sieve impregnated with Mg, produced as high as 92% yield of

TMBs in the aromatic fraction. The selectivity for the smallest 1,2,4 isomer was ~ 97 %, far more than the equilibrium value (63 % at 300K). The 1,2,4 TMB, commonly known as pseudocumene, is an important raw material for the production of trimellitic acid/anhydride which is used in the manufacture of plasticisers, polyesterimides, epoxyresins, high temperature resistant polyimides, 2,3,5 trimethylaniline etc. *[31]*. Though the high selectivity for 1,2,4 TMB has been attributed *[29]* to the shape selective properties of ZSM-5, the yield of TMBs may depend upon the chemical properties (e.g. strength of acid sites) of the catalyst. The reaction (methylation of xylene) was studied over isomorphously substituted analogs (Al-, Ga- and Fe-) of ZSM-11 reaction.

The catalytic halogenation of aromatic compounds with chlorine gas over Lewis acid catalysts, such as $AlCl_3$, $FeCl_3$ or $SbCl_5$, generally produces lower p/o ratio in the product. However, the stochiometric reaction between metal halides and aromatic compounds give higher paraselectivity for chlorinated compounds *[32-44]*. Though the chlorination of toluene over Lewis acid catalysts in the presence of sulfur compounds has also been reported to result in a para-regioselectivity, these methods tend to give lower yields and also lead to di and tri substitution *[43-45]*.

Relatively little attention has been paid to the use of zeolites in the field of aromatic halogenation *[46-56]*. The zeolite catalysts shift the isomer ratio significantly towards para substitution. The chlorination of toluene over metallosilicates of ZSM-11, EU-1, ZSM-48 and Beta will be discussed in the present study.

3.2 EXPERIMENTAL

Syntheses of zeolites and isomorphous substitution in Beta, ZSM-11 and EU-1 and their conversion to H^+ form and K^+ form has been described in detail in chapter 2. The characterization of these zeolites is presented in chapter 2 section 2.2.2.

An on-line reaction analysis set up was used to carry out catalytic studies (Fig. 3.1) on alkylation (toluene and xylenes) and isomerization (of *m*-xylene). It consisted of a quartz reactor of 10 mm inner diameter and 300 mm length with a provision for feeding reactants and carrier gas at the top. A thermowell extended upto the catalyst bed. The catalyst powder was pressed, pelleted and sieved to obtain catalyst particles of ca. 0.3-0.4 mm. The required amount of catalyst was loaded. The catalyst was diluted with inert material (crushed porcelian beads, 40-50 mesh) to a volume of 2 ml. This catalyst was charged in the center of the reactor in such a way that the catalyst bed was sandwiched by inert porcelian beads. The upper portion of the reactor served as a vaporizer-cum-preheater. The reactor was placed in a two zone furnace (Fig. 3.1). The catalyst was activated in a stream of dry air at 723K for 8 h before starting the reaction. The catalyst was flushed with dry nitrogen and cooled to reaction temperature. The reactants were passed at the required rate through preheater to the catalyst bed. The liquid reactant was fed by a syringe pump (SAGE-Instruments, model 352). The flow rate of gaseous reactants were controlled by needle valves and monitored by calibrated flow meter. A Shimadzu gas chromatrograph (GC) with six port heated gas sampling valve was used. At fixed intervals the samples were injected into the GC (Shimadzu R1A with flame ionization detector) through a valve (6 port) for on-line analysis. A two meter long stainless steel column packed with 5% bentone 34 + 10% diisodecyl phthalate on chromorsorb (60-80 mesh) was used for product analysis. The output values gave directly the product distribution in weight percent. The weight of the catalyst used was : 0.35 g, 0.45 g and 1.0 g (on anhydrous basis) for Al-, Ga-, and Fe-ZSM-11 analogs of various zeolites, respectively unless stated otherwise.

The chlorination reactions were carried out in a three necked flask (capacity, 150 ml) fitted with a condenser, gas supply tube and a septum. The temperature of the reaction was maintained using an oil bath. In the reaction flask 0.32 mol toluene and

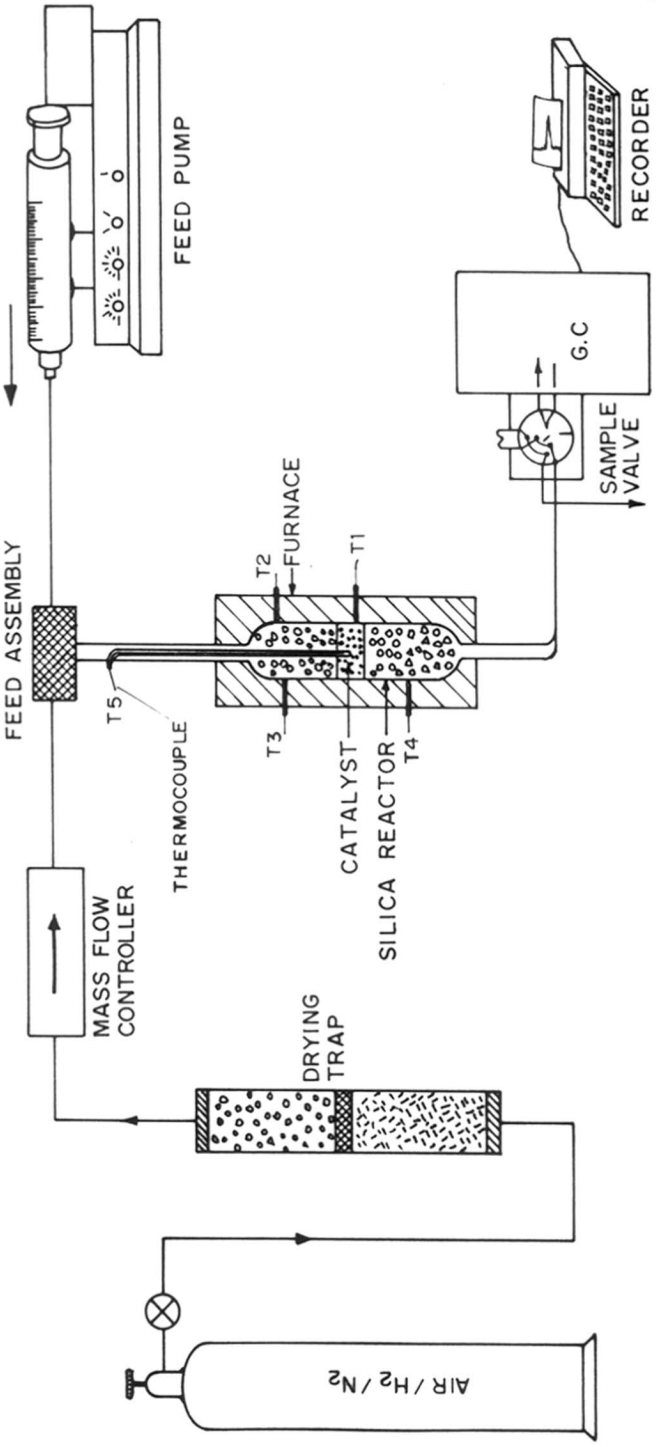

Fig. 3.1 Fixed bed down flow on-line reactor used in this study.

1.63 g catalyst (activated at 438K for 2h) were introduced. The reaction mixture was stirred and heated to attain the reaction temperature (353K) in the presence of purified nitrogen gas. The nitrogen gas was disconnected and chlorine gas was bubbled into the solution at a rate of 0.08 moles h^{-1}. The chlorination was followed by taking samples of reaction mixture at suitable intervals. The analyses of the reaction mixture was done using a gas chromatograph (HP 5890 series II) having a flame ionization detector and 50 X 0.2 mm capillary column with methyl silicone gum. GC/MS and authentic samples were used for product identification.

3.3 RESULTS AND DISCUSSION

3.3.1 Methylation of Toluene

In Fig. 3.2 the amount of toluene passed per gram of the catalyst are plotted against toluene conversion. The resistance towards deactivation followed the order : Fe > Ga > Al. The strength of acid sites of these zeolites follows the reverse order *[25,57]*. As the strength of the acid site increases the products are strongly adsorbed at the site and get converted further to heavier products, which eventually form coke.

Tables 3.1 to 3.3 show the influence of temperature on Al-, Ga- and Fe- silicate analogs of ZSM-11. It can be observed that on increasing the reaction temperature, the conversion of toluene increased with the decrease in selectivity for xylene isomers in aromatic products (S_{xyl}) accompanied with an increase in the selectivity for trimethylbenzenes (S_{TMB}), a secondary product. The distribution of xylene isomers also varied with increase in the reaction temperature and conversion.

In Fig. 3.3, the distribution of xylene isomers and S_{xyl} for Al-, Ga- and Fe- analogs of ZSM-11 is plotted as a function of toluene conversion. S_{xyl} decreases with an increase in the reaction temperature and toluene conversion as expected. The selectivity for total xylene isomers among aromatic products (S_{xyl}) followed the order: Fe > Ga

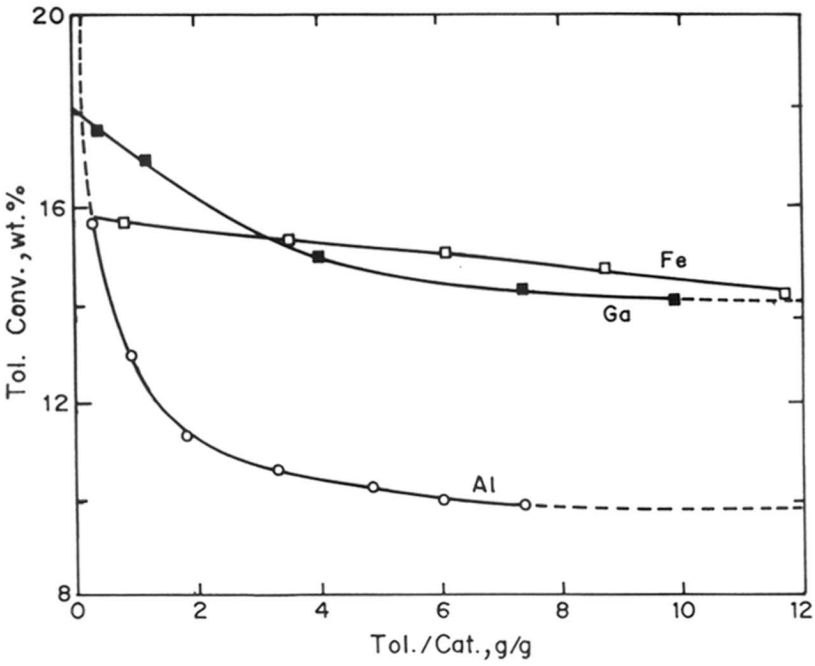

Fig. 3.2 A plot of toluene passed per gram of the catalyst versus toluene conversion over H-[M]-ZSM-11 (M = Al, Ga or Fe).

Table 3.1 Effect of temperature in the methylation of toluene with methanol over H-[Al]-ZSM-11.

Feed : toluene + CH_3OH, 4 : 1 mole; N_2/oil (molar ratio) : 4; feed rate : 4mlh^{-1}; time-on-stream : 20 min

Temperature, K	493	513	533	553	573
Conversion, (wt%)					
Methanol	90	100	100	100	100
Toluene	5.5	9.1	13.0	16.0	18.5
Products, (wt%)					
Methanol	0.1	-	-	-	-
Aliphatics	0.8	1.0	0.7	0.8	0.8
toluene	94.5	90.1	87.0	84.0	81.5
p-xylene	1.2	1.9	2.3	2.5	2.6
m-xylene	1.0	1.8	4.2	5.3	5.8
o-xylene	1.7	2.7	2.7	2.7	2.7
TMBs	0.6	1.2	1.8	2.7	3.7
others[a]	0.1	1.0	1.3	2.0	2.9
$S_{xyl.}$ %[b]	84.8	74.4	74.8	67.9	62.7
S_{TMBs} %[c]	13.0	13.9	14.6	17.5	20.9
Xylene distribution, %					
para	30.8	29.7	25.0	23.8	23.4
meta	43.6	42.2	29.4	25.7	24.3
ortho	43.6	42.2	29.4	25.7	24.3

a: others include benzene, ethylbenzene, ethyltoluenes, Tetramethylbenzenes

b: $S_{xyl.}$,% =(∑xylenes/∑aromatics)X100

c: S_{TMBs}% = (∑TMB/∑aromatics) X 100

Table 3.2 Effect of temperature in the methylation of toluene with methanol over H-[Ga]-ZSM-11.

Feed : toluene + CH_3OH, 4 : 1 mole; N_2/oil (molar ratio) : 4; feed rate 4mlh^{-1}; time-on-stream : 20 min

Temperature, K	493	513	533	553	573
Conversion, (wt%)					
Methanol	80	100	100	100	100
toluene	6.0	11.4	14.1	16.8	19.5
Products, (wt%)					
Methanol	0.2	-	-	-	-
Aliphatics	0.8	0.6	0.7	0.7	0.9
toluene	94.0	88.6	85.9	83.2	81.0
p-xylene	1.5	3.0	3.1	3.0	2.9
m-xylene	1.0	2.2	3.7	5.4	6.4
o-xylene	1.8	3.5	3.3	3.5	3.0
TMBs	0.5	1.5	2.0	2.8	3.8
others[a]	0.2	0.6	1.3	1.8	2.5
$S_{xyl.}$, %[b]	86.0	80.6	75.4	72.1	66.1
S_{TMBs}, %[c]	10.0	13.9	14.9	17.0	20.4
Xylene distribution, %					
para	34.9	34.5	30.7	25.2	23.6
meta	23.2	25.3	36.6	45.4	52.0
ortho	41.9	40.2	32.7	29.4	24.4

[a-c]: see foonotes to Table 3.1

Table 3.3 Effect of temperature in the methylation of toluene with methanol over H-[Fe]-ZSM-11.

Feed : toluene + CH_3OH, 4 : 1 mole; N_2/oil (molar ratio) : 4; feed rate : 4mlh^{-1}; time-on-stream : 20 min

Temperature, K	493	513	533	553	573
Conversion, (wt%)					
Methanol	60	80	100	100	100
toluene	3.4	8.2	12.3	16.0	19.0
Products, (wt%)					
Methanol	0.3	0.2	-	-	-
Aliphatics	0.3	0.5	0.4	0.4	0.5
toluene	96.6	91.8	87.7	84.0	81.0
p-xylene	0.9	2.3	3.2	3.6	3.7
m-xylene	0.5	1.7	2.7	4.7	6.1
o-xylene	1.2	2.9	4.1	4.3	4.4
TMBs	0.1	0.5	1.3	1.9	2.5
others[a]	0.1	0.2	0.6	1.1	1.8
$S_{xyl.}$, %[b]	92.8	90.8	84.3	80.8	76.7
S_{TMBs}, %[c]	3.6	6.6	10.7	12.2	13.5
Xylene distribution, %					
para	34.6	33.3	32.0	28.6	26.0
meta	19.2	24.6	27.0	37.3	43.0
ortho	46.2	42/0	41.0	34.1	31.0

[a-c]: see foonotes to Table 3.1

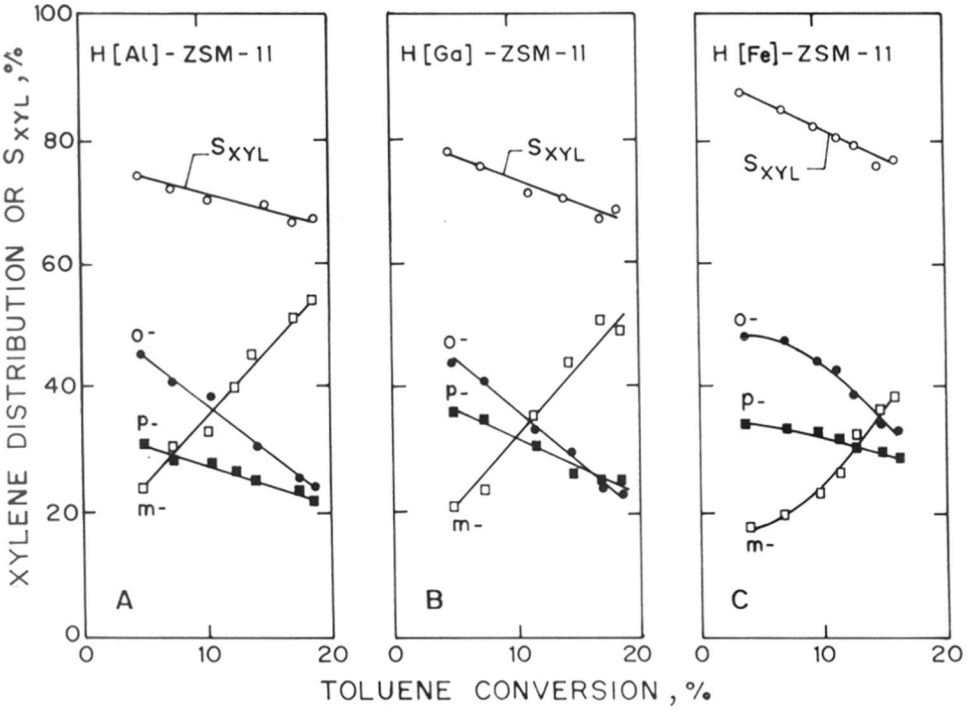

Fig. 3.3 Variation in the distribution of xylenes versus toluene conversion over metallosilicates of ZSM-11. S_{xyl} : selectivity for xylenes in aromatic products; o : *o*-xylene; m : *m*-xylene and p : *p*-xylene.

> Al suggesting that on weaker acid sites the disproportionation of initially formed xylene isomers is suppressed. Among the xylene isomers, *m*-xylene is a secondary products whereas, *p*- and *o*-xylene are formed directly by electrophilic aromatic substitution. The formation of *m*-xylene is favoured in the decreasing order : Al > Ga > Fe. The acidic strength decreases in the same order. The further isomerization of *p*- and *o*- which leads to *m*-xylene is suppressed over Fe-ZSM-11.

The results obtained over Al- and Fe-ZSM-11 are compared with those obtained over Al- and Fe- analogs of zeolite EU-1 and ZSM-48. In Fig. 3.4, the selectivity for xylene isomers in aromatic products, S_{xyl}, is plotted against toluene conversion over Al- and Fe- silicate analogs of ZSM-11, EU-1 and ZSM-48. Once again, ferrisilicate analogs exhibited higher S_{xyl} vis-á-vis their aluminosilicate counterparts. However, this difference in S_{xyl} value on Fe- and Al- zeolites was not very significant in the case of ZSM-48. This difference followed the order: ZSM-48 < ZSM-11 < EU-1. The observations clearly indicate that both chemical nature (e.g. acid strength) as well as pore geometry/structure (e.g. restricted transition state shape selective features) of the zeolites affect S_{xyl}. Since the unidimensional 10-membered ring channel structure of ZSM-48 cannot easily accommodate the larger transition state complex required for the formation of TMB *[28]*, the difference between S_{xyl} exhibited by Fe- and Al-analogs of ZSM-48 is less. Here, the geometric restrictions are playing a dominating role. ZSM-11 with 10-ring intersecting channels and EU-1, with large deep side pockets off unidimensional 10-ring channels, can provide enough void space required for the formation of TMBs. Zeolite EU-1, is also known to catalyze the disproportionation of xylene isomers to a significant extent *[19,58]* leading to xylene loss (lower S_{xyl}). However, in the case of [Fe]-ZSM-11 and to a larger extent in [Fe]-EU-1, the quite high value of S_{xyl} (with respect to their Al-analogs) is better correlated to their (Fe-analogs) weaker acid strength thus suppressing the transalkylation/disproportionation

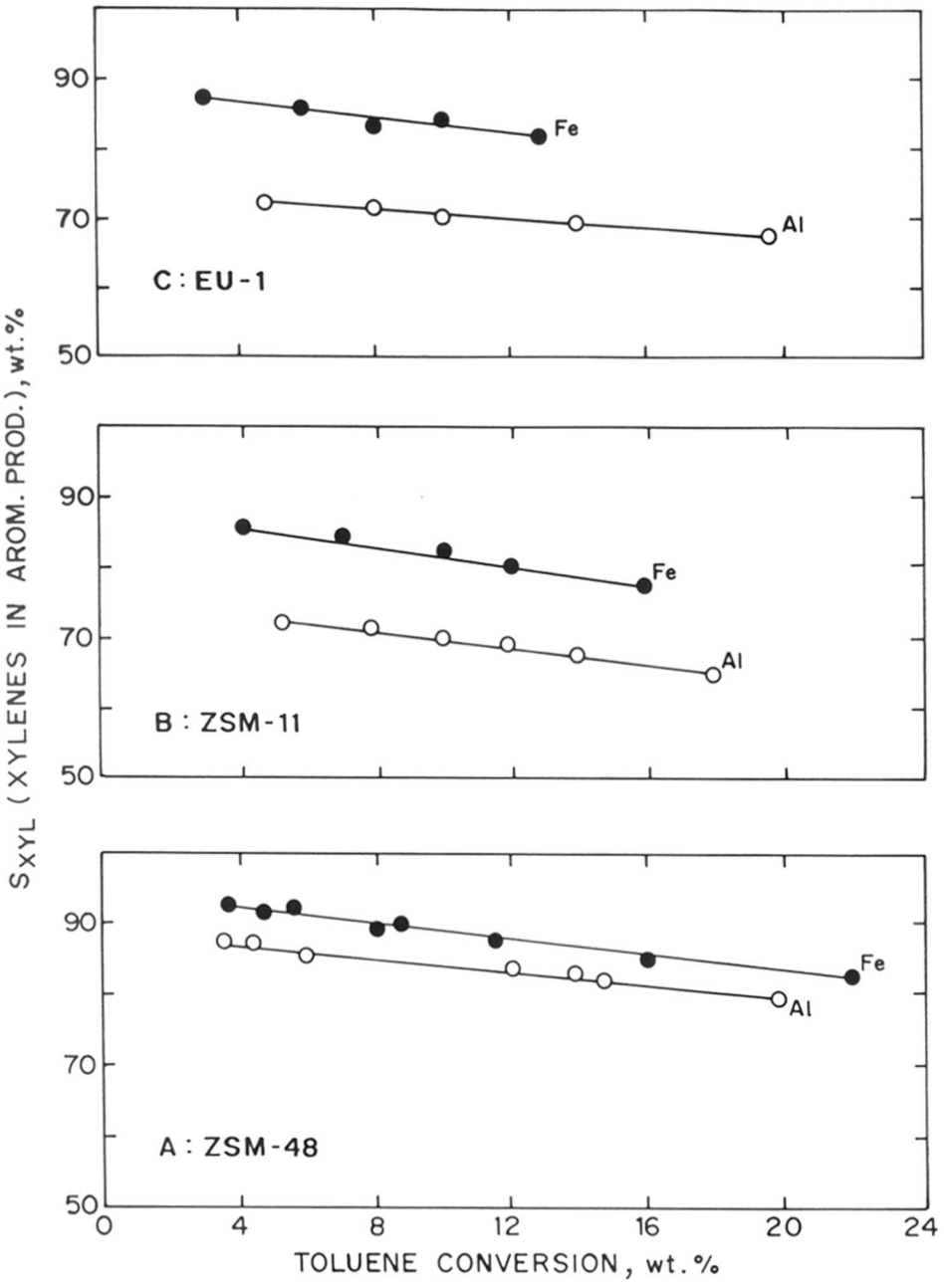

Fig. 3.4 Effect of toluene conversion on the selectivity of xylene in aromatic products (S_{xyl}).

or further alkylation of xylene isomers. Here it is pertinent to mention that the pure toluene or methanol, when used separately as feed under present reaction conditions, did not produce any significant amount of aromatic products.

A comparison of Al- and Fe- analogs of ZSM-11, EU-1 and ZSM-48 is given in Fig. 3.5, where the xylene distribution is plotted against toluene conversion over Al- (left hand side) and Fe- (right hand side) analogs of ZSM-48 (A,B bottom), ZSM-11 (C,D middle) and EU-1 (E,F top) zeolites. At lower or extrapolated zero toluene conversion (where secondary reactions are significantly avoided), ferrisilicates produced higher *p*-xylene compared to their respective Al-counterparts, this difference being more pronounced in the case of ZSM-48 than either ZSM-11 or EU-1.

Further, *p*-xylene is the main product over ZSM-48, *o*-xylene over ZSM-11, while over EU-1 both *p*- and *o*- isomers are produced in almost equal amounts suggesting that, among zeolite structures, the product shape selectivity (a geometric feature) follows the order: ZSM-48 > EU-1 > ZSM-11 in accordance with earlier observations *[19,58]*. However, the lower *m*-xylene selectivity and consequently (i) higher *p*-xylene (ZSM-48), (ii) *o*-xylene (ZSM-11) or (iii) both (*p*- and *o*-xylene) (EU-1) selectivity exhibited by Fe-zeolites, compared to their respective Al- analogs, may be better correlated to the lower acid strength of the former thus suppressing the isomerization of primarily formed *p*- and/or *o*- xylene. The isomerization apparently requires stronger acid sites than those required for the formations of xylenes from toluene by methylation *[59-61]*.

A careful scrutiny of Fig. 3.5 shows that with the increase in toluene conversion, the concentration of *m*-xylene, a secondary product, increases slowly over ZSM-48 and sharply over ZSM-11 with EU-1 following an intermediate path. This follows the trend of product shape selectivity of these zeolite structures *[17,23]*. However, Fig. 3.5 further indicates that on Al-analogs (compared to Fe-isomorphs), m-xylene concentration (among the xylene isomers) increases relatively faster with the toluene

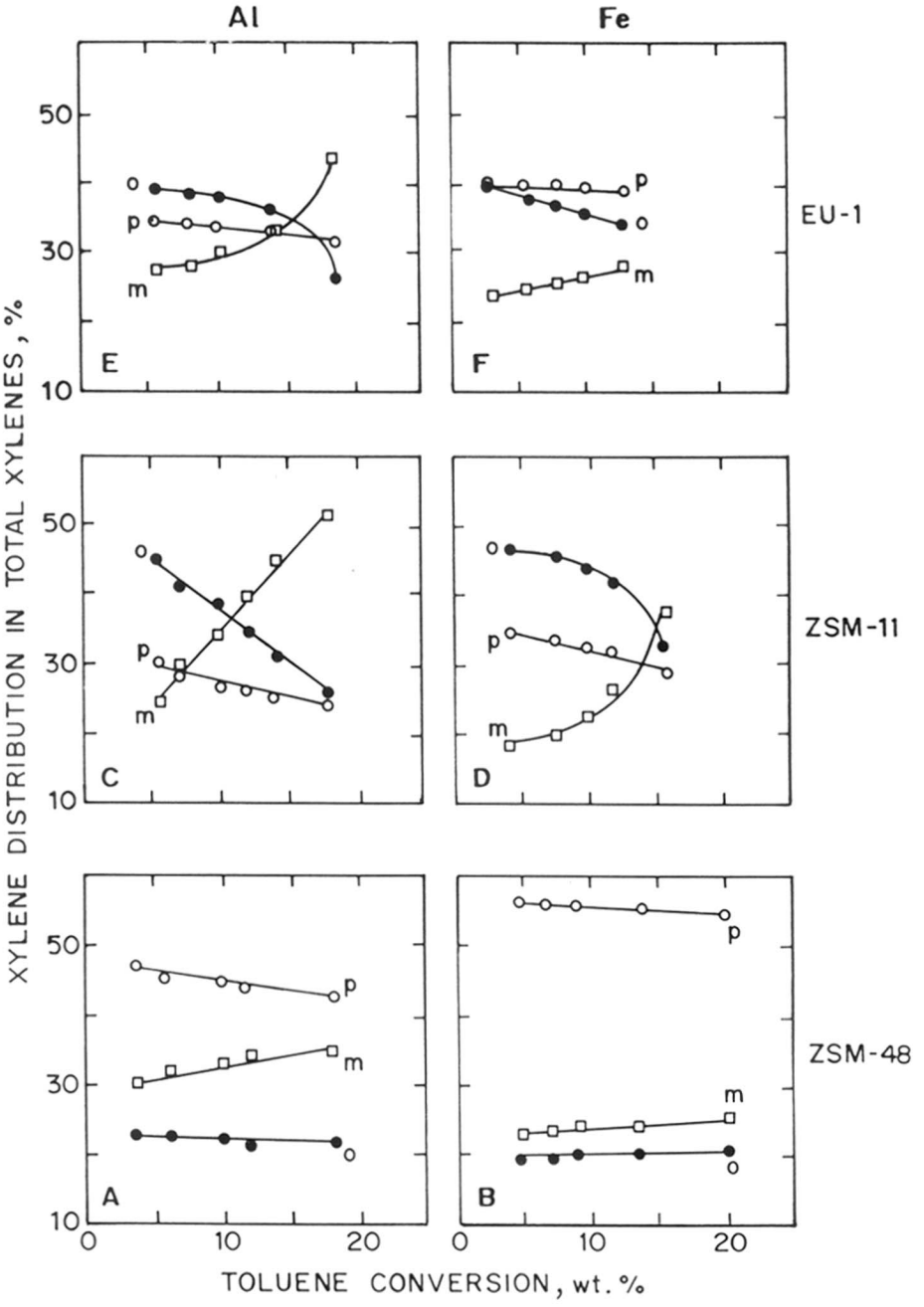

Fig. 3.5 Effect of toluene conversion on the distribution of xylene isomers over metallosilicates of ZSM-11, EU-1 and ZSM-48.
o : *o*-xylene; m : *m*-xylene and p : *p*-xylene.

conversion. This suggests that on Al-zeolites with relatively stronger Brönsted acid sites (vis-á-vis Fe-analogs) *[25,57]*, the isomerization of primarily formed para and/or ortho isomers into *m*-xylene competes favourably with alkylation of toluene as the severity of the reaction conditions, and hence conversion, increases. This is in agreement with the suggestion *[59-61]* that different reactions require active sites having different acid strength.

Recently, Mirth and Lercher *[61]*, on the basis of their in-situ IR spectroscopic studies on toluene methylation over ZSM-5, concluded that *p*-xylene concentration is mainly determined either by the rate of its formation by methylation (at lower temperatures) or by its subsequent isomerization (at higher temperatures). The observed formation of *m*- and *o*-xylene are on the other hand, strongly influenced by their diffusion rates.

The results of the present study suggest that in the methylation of toluene, the isomerization as well as transalkylation of primarily formed xylene isomers is suppressed over ferrisilicate zeolites, having weaker acid sites (compared to their respective Al-analogs), leading to higher selectivity of *p*-and/or *o*-xylene (depending upon the zeolite structure) and S_{xyl}.

3.3.2 Isomerization of *m*-xylene

The influence of temperature over Al-, Ga- and Fe-ZSM-11 is given in Table 3.4 to 3.6. It can be seen that contrary to higher paraselectivity obtained in the methylation of toluene for Fe-zeolites in comparison with Al- and Ga- analogs, they (Fe-zeolites) exhibited a lower *p/o* xylene ratio indicating that the ferrisilicates are certainly not more para-selective, if not less, than the corresponding aluminosilicates. Similar observation have been reported in the case of [M]-ZSM-5 *[5]*.

Recently, Vorbeck *et al.[5]* have reported that H-Fe-ZSM-5 exhibited lower paraselectivity compared to H-Al-ZSM-5. The samples containing both Al- and Fe-, H-[Al,Fe]-ZSM-5 followed the intermediate path. They correlated this to somewhat larger size of Al-ZSM-5 crystals (vis-á-vis Fe-). However, in the present work, all the samples were having same crystal size and shape, adsorption as well as SiO_2/M_2O_3 molar ratio (M = Al, Ga or Fe) (see Table 2.2 chapter 2). Hence the lower paraselectivity exhibited by Fe vis-á-vis Al- and Ga- cannot be correlated to the morphological features of the catalyst.

3.3.2.1 Influence of silylation

The presence of active sites on the external surface of the catalyst may contribute to the non-shape selective formation of para and ortho isomers. It has been suggested *[5]* that for Fe-zeolites, the presence of active sites may be preferentially on the external surface of the crystal. To check whether the effect is due to acid sites on external surface, the external surface of Fe-ZSM-11 crystals was silylated using tetraethy-lorthosilicate. The results are presented in Table 3.7. At similar conversions, the *p/o* xylene ratio and selectivity for isomerization did not differ significantly suggesting that the influence of external surface sites on the paraselectivity is not significant atleast in the present case.

Table 3.4 Effect of temperature in the isomerization of *m*-xylene over H-[Al]-ZSM-11.

Feed : *m*-xylene; H_2/oil (molar ratio) : 4; feed rate 4mlh^{-1}; time-on-stream : 20 min

Temperature, K	493	513	533	553
Conversion, (wt%)				
m-xylene	4.7	10.9	16.3	22.2
Products, (wt%)				
toluene	0.1	0.1	0.2	0.2
p-xylene	2.5	6.6	10.7	14.0
m-xylene	95.3	89.1	83.7	77.8
o-xylene	2.1	4.0	5.2	7.5
TMBs	-	-	0.1	0.1
others	-	0.2	0.1	0.4
p/*o*[a]	1.2	1.6	2.0	1.9
S_{isom} %[b]	97.8	97.2	97.5	96.8

a: *p*-xylene/*o*-xylene

b: $S_{isom.}$ = ∑xylenes/*m*-xylene conversion

Table 3.5 Effect of temperature in the isomerization of *m*-xylene over H-[Ga]-ZSM-11.

Feed : *m*-xylene; H_2/oil (molar ratio) : 4; feed rate 4mlh^{-1}; time-on-stream : 20 min

Temperature, K	493	513	533	553
Conversion, (wt%)				
m-xylene	3.9	8.9	15.5	24.4
Products, (wt%)				
toluene	-	0.1	0.2	0.2
p-xylene	1.8	5.1	9.2	14.6
m-xylene	96.1	91.1	84.5	75.6
o-xylene	2.0	3.6	6.0	9.1
TMBs	-	-	0.1	0.1
others	0.1	0.2	0.2	0.4
p/*o*[a]	0.9	1.4	1.5	1.6
S_{isom}, %[b]	97.4	97.8	98.0	97.1

[a] & [b]: see footnotes to Table 3.4

Table 3.6 Effect of temperature in the isomerization of *m*-xylene over H-[Fe]-ZSM-11.

Feed : *m*-xylene; H_2/oil (molar ratio) : 4; feed rate : 4mlh^{-1}; time-on-stream : 20 min

Temperature, K	493	513	533	553
Conversion, (wt%)				
m-xylene	5.9	9.0	15.6	22.8
Products,(wt%)				
toluene	0.1	0.1	0.2	0.2
p-xylene	2.8	4.4	8.2	12.8
m-xylene	94.1	91.0	84.5	77.2
o-xylene	3.0	4.4	6.9	9.5
TMBs	-	-	0.1	0.1
others	-	0.1	0.2	0.2
p/*o*[a]	0.9	1.0	1.2	1.3
S_{isom}, %[b]	98.3	97.8	98.1	98.2

[a & b]: see footnotes to Table 3.4

Table 3.7 Effect of temperature in the isomerization of *m*-xylene over silylated H-[Fe]-ZSM-11.

Feed : *m*-xylene; H_2/oil (molar ratio) : 4 ; feed rate : 4mlh^{-1}; time-on-stream : 20 min

Temperature, K	493	513	533	553
Conversion, (wt%)				
m-Xylene	5.4	9.1	13.3	23.1
Products, (wt%)				
toluene	0.1	0.2	0.2	0.2
p-xylene	2.8	5.0	7.2	12.5
m-xylene	94.7	91.1	87.0	76.9
o-xylene	2.4	3.8	5.7	10.0
TMBs	-	-	-	0.1
others	-	-	0.1	0.2
p/*o*[a]	1.2	1.3	1.3	1.3
S_{isom}, %[b]	96.3	96.7	97.0	97.4

[a & b] :see footnotes to Table 3.4

3.3.2.2 Comparison of zeolites

In Fig. 3.6 the *p/o* xylene ratio and selectivity to isomerization is plotted against *m*-xylene conversion over Al- and Fe-analogs of ZSM-11, EU-1 and ZSM-48. In agreement with the topological feature of these zeolite structures, the trend for *p/o* ratio and selectivity for isomerization followed the order ZSM-48 > ZSM-11 > EU-1 *[19,58]*. However, the Fe- zeolites exhibited lower values of *p/o* xylene ratio (vis-á-vis Al-analog, Fig. 3.6). The higher selectivity to isomerization for Fe- indicates lower transalkylation or cracking as compared to Al- analog.

In literature, the high *p*-xylene selectivity of the zeolites has been correlated to a number of factors (over Al zeolites), which can broadly be classified into two main categories (i) geometrical /topological features (see Chapter 1 § 1.6) *[62,63]* and (ii) chemical nature/electronic factor of active sites *[60,65]*.

Corma *[60]* has invoked the concept correlating hardness/softness of the acid sites to the lower paraselectivity of Fe-ZSM-5 (vis-á-vis Al-) in *m*-xylene isomerization reaction. According to this the preferential formation of a product is influenced by "orbital control" effects due to the difference in the energy gap between HOMO and LUMO of the isomorphously substituted transition metal ions. Pellet *et al. [65]*, on the basis of their systematic study of on SAPOs and MeAPSOs (-11, -31; Me = Mn and Co) in xylene isomerization, concluded that the observed paraselectivity cannot be accounted solely to the geometry induced shape selective effects. The presence of metal ions exert special effects independent of the acid strength and spatial constraints *[65]*.

Recently, Dewing and Dwyer *[62]*, have reported that the product selectivity in *m*-xylene isomerization over Al- and Fe- zeolites, depend upon the relative rates of diffusion vis-á-vis rate of reaction. They *[62]* suggested that over Al- analogs, being highly active (due to stronger Brönsted acidity), the rate limiting factor may be the

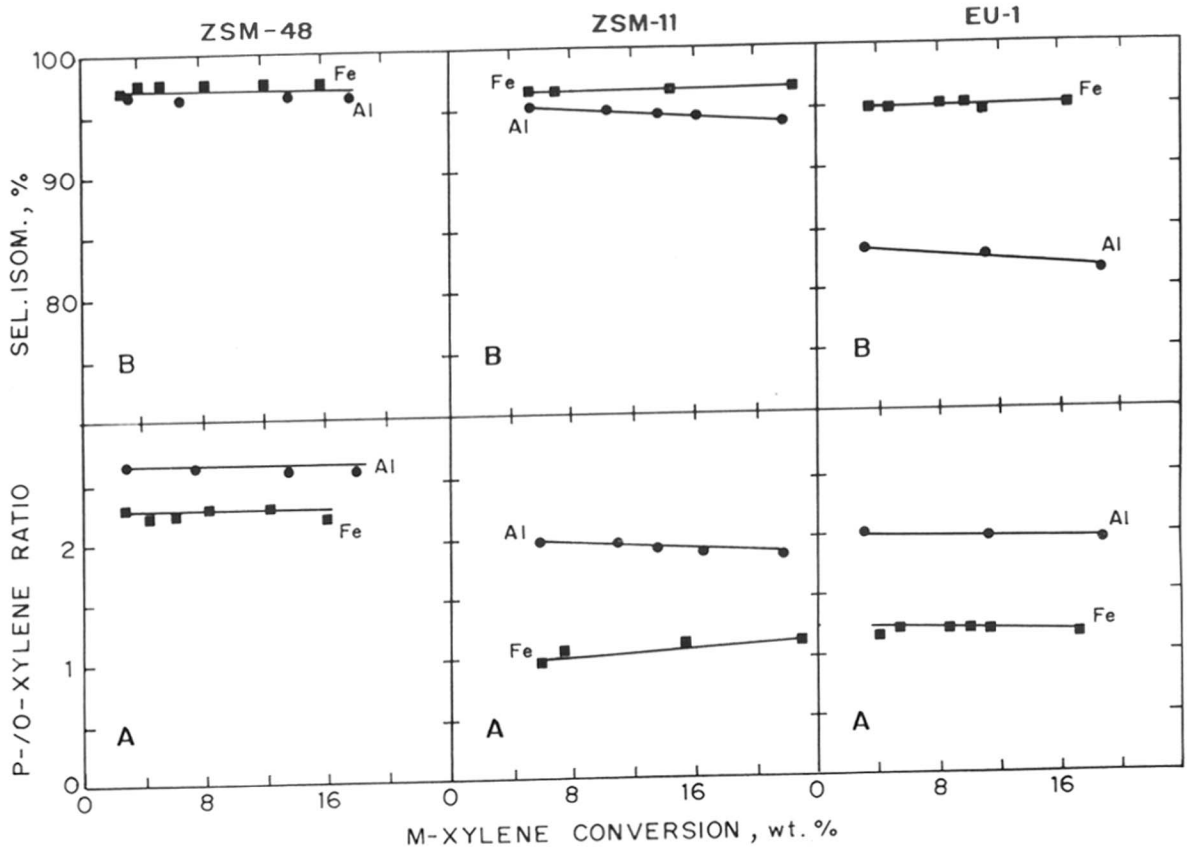

Fig. 3.6 Effect of *m*-xylene conversion on *p/o* xylene ratio and selectivity for isomerization.

diffusion of the products from the active sites. Hence the overall selectivity exhibited by Al-analogs is primarily controlled by diffusional limitation. Over Fe-analogs, with lower activity (due to weak Brönsted acid sties), the rate limiting factor may be the intrinsic activity of the zeolite, Para shape selectivity can be observed only when the overall rate is controlled by transport (diffusion) phenomenon.

3.3.3 Methylation of xylenes

In this section, Al-, Ga- and Fe- silicate analogs of ZSM-11 (MEL) are compared in the methylation of *m*-xylene, *o*-xylene as well as an equilibrium mixture of xylenes.

3.3.3.1 Influence of temperature

The influence of reaction temperature on *m*-xylene conversion (wt.%) and selectivity of various products (S, wt.% = (wt.% of a particular product/wt.% of total products) x 100) in the methylation of *m*-xylene with methanol over H-Al-ZSM-11, H-Ga-ZSM-11 and H-Fe-ZSM-11 is illustrated in Fig 3.7A, 3.7B and 3.7C, respectively. At similar temperature and conversion levels the selectivity for trimethylbenzenes (S_{TMB}) followed the order : Al- < Ga- < Fe-. The selectivity for isomerization products ($S_{(o\text{-}x+p\text{-}x)}$) followed the reverse order (Fig 3.7A-3.7C, curves b and c). The selectivity for aliphatics (from methanol) decreased with the increase in temperature/conversion in all the cases. At lower conversion levels (around 5-10%), the Al- analog produced more aliphatics vis-á-vis Ga- and Fe- analogs (curve d, Fig. 3.7A-3.7C). However, the selectivity for 1,2,4 TMB in total TMBs was very high ($\approx$ 98.5±1 %) in all the cases in accordance with the reported *[30,29]* values over ZSM-5.

3.3.3.2 Influence of WHSV

The effect of varying feed rate on the *m*-xylene conversion and various selectivities over H-Fe-ZSM-11 is compared in Table 3.8. With an increase in feed rate, the conversion slightly decreased and selectivity for TMBs increased.

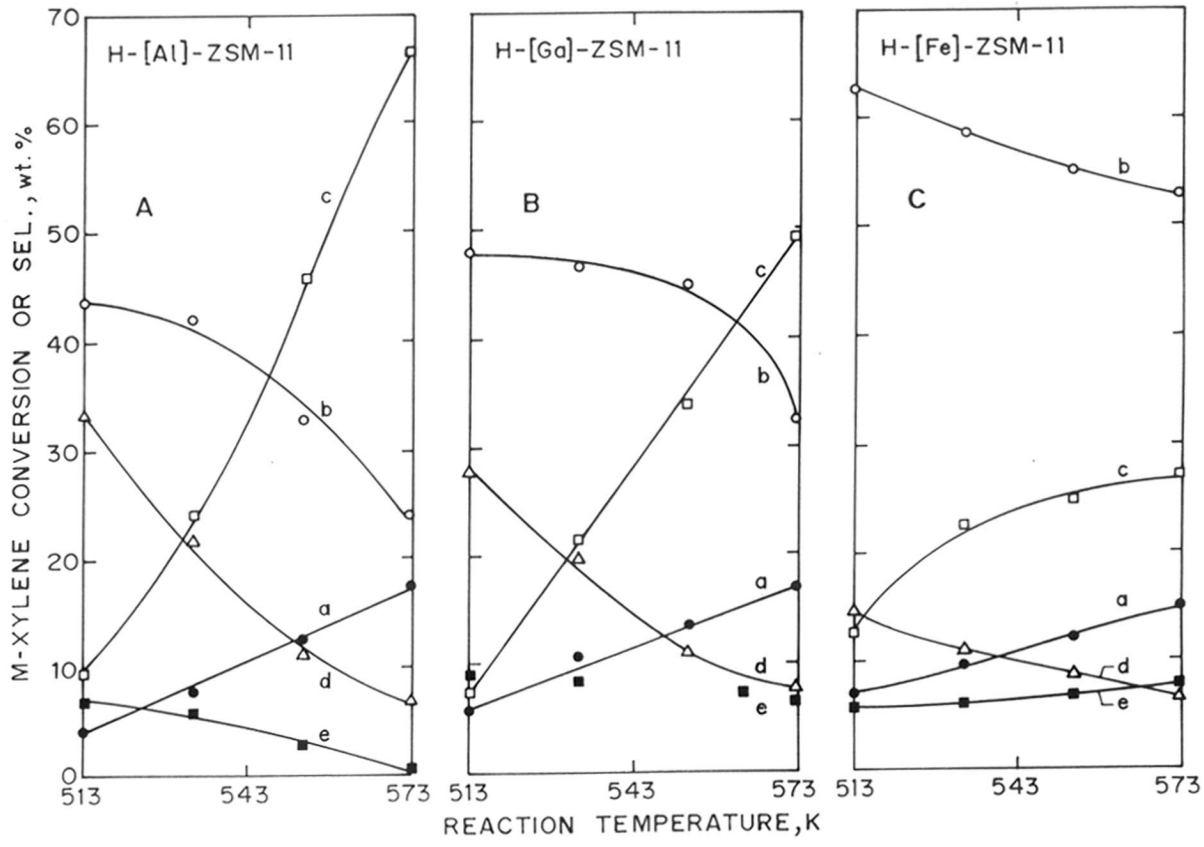

Fig. 3.7 Effect of temperature on *m*-xylene conversion or yield over A: H-[Al]-ZSM-11; B: H-[Ga]-ZSM-11; C: H-[Fe]-ZSM-11. a: *m*-xylene conversion, b: TMBs, c: *o*- + *p*-xylene, d: aliphatics and e: others (toluene, benzene, tetramethylbenzenes etc.).

3.3.3.3 Alkylation/isomerization ratio

In Fig. 3.8, the log of the alkylation/isomerization ratio (A/I, molar ratio of total TMBs/(*o*-xylene + *p*-xylene)) is plotted against *m*-xylene conversion over Al-, Ga- and Fe-silicates. The value of log (A/I), decreased with the increase in conversion in all the three cases, following the order: Al- < Ga- < Fe-. The positive value of log (A/I) reflects the predominance of alkylation over isomerization, while the negative values of this ratio (at higher *m*-xylene conversion) indicate the importance of the isomerization. Here it may be pertinent to mention that under identical reaction conditions neither pure methanol nor pure *m*-xylene produced any significant amount of TMBs over Al-, Ga- or Fe- analogs of ZSM-11. This observation suggests that the TMBs were formed through methylation of *m*-xylene and not by its disproportionation/transalkylation or from methanol alone.

The possible reactions *m*-xylene can undergo during methylation are given in Scheme-1. Under the reaction conditions studied here, we have established that neither dealkylation (A) nor disproportionation/transalkylation (B) of xylenes occurs to any significant extent. Almost no TMBs and insignificant amount of toluene were obtained when *m*-xylene (or an equilibrium mixture of xylenes) was converted over Al-, Ga- and Fe-ZSM-11 at the same reaction temperature and feed rate (WHSV) used during methylation (see section 3.3.2). Hence, the higher selectivity of TMBs and lower selectivity of aliphatics over Fe- and Ga- vis-á-vis Al- analog (curve d, Fig 3.7A-C) is probably due to the reason that at the weaker acid sites (on the Fe- and Ga- analogs) the alkylation reaction is able to compete more successfully with the isomerization (D) as well as methanol to aliphatics reactions.

3.3.3.4 Comparison of xylenes

In Fig. 3.9 the conversion as well as selectivity of trimethylbenzenes among products (S_{TMB}) in the methylation of *m*-xylene, *o*-xylene and equilibrium mixture (24

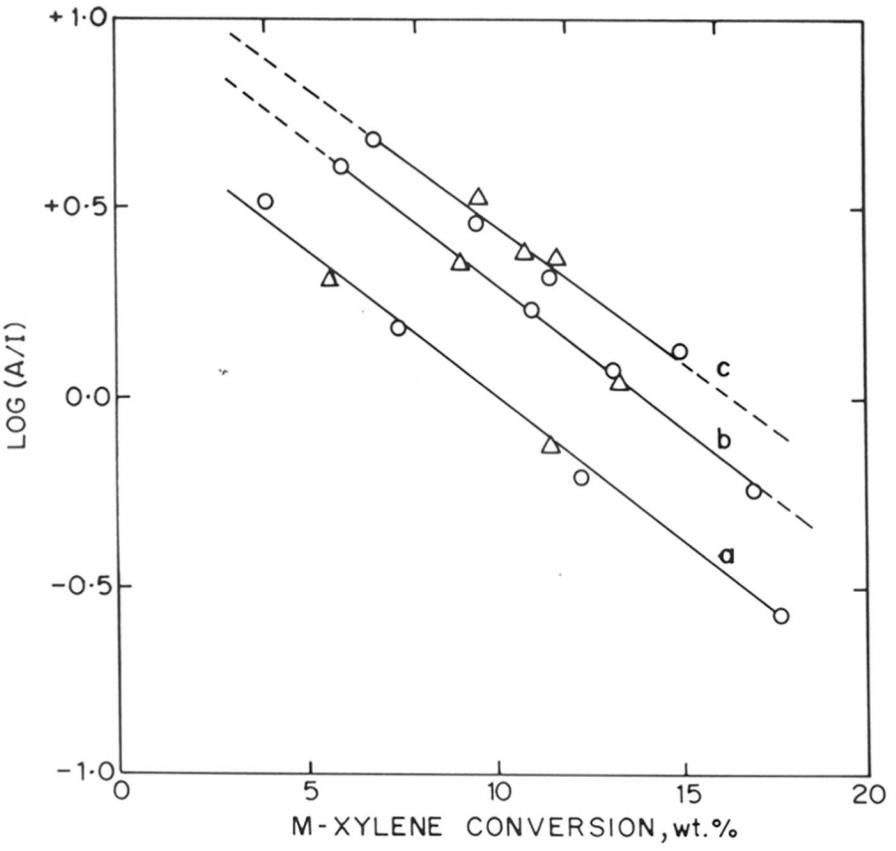

Fig. 3.8 Log (A/I) vs *m*-xylene conversion, A/I = moles of total TMBs/ moles of p-xylene + *o*-xylene a: H-[Al]-ZSM-11; b: H-[Ga]-ZSM-11 and c: H-[Fe]-ZSM-11; Conversion was varied by changing (o): Temperature and (Δ): WHSV.

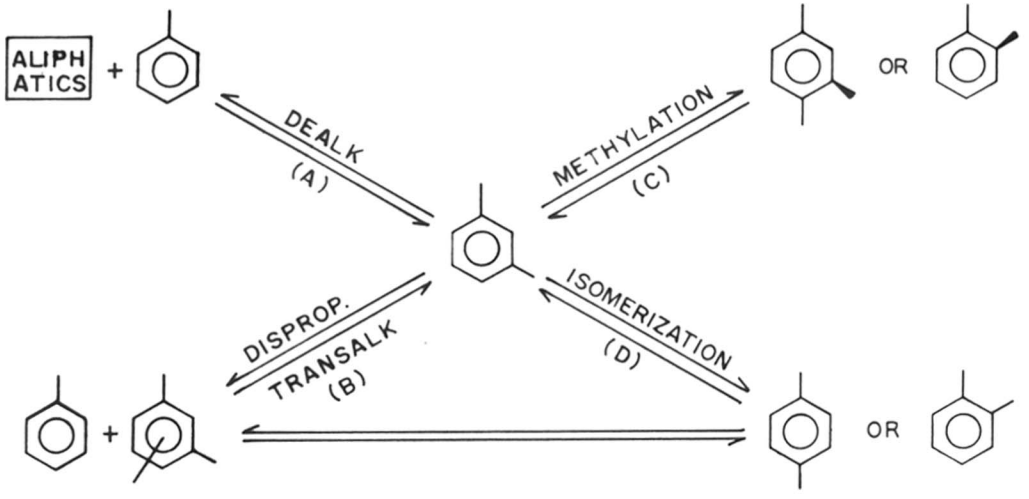
ALIPH
ATICS
+
DEALK
(A)
METHYLATION
(C)
OR
DISPROP.
TRANSALK
(B)
ISOMERIZATION
(D)
+
OR

SCHEME-1

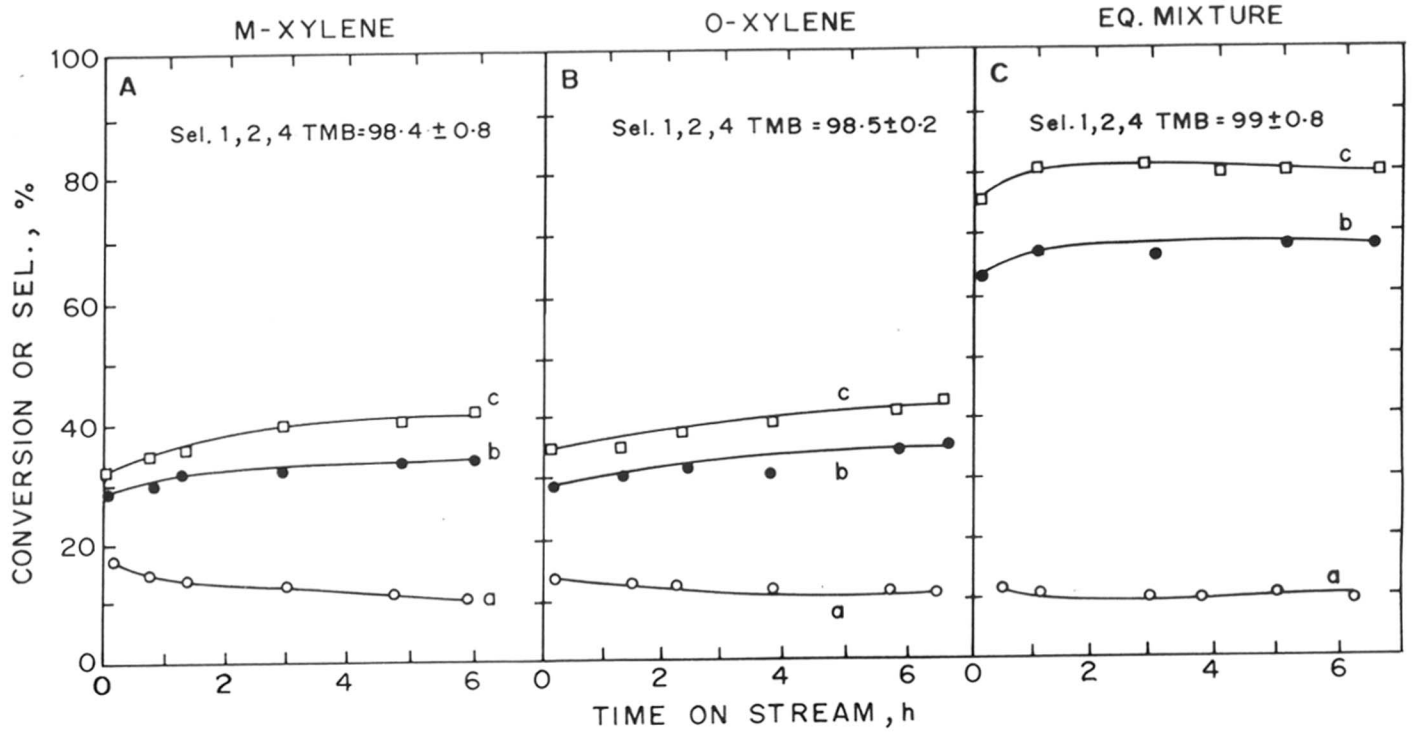

Fig. 3.9 Effect of time-on-stream on the conversion and selectivity during methylation of A: *m*-xylene; B: *o*-xylene and C: Equilibrium mixture of xylenes; Curves a: conversion; b: S_{TMB} in total products, c: $S_{TMB(arom.)}$ in aromatic products.

Table 3.8 Influence WHSV in the methylation of *m*-xylene

Feed: *m*-xylene + CH_3OH, 4 : 1 mole; N_2/Oil (molar ratio): 4; Temperature = 553 K; Catalyst : H-Fe-ZSM-11

	Feed rate, ml/h		
	4	6	10
Conversion, (wt %)			
methanol[a]	100	90.0	75.0
m-xylene[b]	11.7	10.8	9.4
Products, (wt%)			
aliphatics	1.2	0.8	0.7
p-xylene	1.2	0.8	0.6
m-xylene	88.3	89.2	90.6
o-xylene	1.2	1.6	1.2
1,3,5 TMB	-	-	-
1,2,4 TMB	6.2	6.4	6.1
1,2,3 TMB	0.03	0.03	0.02
TeMBs	0.8	0.9	0.6
others	0.8	0.2	0.2
S_{TMB}[c]	53.3	58.7	65.1
$S_{TMB\ (arom.)}$[d]	59.4	63.7	70.3
$S_{(o\text{-}xyl.+p\text{-}xyl.)}$	22.2	22.0	19.1
$S_{aliphatics}$	10.3	7.3	7.4
S_{TeMB}	6.8	8.3	6.3
S_{others}[e]	4.2	1.0	2.1
log (A/I)[f]	0.36	0.38	0.48

a: (methanol in feed - methanol in products/methanol in feed) x 100,

b: 100 - ∑unconverted xylenes, wt% in products

c: $S_{TMB} = \frac{\sum TMBs \times 100}{total\ products}$, % .

d: $S_{TMB(arom.)} = \frac{\sum TMB}{\sum aromatic\ products}$, %.

e: Others include benzene, toluene, ethyltoluenes, dimethylether etc.

f: $\log \frac{A}{I} = \frac{\sum TMBs}{p + o xylene}$

% *p*-xylene; 54 % *m*-xylene; 22 % *o*-xylene) of xylenes over H-Ga-ZSM-11 are plotted as a function of time-on-stream. Although the xylene conversion decreased slightly, the yield for TMBs did not change significantly with the reaction time. Similar observations have been recorded earlier in the methylation of *m*-xylene over H-Al-ZSM-5 *[29]*. Although the conversion levels in all the cases (*m*-xylene, *o*-xylene and mixture of xylenes) were similar, the yield for TMB followed the order: xylene mixture >> *m*-xylene ≈ *o*-xylene, probably due to the suppression of isomerization reaction in the case of xylene equilibrium mixture. A similar trend was observed in the case of Al- and Fe- ZSM-11 also (Table 3.9 and Fig. 3.7). The increased yield of TMBs (by about 30%, 80 vs 50%) is significant from an economic point of view. The selectivity for the 1,2,4 isomer was, however maintained at about 99 %.

3.3.3.5 Influence of molar feed ratio

The effect of varying the molar feed ratio (xylenes to methanol = 2, 4 and 6) over H-Fe-ZSM-11 is shown in Table 3.10. Although the xylene conversion slightly decreased with an increase in the xylene to methanol feed ratio, the utilization of methanol to yield TMBs was enhanced, probably due to the reason that with the decrease in methanol concentration in the feed the alkylation reactions compete more successfully with the pure methanol reactions leading to higher yield for TMBs.

In the methylation of xylenes, *m*- or *o*- isomer can provide either 1,2,4 or 1,2,3 TMBs. The *p*-xylene can, however, produce only 1,2,4 TMB as the primary product *[29]*. 1,3,5 TMB can be obtained either by isomerization of 1,2,4 or 1,2,3 TMB or by disproportionation of xylenes. During the present study, 1,3,5 TMB was not observed at all. The formation of 1,2,3 isomer was also suppressed drastically resulting in the very high selectivity for 1,2,4 TMB (98.5 ± 1 %), much more than equilibrium value (Equilibrium Composition at 600 K = 63 : 24 : 13 for 1,2,4, 1,3,5 and 1,2,3 TMBs, respectively) *[66]*. Since the kinetic diameter of 1,2,4 TMB is the smallest (0.68 nm)

Table 3.9 Effect of isomorphous substitution in the methylation of Equilibrium mixture of xylenes

Feed : xylenes + CH_3OH, 4 : 1 mole; N_2/oil (molar ratio) : 4; feed rate 4mlh^{-1}; temperature : 553 K; time-on-stream : 1h; methanol conversion[a]: 100%

Catalyst	H-Al-ZSM-11	H-Ga-ZSM-11	H-Fe-ZSM-11
Conversion (wt%)			
Xylenes[b]	9.9	10.0	10.2
Products, wt%			
aliphatics	2.6	1.7	1.4
p-xylene	21.5	21.4	23.3
m-xylene	48.6	45.6	44.6
o-xylene	20.0	22.9	21.9
1,3,5 TMB	-	-	-
1,2,4 TMB	5.2	6.9	7.3
1,2,3 TMB	0.1	0.1	0.1
TeMB	0.9	0.6	0.8
others	1.1	0.6	0.5
S_{TMB}[c]	53.5	68.3	72.6
$S_{TMB(arom.)}$[d]	71.7	81.8	84.1
$S_{aliphatics}$	26.3	17.0	13.7
S_{TeMB}	9.1	9.3	8.8
S_{others}[e]	11.1	6.0	4.9

[a-c]: see footnotes to Table 3.8.

Table 3.10 Influence of xylenes to methanol ratio in the methylation of Equilibrium mixture of xylenes

Temperature = 563 K; WHSV = 3.5 h^{-1}; Catalyst : H-Fe-ZSM-11

	xylenes/methanol ratio		
	2	4	6
Conversion, (wt%)			
methanol[a],	70	100	100
xylenes[b]	13.7	12.7	11.4
Products (wt%)			
Aliphatics	3.0	1.4	0.5
p-xylene	23.6	23.6	23.0
m-xylene	41.1	42.3	42.9
o-xylene	21.7	22.0	22.7
1,3,5 TMB	-	-	-
1,2,4 TMB	8.4	9.3	9.5
1,2,3 TMB	0.07	0.05	0.01
TeMB	1.6	1.7	1.2
others	0.5	0.5	0.3
Sel. 1,2,4 TMB, %	99.0	99.5	99.9
S_{TMB}[c]	62.3	73.4	83.3
$S_{TMB\ (arom.)}$[d]	79.8	82.7	86.4
$S_{aliphatics}$	22.0	11.2	3.5
S_{TeMB}	11.9	11.9	10.5
S_{others}[e]	3.8	3.9	2.6

[a-e]: see footnotes to Table 3.8

among TMBs, the very high selectivity of 1,2,4 isomer during the methylation of xylenes over metallosilicate analogs of ZSM-11 can be attributed to their shape selective properties. Although the enrichment of 1,2,4 TMB seems to be the manifestation of product shape selectivity, the restricted transition state shape selectivity may also contribute to this phenomenon owing to the fact that the transition state complex required to form 1,2,4 TMB will be smaller than that required for either 1,2,3 or 1,3,5 TMB *[28]*.

Recently, Corma *[60]* has elaborated on the relationship between acid strength (or more accurately, softness/hardness) of the acid sites on the selectivities in various acid catalyzed reactions, supporting the view that different acid catalyzed reactions may require sites with different acid strength. Since the acid strength of metallosilicate molecular sieves decreases in the order Al > Ga > Fe *[2-4,25,57]*, the higher yield of TMBs (alkylation product) over ferrisilicate ZSM-11 may be due to its weaker acid sites (vis-á-vis Al- or Ga-).

3.3.4 chlorination of toluene

The results of the influence of various zeolites, isomorphous substitution (of Al by Fe) and cations (H^+ and K^+) in zeolites on the *p/o* selectivity in the chlorination of toluene with chlorine gas is presented in Table 3.11. The isomer distribution (*p*-CT/*o*-CT) obtained using a conventional catalyst, $FeCl_3$, is also included for comparison. In all experiments, para-chlorotoluene (*p*-CT) and ortho-chlorotoluene (*o*-CT) were major products. Small amounts of benzyl chloride (BC) and polychlorinated toluenes (others) were also detected. meta-Chlorotoluene (*m*-CT) was found in an amount less than 2% in all cases. The products are found to be similar to those reported over conventional catalysts *[37]*.

Table 3.11 Chlorination of toluene over various zeolites

Catalyst: 5 g/ mole toluene; reaction temperature : 363 K; toluene = 0.32 moles; Cl_2 flow (mol./h) = 0.08

Catalyst	Tol. Conv. wt%	YIELDS[a], wt%				*p*/*o*[b]
		p-CT	*o*-CT	BC	others	
H-Al-Beta	25.2	11.6	13.5	0.1	-	0.86
H-Fe-Beta	20.3	5.2	12.4	-	2.7	0.42
K-Al-Beta	28.9	15.1	13.7	0.1	-	1.10
K-Fe-Beta	21.2	6.0	13.3	-	1.9	0.45
K-Al-ZSM-11	24.6	11.2	13.3	0.1	-	0.84
K-Fe-ZSM-11	25.6	10.5	14.8	0.3	-	0.71
K-Al-EU-1	22.6	10.1	12.3	0.2	-	0.82
K-Fe-EU-1	27.2	10.2	14.7	0.7	1.6	0.69
$FeCl_3$	22.3	5.9	12.1	2.8	1.5	0.49

[a] *p*-CT : para chlorotoluene; *o*-CT : ortho chlorotoluene; BC : Benzyl chloride; others : include di, tri and polychlorinated toluenes

[b] $\frac{p}{o} = \frac{parachlorotoluene}{orthochlorotoluene}$

The *p/o* ratios over various zeolites were obtained in the chlorination of toluene at similar levels of conversion and under same reaction conditions. The chlorination of toluene results first in para and ortho substituted products (parallel reaction) followed by a slow consecutive reaction to di-, tri- and tetra- chlorotoluenes. The selectivity for the parallel reaction is expressed as *p/o* ratio. This ratio in parallel reaction is controlled by several variables such as the type of cation, the extent of cation exchange, the type of zeolites and the metal ion in the framework of zeolites. It was observed that selective formation of *p*-CT over zeolites is not a geometry related shape selectivity *[67]*. The size, charge and position of the cations in the zeolite channels may be responsible for the shape selectivity and activation of chlorine molecule in the chlorination of toluene *[46,48]*. The results show a strong influence of different catalysts on the *p/o* selectivity in the chlorination of toluene which increase from 0.42 to 1.10. The catalyst used in this study could be arranged in the decreasing order of their *p/o* selectivity as follows :

K-Al-Beta > H-Al-Beta > K-Al-ZSM-11> K-Al-EU-1 > K-Fe-ZSM-11 > K-Fe-EU-1 > $FeCl_3$ > K-Fe-Beta > H-Fe-Beta

In Table 3.11 the effect of isomorphous substitution of Al by Fe in zeolites Beta, ZSM-11 and EU-1 on the *p/o* selectivity is also shown. When ferrisilicates were used in the reaction the *p/o* ratio was lower compared to the Al-zeolites.

A strong influence of the cation exchange (K^+) in zeolites on the *p/o* selectivity is observed. The higher *p/o* ratio is obtained over all K-zeolites compared to the H-zeolites (Table 3.11). The higher para-selectivity of K-zeolites may be due to the following reasons :

I The coordination of the reactants to the cations

II The change in the acidic centers due to K

III The change in the electrostatic field in the zeolite channels

The ring (nuclear) and side chain chlorination of toluene takes place by ionic and radical mechanisms, respectively over zeolites *[68]*. Electrophilic aromatic chlorination is feasible over Lewis and Brönsted acid catalysts *[70]*. These sites polarize the chlorine molecule and produce the required positive chlorine by heterolytic dissociation which acts as electrophile *[69]*. Among the catalyst used K-Al-Beta was found to be more most paraselective. Hence, all further studies were carried out using this catalyst.

3.3.4.1 Influence of catalyst concentration

Increasing the catalyst concentration of zeolite K-Al-Beta (5 g/mole toluene) increases the yield of *p*-CT and the *p/o* ratio (Table 3.12). The maximum yield of benzyl chloride was obtained in the absence of any catalyst which may be attributed to the photochlorination of the side chain in toluene *[69]*. The measured product ratio (*p/o*) over different catalyst concentration 0, 3 and 5 (g/mole toluene) were found to be 0.68, 0.92 and 1.10, respectively at nearly similar levels of conversions. Mostly benzyl chloride (84.5%) was obtained in the absence of any catalyst.

3.3.4.2 Influence of reaction temperature

The influence of reaction temperatures in the range of 323 to 378 K on the product distribution in the chlorination of toluene over K-Al-Beta was investigated. At 323 K, the *p/o* selectivity is lower compared to those obtained at 363 and 378 K. The results show that an increase in the reaction temperature from 323 to 363 K increases the *p/o* ratio from 0.90 to 1.10. No appreciable change in the *p/o* ratio was observed on further increase in temperature to 378K (Table 3.13).

Table 3.12 Influence of catalyst amount on the chlorination of toluene[a]

	catalyst/toluene, g/mole		
	0	3	5
Toluene conversion, (wt%)	27.1	22.1	28.9
Products[b] (wt%)			
p-Chlorotoluene	1.1	10.5	15.1
o-Chlorotoluene	1.6	11.4	13.7
Benzyl chloride	22.9	0.1	0.1
others	1.5	-	-
p/*o* ratio	0.68	0.92	1.10

[a&b] : see table 3.11

Table 3.13 Influence of reaction temperature on the chlorination of toluene.

	Temperature, K		
	323	363	378
Toluene conversion, (wt%)	24.1	28.9	27.9
Products[b], (wt%)			
p-Chlorotoluene	11.3	15.1	14.6
o-Chlorotoluene	12.6	13.7	13.2
Benzyl chloride	0.1	0.1	0.1
Others	0.1	-	-
p/o ratio	0.90	1.10	1.11

3.3.4.3 Influence of duration of the run

The influence of duration of the run on the *p/o* selectivity and secondary chlorinated products are presented in Table 3.14. *P/o* selectivity decreases marginally with time.

3.4 CONCLUSIONS

In toluene methylation, a comparison of Al-, Ga- and Fe- analogs, shows that the selectivity for primarily formed para and/or ortho xylene follows the order Fe > Ga > Al which is a consequence of the suppression of the secondary reactions on Fe-zeolites with weaker acid sites compared to the Al- and Ga- analogs. Similarly, S_{xyl} (total xylenes among aromatic products) follows the order : Fe > Ga > Al indicating that on weaker acid sites the transalkylation and dealkylation of xylenes is hindered. Probably, suppression of the side reactions also makes Fe- stable to deactivation by decreasing the higher aromatics which may cause pore blocking and coke formation.

In the isomerization of *m*-xylene the *p/o* ratio, an indicator of paraselectivity is found to decrease with the acidic strength of the metallosilicate for a given zeolite. The crystal structure, however influenced the absolute value. Depending upon the void space available the overall selectivity for xylenes, S_{xyl}, varied. For a given structure Fe- showed higher values indicating the lower occurrence of side reactions (such as transalkylation) compared to its Al- analog. The higher selectivity for isomerization and the lower *p/o* ratio is attributed to the weaker acidic strength of the metallosilicate.

The shape selective properties of medium pore 10 ring MEL molecular sieve, lead to highly selective formation of 1,2,4 isomer (98.5 ± 1%) among TMBs during methylation of xylenes (individual isomers or their equilibrium mixture). The isomorphous substitution of Al by Ga or Fe significantly enhances the yield of TMBs probably due to the reason that on weaker acid sites (of the Ga- and Fe- vis-á-vis Al-analogs) the alkylation of xylenes is able to compete more efficiently with other

Table 3.14 Influence of reaction on the chlorination of toluene.

	Duration of run (h)			
	1.5	3.0	4.0	4.5
Toluene conversion, (wt%)	28.9	64.2	82.0	92.3
Products[b], (wt%)				
p-Chlorotoluene	15.1	33.4	42.3	47.4
o-Chlorotoluene	13.7	30.3	38.8	43.9
Benzyl chloride	0.1	0.3	0.4	0.4
Others	-	0.2	0.5	0.6
p/o ratio	1.10	1.10	1.09	1.08

[a&b] : see footnotes in Table 3.11

reactions such as isomerization of *m*-xylene and conversion of methanol to aliphatics. The yield for TMBs in the product can be increased considerably by methylating the equilibrium xylene mixture (instead of individual isomers) due to the suppression of isomerization reaction.

In the chlorination of toluene over various Al- and Fe- silicate analogs of ZSM-11, EU-1, ZSM-48 and Beta, para-chlorotoluene is produced more selectively over K-Al-Beta compared to other zeolites. When ferrisilicates are used, the *p/o* selectivity is reduced. The formation of *p*-CT is higher over K-exchanged zeolites than their protonic form. Higher *p/o* selectivity is also obtained by increasing the catalyst concentration, and reaction temperature in the range of 363 to 378 K.

3.5 REFERENCES

1. R.M. Barrer, *Hydrothermal chemistry of Zeolites*, Academic Press, London/New York, 1982 p.251.
2. R. Szostak, *Molecular Sieves : Principle of synthesis and Identification*, Reinhold, New York, 1989, p.213.
3. P. Ratnasamy and R.Kumar, *Catal. Today* **9**, 329 (1991).
4. R. Kumar and P. Ratnasamy, *Stud. Surf. Sci. Catal.* **60**, 43 (1990).
5. G. Vorbeck, M. Richter, R. Fricke, B. Parlitz, E. Schreier, K. Szulewsky and B. Zibrowius, *Stud. Surf. Sci. Catal.* **65**, 631 (1991).
6. a.Anuj Raj, J.S. Reddy and R. Kumar, *Proc. 9th Intern. Zeolite Conf.*, Montreal, 1992, Eds. R. von Ballmoos, J.B Higgins and M.M.J. Treacy, Butterworth-Heinmann, USA, 1993 p.551.
   b. Anuj Raj, K.R. Reddy, J.S. Reddy and R. Kumar, *Stud. Surf. Sci. Catal.* **75B**, 1715 (1993).
7. Anuj Raj, J.S. Reddy and R. Kumar, *J. Catal.* **138**, 578 (1992).
8. G.T. Kokotailo, P. Chu, S.L. Lawton and W.M. Meier, *Nature* **275**, 119 (1978).
9. N.A. Briscoe, D.W. Johnson, M.D. Shanon, G.T. Kokotailo and L.B. McCusker, *Zeolites* **8**, 74 (1988).
10. J.L. Schlenker, W.J. Rohrbaugh, P. Chu, E.W. Valyocsik and G.T. Kokotailo, *Zeolites* **5**, 555 (1985).
11. W.W. Kaeding, C. Chu, L.B. Young, B. Weinstein, S.A. Butter, *J. Catal.* **67**, 159 (1981).
12. W.W. Kaeding, C. Chu, L.B. Young and S.A. Butter, *J. Catal.* **69**, 159 (1981).
13. N.Y. Chen, W.W. Kaeding and F.G. Dwyer, *J. Amer. Chem. Soc.* **101**, 392 (1979).
14. L.B. Young, S.A. Butter and W.W. Kaeding, *J. Catal.* **76**, 418 (1982)
15. T. Yashima, Y. Sakaguchi and S. Namba, *Stu. Surf. Sci. Catal.* **7**, 739 (1981).
16. J.H. Kim, S. Namba and T. Yashima, *Stud. Surf. Sci. Catal.* **46**, 71 (1989).
17. J.H. Kim, S. Namba and T. Yashima, *Bull. Chem. Soc. Japan* **61**, 1051 (1988).
18. N.R. Meshram, *J. Chem. Technol. Biotechnol.* **37**, 111 (1987).
19. G.N.Rao, R.Kumar and P.Ratnasamy, *Appl. Catal.* **49**, 307 (1989).
20. G. Vayssilov, M. Yankov and Abdul Hamid, *Appl. Catal. A* **94**, 117 (1993).
21. T. Yashima, K. Yamazaki, H. Ahamad, M. Katsuta and Nottra, *J. Catal.* **17**, 151 (1970).
22. K.J. Chao and L.J. Len, *Zeolites* **9**, 193 (1989).

23. F. Lonyi, J. Engelhardt and D. Kallo, *Zeolites*, **11**, 169 (1991).
24. P. Ratnasamy, R.N. Bhat, S.K. Pokhriyal, S. Hegde and R. Kumar, *J. Catal.* **119**, 65 (1989).
25. J.H. Kim, S. Namba and T. Yashima, *Zeolites* **11**, 59 (1991).
25a. G. Paparatto, E. Moretti, G. Leofanti and F. Gatti, *J. Catal.* **105**, 227 (1987)
26. J. Dewing. *J. Mol. Catal.* **27**, 25 (1984).
27. N.S. Gnep, J. Tejida and M. Guisnet, *Bull. Soc. Chim.* **12**, 5 (1982).
28. J.A. Martens, J. Péréz-Pariente, E. Sastre, A. Corma and P.A. Jacobs, *Appl. Catal.* **45**, 85 (1988).
29. S. Namba, K.Inaka and T. Yashima, *Zeolites* **3**, 106 (1983).
30. R.E. Desimone, US Patent 4,665, 254 (1987) assigned to Amoco Corp.
31. H.G. Frank and J.W. Stadehofer,"*Industrial Aromatic Chemistry*" p.292, Springer verlag, Berlin, Heidelberg, 1988.
32. G.A. Olah," *Friedel Crafts chemistry*", J.Wiley & Sons, New York, (1973) p.509
33. X.P. Hugust and A. Ylla-Catala, *Afinidad*, **20**, 15 (1964). Chem.Abstr. 60 15700d (1964).
34. K. Sawazak, H. Fujii and M. Dehura, *German Patent* 2 230 369 (1973).
35 P. Kovacic and C. Wu, *J. Org. Chem.* **26**, 759 (1961).
36. E. Dibella, *U.S. Patent* 3 000 975 (1959).
37. P. Kovacic and A.K. Sparks, *J. Amer. Chem. Soc.* **82**, 5740 (1960).
38. P. Kovacic and C. Wu, *J. Org. Chem.* **26**, 214 (1961).
39. P. Kovacic, C. Wu and R.W. Stewart, *J. Amer. Chem. Soc.* **82**, 1917 (1960).
40. J.C. Graham, *U.S. Patent* 4 013 730 (1977); Chem. Abstr. 87, 5605g (1977).
41. J.C. Graham, *U.S. Patent* 4 031 147 (1977); Chem. Abstr. 87, 39074r (1977).
42. J.C. Graham, *U.S. Patent* 4 031 147 (1977); Chem. Abstr. 87, 39074r (1977).
43. E.P. Dibella and J. Wardzel, *French Patent* 1 491 143 (1969); Chem. Abstr., 69, 35666y (1967).
44. F. Muhtadi and M. Mass, *Brit. Patent* 1153746 (1970); Chem. Abstr., 69, 3566y (1970).

45. N. Kamigata, T. Satoh, M. Yoshida, H. Matsuyama and Kameyama, *Bull. Chem. Soc. Jpn.* **61**, 2226 (1988).

46. A. Botta, H.J. Buysch and I. Puppe, *Angew. Chem. Int. Ed. Engl.* **30**, 1689 (1991)

47. T. Nakamura, K. Shihoda and K. Yasuda, *Chem. Lett.*, 1881 (1992).

48. Th. M. Wortel, D. Oudijn, C.J. Vleugel, D. P. Roelofsen and H. van Bekkum, *J. Catal.* **60**, 110 (1979).

49. T. Suzuki and C. Komatsu, *U.S. Patent* 4 831 199 (1989).

50. Ihara, Chem. Ind., *Japanese Patent* 63-12450; 63-34129.

51. Kureha, Chem. Ind., *Japanese Patent* 63-34132.

52. A.G. Bayer, *German Patent*, DE 3 930 839 (1989).

53. P. Ratnasamy, A.P. Singh and P.N. Joshi, *Ind. Pat.*, 926/DEL/1992.

54. A.P. Singh, S.B. Kumar and P.N. Joshi, *Ind. Pat.* (applied)

55. A.P. Singh, S.B. Kumar and Anuj Raj, *J. Catal.*, (communicated)

56. A.P. Singh and S.B. Kumar, *J. Chem. Soc. Chem. Commun.* (communicated)

57. C.T.W. Chu and C.D. Chang, *J. Phys. Chem.* **89**, 1569 (1985).

58. R. Kumar, G.N. Rao and P. Ratnasamy, *Stud. Surf. Sci. Catal.* **49B,** 1141 (1989).

59. L. Yang, Y. Aizhen and Q. Xu, *Appl. Catal.* **67**, 169 (1991).

60. A. Corma, in *"Guidelines for Mastering the Properties of Molecular Sieves"*, (D.Barthomeuf, E.G Derouane and W. Hölderich, Eds.) NATO, ASI Ser. B: Physics, Vol. 221, p.299. Plenum Press, New York, 1990.

61. G. Mirth and J.A. Lercher, *J. Catal.* **132**, 244 (1991).

62. J. Dewing and J. Dwyer, *Zeolites* **12**, 431 (1992).

63. a. J. Wei, *J. Catal.* **76**,433 (1982).

b. C. Bezouhanova, C. Dimitrov, V. Nrnova, B. Spassov and H. Lechert, *Appl. Catal.* **21**, 149 (1986).

64. J.S. Reddy, K.R. Reddy, R. Kumar and P. Ratnasamy, *Zeolites*, **11**, 553 (1991).

65. R.J. Pellet, P.K. Coughlin, E.S. Shamshoum and J.A. Rabo, in "*Perspectives in Molecular Sieve Science*", ACS Symp.Ser. **368**, 1988, pp. 512.

66. S.M. Csissery, *J. Chem. Engg. Data* **12**, 118 (1967).

67. S.M. Csissery, *Pure Appl. Chem.* **58**, 841 (1988).

68. H.P. Braendlin, E.T. McBee, "*Friedel Crafts and Related Reactions*" Vol. 3, p. 1517. Wiley Interscience, New York, 1964 p.1517.

69. L. Delaude and P. Laszlo, *J. Org. Chem.* **55**, 5260 (1990).

70. P. De la Mare, "*Electrophilic Halogenation*", p.24. Cambridge Univ. Press, London/ New York, 1976.

Chapter 4

A CONVENIENT METHOD FOR THE SYNTHESIS OF TRANSITION METAL SILICATE ZEOLITES

4.1 INTRODUCTION

The hydrothermal synthesis of metallosilicate molecular sieves (metal ions = Al^{3+}, B^{3+}, Fe^{3+}, Ga^{3+}, Ge^{4+}, Ti^{4+}, V^{4+} etc.) is an important area in the field of molecular sieve chemistry. Metallosilicate molecular sieves are often prepared from basic gel under hydrothermal conditions. Much depends on the solubility of the metal oxides in basic medium. Thus the metal ions may, broadly, be classified into two types 1) metal ions which form insoluble metal oxides (e.g. Fe^{3+}, Ti^{4+}, Zr^{4+}) in basic medium and 2) metal ions which form soluble metal oxides in basic medium (e.g. Si^{4+}, Al^{3+}, Ga^{3+}, V^{4+}). In the case of type 1 metal ions, it is necessary to avoid the formation of metal oxide/hydroxide phases. The precipitation as oxides in such cases inhibits the incorporation of the metal ions into the framework of zeolite. Therefore, the gel preparation procedures of type 1 metallosilicates require rigid precautions such as definite sequence of addition of specific reactants, and their careful and slow addition. In conventional procedures, it is a prerequisite to use the silica source having low molecular weight silicate species *[1,2]* which can combine easily with metal ions to form metallosilicate species. Tetraethylorthosilicate (TEOS) or sodium silicate are commonly used as silicate sources. The basic silicate solution is added to the metal ion solution very carefully to avoid the precipitation of oxides/hydroxides *[2]*. To hydrolyze the ester bonds in TEOS, acidic metal salt solution or basic template solution is added followed by the slow addition of the metal ion solution in a diluent such as isopropyl alcohol (in case of titanium) *[1]* or dilute sulfuric acid (in case of iron) *[2]*. Jacobs *et al. [3]* prefer the addition of titanium solution at 0°C till the formation of a small amount of precipitate. On appearance of a precipitate the addition should be stopped till a clear solution is obtained. The addition is continued in a similar way to get a clear solution. Though

these methods alongwith others are claimed to produce metallosilicates, a more general, convenient and reproducible synthesis method for the preparation of these metallosilicates is desirable. Aiming for the successful preparation of type 1 metallosilicates, the use of chelating ligands to complex the type 1 metal ions to avoid their instantaneous precipitation in basic medium was explored. Oxalic acid and acetylacetonate form stable metal chelate complexes with metal ions at low pH. However, these tend to dissociate at high pH *[4-6]* to give the corresponding metal ions. The dissociation takes place in a stepwise manner to liberate metal ions which precipitate as metal oxide. However, in the presence of silica they form a stable metallosilicate complex, thus avoiding the precipitation of metal oxide.

In this chapter, a general procedure for the preparation of the metallosilicates of type 1 metal ions using chelating agents is described. The use of complexes for the synthesis of titanium and ferrisilicates is described to illustrate the utility of the method. The methodology provides a flexibility in the synthesis procedures used conventionally and can be applied to other metal ions to incorporate them in the zeolite framework with the appropriate choice of ligand.

4.2 EXPERIMENTAL

The syntheses were carried out in 100 ml stainless steel autoclaves (Fig 2.1). The autoclaves were cleaned thoroughly with HF (10% aqueous) before use in synthesis. The raw materials used for the synthesis are given in Table 4.1

4.2.1 Hydrothermal Synthesis of Titanium Silicate Molecular Sieves

Following procedures were adopted during the synthesis of titanium silicate molecular sieves

Ti-MFI-A : To a mixture of 1.1 g $Ti(OBu)_4$ and 1 g acetylacetone, 21 g TEOS was added with stirring. To this mixture 30 g tetrapropyl ammonium hydroxide was added

Table 4.1 specification of the reactants used in the synthesis

	Reagent & Source	Chemical formula	purity%
1.	Fumed Silica, S-5005, Sigma	SiO_2	99.8%
2.	Tetraethyl orthosilicate	$Si(C_2H_5)_4$	98%
3.	Ferric nitrate, BDH	$Fe(NO_3)_3.9H_2O$	98%
4.	Ferric sulphate, BDH	$Fe_2(SO_4)_2.5H_2O$	98%
5.	Oxalic acid	$(COOH)_2$	>95%
6.	Tetrapropyl ammonium hydroxide Aldrich	$(C_3H_7)_4NOH$	20% aqueous
7.	Acetylacetone BDH	CH_3COCH_3	>98%
8.	tetrabutyl orthotitanate Fluka	$Ti(OBu)_4$	98%
9.	Triethylbutyl ammonium bromide, Aldrich	$(C_2H_5)_3(C_4H_9)NBr$	98%
10.	Sodium silicate	Na_2SiO_3	SiO2 28%, Na_2O 8.8%, 63.2 H_2O

with vigorous stirring. This mixture was stirred for 20 min. To the resultant clear solution 15 g of water was added. The final reaction mixture was a clear solution (pH 11.9). This solution was autoclaved and crystallized at 433 K for 30 hours. Using this method three more sample with Si/Ti 17, 78 and 140 in gel were prepared. These sample were labelled Ti-MFI-A_1-A_4 in the increasing order of their Si/Ti ratios.

Ti-MFI-B : This method B is similar to method A used for synthesizing Ti-MFI-A sample except that acetylacetone was not added. The solution thus obtained showed the presence of a white precipitate during the gel preparation. The pH of the gel was 12.2. The crystallization was carried out at 433 K for 30 h.

Ti-MFI-C : In this case, 30 g tetrapropyl ammonium hydroxide was added to 21 g tetraethylorthosilicate. The mixture was stirred for 1 h to hydrolyze TEOS. Then a mixture of 1 g tetrabutylorthotitanate ($Ti(OBu)_4$) in 10 g isopropyl alcohol was added very slowly to form a clear titanium silicate solution. This solution was stirred for another 30 min before adding 15 g water. The pH of the final solution was 12.2. It was crystallized at 433 K for 30 h.

Ti-MFI-D : 6 g fumed silica was mixed with 30 g of TPAOH (20% aqueous) and stirred for one hour followed by the addition of a mixture of 1.1 g $Ti(OBu)_4$ and 1.0 g acetylacetone. The resultant mixture was stirred for 20 min. Finally, 20 ml water was added and stirred for another 20 min before autoclaving for crystallization. The pH of the final gel was 11.7. The crystallization was carried out at 433K for 48 h.

4.2.2 Hydrothermal Synthesis of Ferrisilicate Molecular Sieves

Following procedures were adopted during the synthesis of ferrisilicate molecular sieves

ZSM-5

Fe-MFI-A : A solution of 0.9 g oxalic acid in 10 g water was mixed with ferric nitrate (2.16 g in 10 g water) solution. This solution was added to 23 g sodium silicate (SiO_2 28.5%, Na_2O 8.8, H_2O 62.7%). The resultant mixture was stirred for 20 min before adding to it a solution of 6.36 g TEBABr (triethylbutyl ammonium bromide) in 13 g water. The color of final gel was pale lemon (pH 11.5). The crystallization was carried out at 433 K for 7 d. The color of final crystalline product was white.

Fe-MFI-B : Ferric nitrate solution was added to basic sodium silicate followed by the addition of template (TEBABr). No oxalic acid was added to ferric salt solution. The gel (pH 11.4) thus obtained was brownish red. The crystallization was carried out at 433 K for 7 d. The final product was off-white in color.

Fe-MFI-C : Sodium silicate (23 g) was very slowly added to a solution comprising ferric nitrate (2.16 g), sulfuric acid (0.75g, 98 wt.%) and water (20 g). The resultant mixture was stirred for 20 min before adding to it a solution of TEBABr in 13 g water. The final gel thus obtained (pale lemon colored; pH 11.3) was crystallized at 433 K. A white crystalline product formed after crystallization for 7 d.

The molar gel composition obtained from the method Fe-MFI-A-C is given below :

$$0.025\ Na_2O : 0.0027\ Fe_2O_3 : 0.107\ SiO_2 : 0.028\ TEBABr : 3\ H_2O : 0.007\ OX$$

Beta

Fe-BEA-A : In this method, Fe-Beta was prepared by mixing 0.62 g sodium hydroxide 0.46 g potassium hydroxide and 74 g tetraethyl ammonium hydroxide. This solution was added to 24 g fumed silica and stirred for 4 h to give a clear silicate solution. To this solution, another solution comprising of 3.74 g ferric sulfate and 2.9 g oxalic acid in 30 g water was added. A dark grey colored solution (pH= 12.5) thus formed was crystallized at 413K for 15 d.

Fe-BEA-B : This method was similar to the above method, Fe-BEA-A in all respects except that oxalic acid was not used in the synthesis. The final gel formed here was red in color. The gel remained amorphous even on heating for 20 d at 413 K.

Fe-BEA-C : The silicate solution prepared as in mehtod Fe-BEA-A was added very slowly to a solution containing 3.74 g ferric sulfate in 40 g water. The resultant grey colored gel was crystallized at 413K for 15 days.

The final gel composition was :

$0.023(Na+K)_2O$: 0.4 SiO_2 : 0.0067 Fe_2O_3 : 0.01 $(TEA)_2O$: 8 H_2O : 0.023 OX

The crystalline products were washed thoroughly in water till the pH of the solution was 7-8. The samples after drying at 393 K were further calcined to remove the template (for details see chapter 2 section 2.2.1).

4.2.3 CHARACTERIZATION

The experimental procedure for X-ray diffraction, infrared spectroscopy, ESR spectroscopy, Mössbauer spectroscopy, Scanning electron microscopy and ion-exchange capacities is described in Chapter 2 in sections 2.2.2.1 through 2.2.2.8.

4.2.3.1 Chemical Analysis

The details of procedure for chemical analysis is described in chapter 2 section 2.2.2.1. The analyses of titanium in samples was conducted by inductively coupled plasma (ICP, Perkin Elmer, model PE 1000).

4.2.3.2 Thermal Analysis

Simultaneous TG-DTA-DTG analysis of the crystalline samples were performed on an automatic derivatograph (Setaram TG-DTA92) with finely powdered alumina as reference. The thermograms of the samples were recorded under the following conditions :

Weight of the sample = 50 mg ; Heating rate = 10K min^{-1}

Sensitivity :

TG = 25 mg; DTA = 0.1 mv; DTG = 0.2 mv; Atmosphere = flowing air

4.2.3.3 Catalytic Reactions

The oxyfunctionalization of n-hexane (Aldrich 99%) was carried out in an autoclave of 100 ml capacity (Fig. 2.1) at 353K under autogeneous pressure and static conditions. Typically, 200 mg of TS-1 catalyst, 10 g of alkane (n-hexane) and required amount of 28 wt% aqueous H_2O_2 were mixed in 20 ml acetone (solvent). The reaction was carried out for 10 h at 353 K. After completion of the reaction the autoclave was cooled to 273 K and the reaction mixture was filtered to separate the catalyst. The products were analyzed by G.C. (HP 5890 series II) using a capillary (50m; crosslinked methylsilicone gum) column and flame ionization detector (FID).

Phenol hydroxylation was carried out in a batch reactor. In a typical reaction, 200 mg of TS-1 catalyst was added to 1 g phenol and 8 g of acetone. The mixture was vigorously stirred and the required amount of 28 wt% aqueous H_2O_2 was then added. After completion of the reaction, the products were analyzed by G.C. (50m; crosslinked methylsilicone gum) column and flame ionization detector (FID).

4.3 RESULTS AND DISCUSSION

4.3.1 Titanium silicate molecular sieves

4.3.1.1 Synthesis

Titanium silicate molecular sieves (TS-1) were first reported by Taramasso et al.*[7]*. They were found to be active in oxidation reactions like oxidation of phenol to dihydroxybenzenes, primary alcohols to aldehydes, secondary alcohols to ketones, ammoximation of ketones to oximes etc. In the synthesis of titanium silicates, the

precipitation of titanium as oxides inhibits the incorporation of titanium into zeolite framework. The use of acetylacetone as a complexing agent for titanium prevents the precipitation of TiO_2 during the addition of basic template to the titanium containing silicate mixture.

The molecularity of titanium alkoxides conventionally used in the synthesis of titanium silicates molecular sieves is four in the pure forms (Fig.4.1) and three in solution *[8,9]*. β-diketones (e.g. acetylacetone) with titanium alkoxides forms monomeric $Ti(OR)_2(acac)_2$ species *[9]*. These species can further undergo hydrolysis or ligand exchange reaction to form, Si-O-Ti linkages. The formation of titanosilicate (through formation Si-O-Ti linkages) prevents the precipitation of titanium. This is a prerequisite for the formation of a good titanium silicate zeolite. Further, β-diketones act as chelates and liberate metal ions (Ti) slowly (through stepwise dissociation of the bonds), facilitating its complexation with silica.

These facts are demonstrated using different procedures of synthesis. In method A, titanium alkoxides and acetylacetone are mixed to form a complex. This solution is added to TEOS followed by the addition of TPAOH. The basic template can be added immediately since the dissociation of complex takes place slowly and in stepwise manner avoiding the instantaneous formation of titanium oxide. To demonstrate the effect of the addition of acetylacetone, Ti-MFI-B sample was prepared by similar procedure used for Ti-MFI-A except that acetylacetone was not added. A reference sample is prepared (Ti-MFI-C) using proven methods for Ti-silicates *[10]* for comparison. This method involves the hydrolysis of TEOS with basic template (TPAOH) to generate monomeric silicate species. At this stage tetrabutyl orthotitanate (having a dissociation constant lower than TEOS) in isopropyl alcohol can be added very slowly to avoid precipitation of titanium.

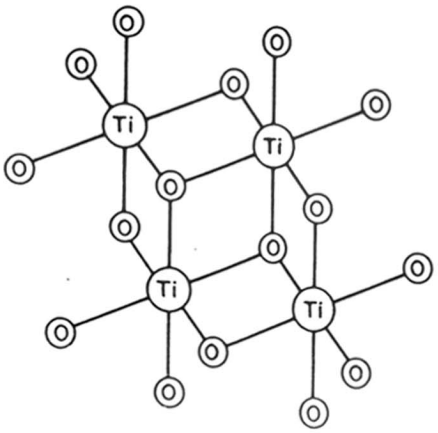

A

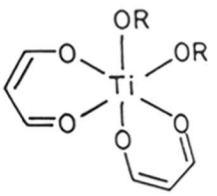

B

Fig. 4.1 A: Tetrameric titanium alkoxide species *[9]* and B: Monomeric titanium dialkoxide bis(acetylacetone)*[10]*.

In Ti-MFI-D, the successful use of silica gel is demonstrated using complexing agents. In our method, Fumed silica is hydrolysed using basic template before adding to it the titanium acetylacetone complex solution. The final mixture was a clear solution indicating the absence of any oxide or hydroxide phases.

4.3.1.2 Characterization

4.3.1.2.1 Chemical analysis

The chemical analyses of the samples Ti-MFI-A to D are given in Table 4.2. Sample Ti-MFI-A_1 to A_4 were prepared according to method A (Sample Ti-MFI-A_2) having different Si/Ti molar ratio. The incorporation of titanium for samples in gel and products are similar except for sample Ti-MFI-B. This shows that the use of acetylacetone does not hamper the incorporation of titanium into the zeolite framework.

4.3.1.2.2 Powder X-ray diffraction

The powder X-ray diffraction pattern of the calcined TS-1 samples were similar to that of ZSM-5 zeolites. The symmetry of the calcined TS-1 was orthorhombic (Fig 4.2 B-H). As expected, calcined silicalite-1 had a monoclinic symmetry (Fig 4.2 A). The persistence of the orthorhombic symmetry even in the calcined state in the titanium silicates is probably indicative of the location of Ti in the zeolite framework *[11]*. The replacement of Si by the larger titanium ions in the tetrahedral zeolite framework causes an expansion in the unit cell volume with the increasing Ti content. In Fig 4.3, the unit cell volume for sample Ti-MFI-A_1 to A_4, B, C, D and Silicalite-1 (Si-1) are plotted against mole fraction of titanium. A linear increase in the unit cell volume with increase in the mole fraction of Ti (X = Ti/Si+Ti) suggests the presence of titanium in the framework. However, a slight deviation from the line is observed for sample A_1 (x = 0.0526) and B (x=0.0212) indicating the presence of some titanium in extra framework positions. Further, the sample Ti-MFI-B shows a lower value for unit cell

Table 4.2 : Physico-chemical Characterization of titanium silicate molecular sieves prepared by complex method.

Sample	Si/Ti		Ti/Si+Ti	unit cell volume	I_{960}/I_{550}	crystal size μm
	Gel	product				
Ti-MFI-A_1	17	18	0.0526	5362.51	0.62	nd
Ti-MFI-A_2	33	32	0.0303	5357.77	0.61	0.8
Ti-MFI-A_3	78	77	0.0128	5349.75	0.30	nd
Ti-MFI-A_4	140	135	0.0074	5347.40	0.24	nd
Ti-MFI-B	33	45	0.0212	5347.72	0.34	1.2
Ti-MFI-C	33	27	0.0357	5358.24	0.62	0.3
Ti-MFI-D	33	30	0.0322	5356.50	0.60	1.0
Si-MFI	-	>2000	0.000	5345.12	0.00	nd

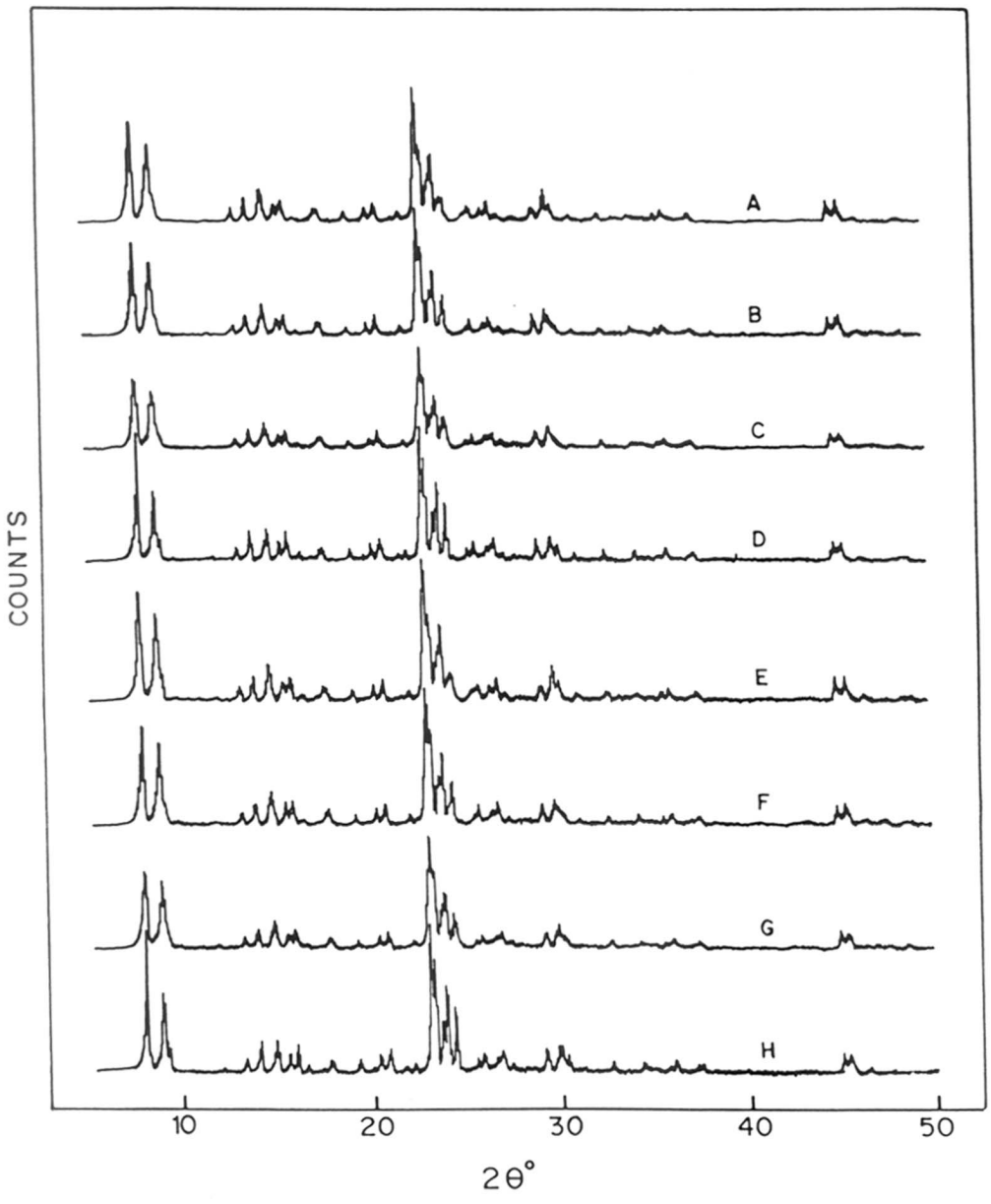

Fig. 4.2 X-ray diffraction patterns of silicalite-1 (A) and various Ti-MFI samples B-E :samples Ti-MFI-A_1-A_4 and F-H: Ti-MFI-B, Ti-MFI-C and Ti-MFI-D, respectively.

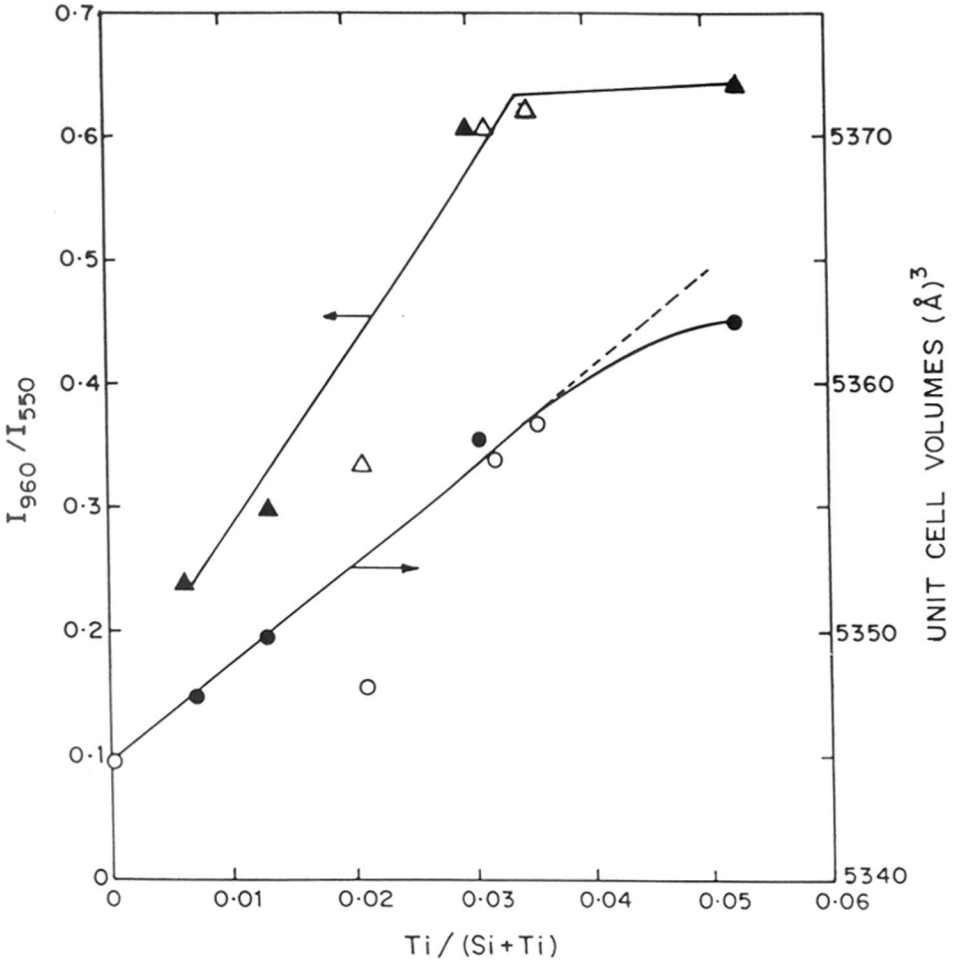

Fig. 4.3 A plot of the ratio of intensities of 960 and 550 cm^{-1} IR bands and the unit cell volume vs mole fraction of titanium in various TS-1 samples. ratio of IR intensities, I_{960}/I_{550}, ▲, A_1-A_4, Δ; B-D, XRD unit cell volumes, ●, samples A_1, A_2, A_3 and A_4 and o, samples B-D.

volumes compared to the reference sample Ti-MFI-C. The unit cell volume for Ti-MFI-D is also similar compared to that of sample Ti-MFI-A_2 and C indicating the incorporation of titanium in the framework.

4.3.1.2.3 Framework infrared spectroscopy

Fig 4.4 illustrates the IR spectra of calcined samples Ti-MFI-A through D. An absorption band at 960 cm^{-1} has been observed in case of all titanium containing samples. Infrared spectra of samples Ti-MFI-A_1 to A_4 and silicalite-1 (Si-MFI) are given in Fig. 4.5. The relative intensity of 960 cm^{-1} to the intensity of the band at 550 cm^{-1} versus mole fraction of titanium is plotted in Fig 4.3. A linear increase in the I_{960}/I_{550} ratio with titanium content indicates the incorporation of titanium in the framework. Boccuti *et al.[13]* assigned this band to the Si-O stretching vibration of the polarized Si-O-Ti bond.

4.3.1.2.4 UV-VISIBLE spectroscopy

The diffuse reflectance electronic absorption spectroscopy (DREAS) is a sensitive technique to qualitatively evaluate the presence of framework and extraframework forms of titanium *[15,16]*. The presence of an absorption band at ≈ 212 nm indicates the presence of titanium in the framework *[15]*. The presence of extraframework titanium species appear at 250-280 nm, while the presence of any anatase impurity is seen around 330 nm.

The diffuse reflectance spectra of samples Ti-MFI-A-D are presented in Fig. 4.6. While samples Ti-MFI-A, C and D possess a strong peak at ≈210±5 nm, sample Ti-MFI-B shows a weak peak in this region and also has an additional peak at ≈ 274 nm indicating the presence of octahedral titanium. Samples Ti-MFI-A_1 to A_4 also exhibit a peak at 212 nm (Fig. 4.7). The presence of an additional peak in sample Ti-MFI-A_1 around 330 nm may be due to the presence of an anatase phase in the

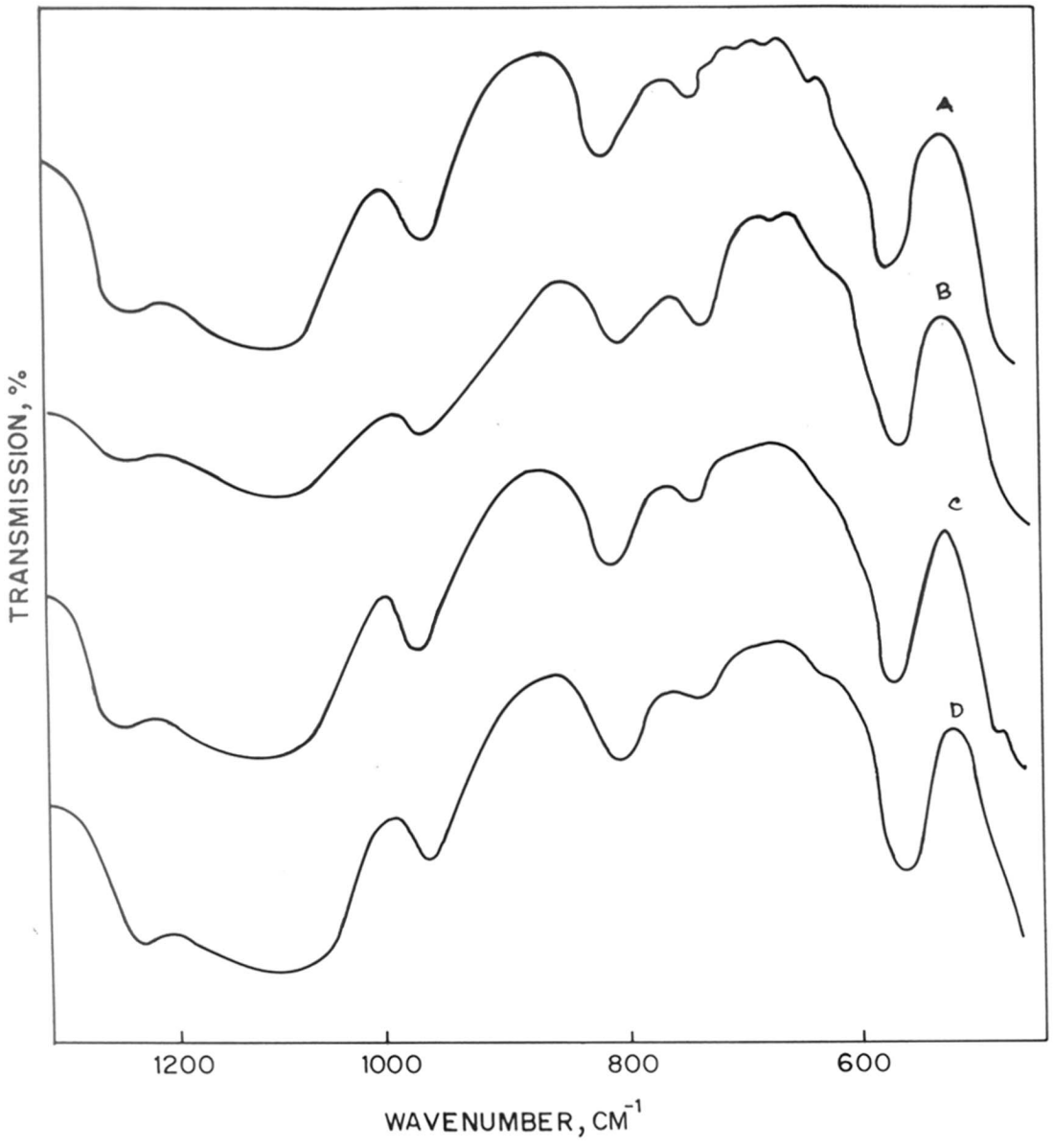

Fig. 4.4 Framework infrared spectra of TS-1 samples. Curves A-D represent samples Ti-MFI-A, B, C and D, respectively.

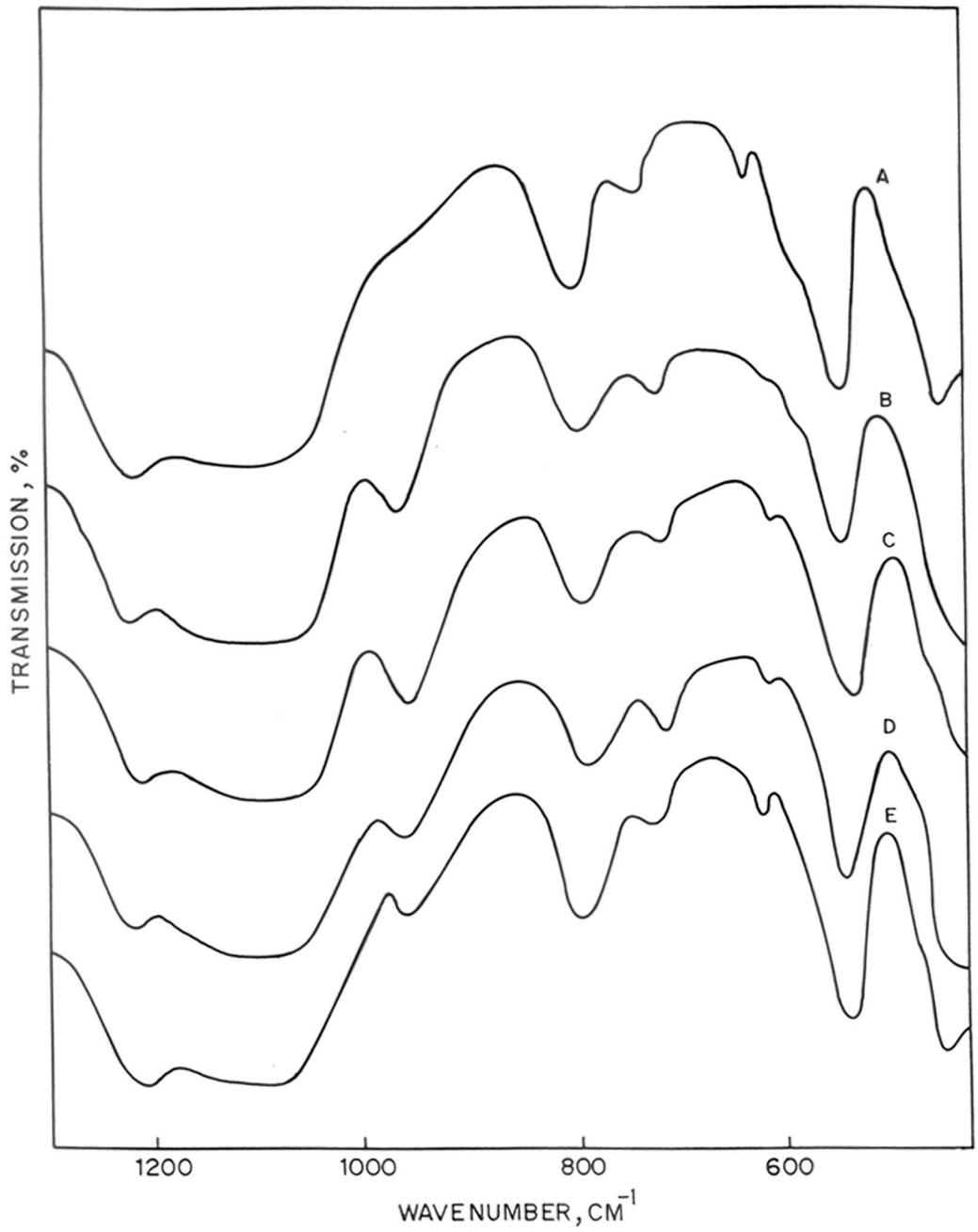

Fig. 4.5 Framework infrared spectra of silicalite-1 and TS-1 samples
Curve A : Si-MFI, B-E represent samples Ti-MFI-A_1, A_2, A_3 and A_4, respectively.

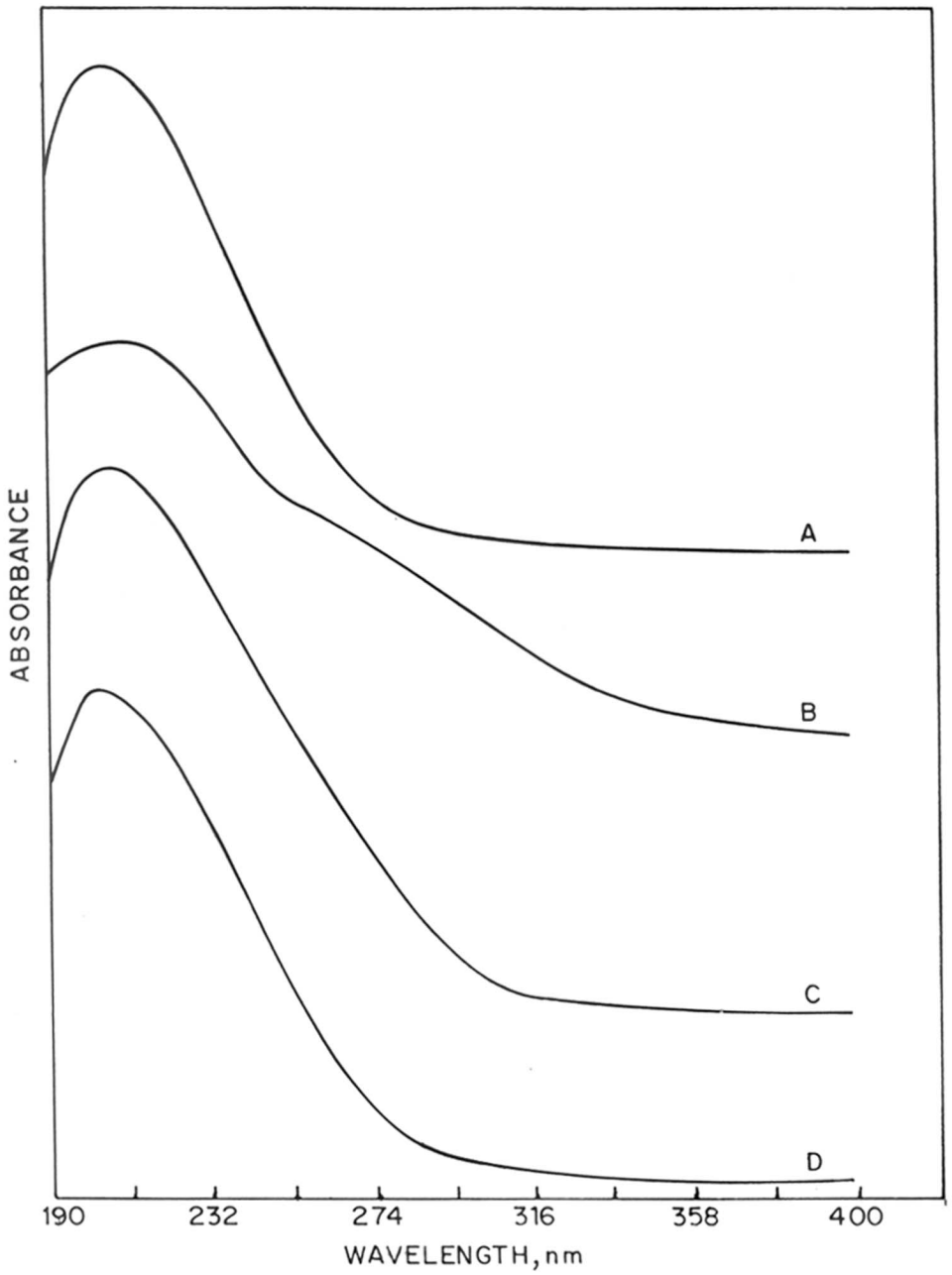

Fig. 4.6 Diffuse reflectance electronic absorption spectra for TS-1 samples curves A-D represent samples Ti-MFI-A_2, B, C and D, respectively.

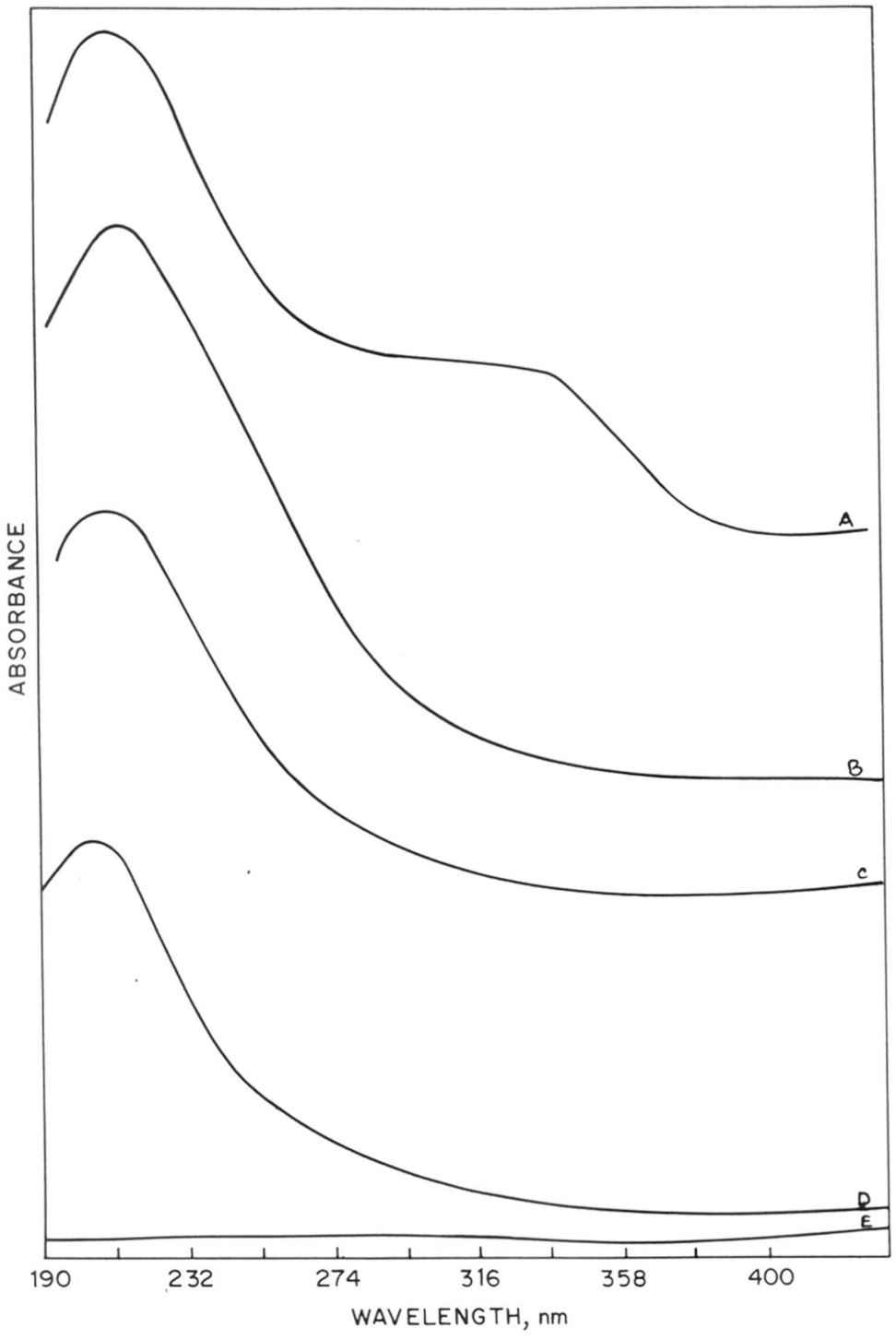

Fig. 4.7 Diffuse reflectance electronic absorption (DREA) spectra for TS-1 samples. Curves A-D represent samples Ti-MFI-A_1, A_2, A_3 and A_4, respectively and E : Si-MFI.

sample.

4.3.1.2.5 ^{29}Si MAS NMR spectroscopy

Fig. 4.8 illustrates the ^{29}Si MAS NMR spectra of sample Ti-MFI-A to D calcined at 823K. The samples from Ti-MFI-A, C and D show the presence of a broad peak at δ = -116 ppm. This peak has been attributed to the distorted silicon environment in the tetrahedra containing Si-O-Ti bonds of the zeolitic framework *[10,11,16]* . It is known for titanium silicates that as the titanium content increases, the linewidths broaden progressively *[11,16]*. The sharpening of peaks in sample Ti-MFI-B imply lower incorporation of titanium in the framework.

4.3.1.2.6 ^{13}C NMR spectroscopy

Fig 4.9 shows the ^{13}C CP MASNMR of the as-synthesized samples of Ti-MFI-A_2 (using acetylacetone, Si/Ti =33) and Ti-MFI-C (reference, Si/Ti = 33). Both samples exhibit the same ^{13}C lines (at δ =9.63 ppm and 10.44 for -CH_3, δ = 62.16 for -CH_2- and δ = 105.40 ppm for N-CH_2- characteristic of template TPA^+ (Tetrapropyl ammonium cation)*[18]*. The peaks for acetylacetone are present at 25 and 31 ppm for methyl carbons of keto and enol forms, and 101.3 ppm for enol form. Two peaks are present in the range of 180-205 ppm for carbonyl carbon of both enol and keto forms *[19]*. The absence of such peaks in the sample Ti-MFI-A_2 show the absence of any occluded acetylacetone in the zeolite as detected by NMR.

4.3.1.2.7 X-ray Photoelectron Spectroscopy or ESCA

The presence of a peak at 459 e.v. indicates titanium in the silicate framework while the oxidic titanium has a shift to the lower binding energy side and is seen around 456 e.v. Carati *et al. [12]* have characterized the presence of non-framework titanium species by this technique in TS-1. Similar results are reported for TS-2 (titanium silicate with MEL structure) *[21]*.

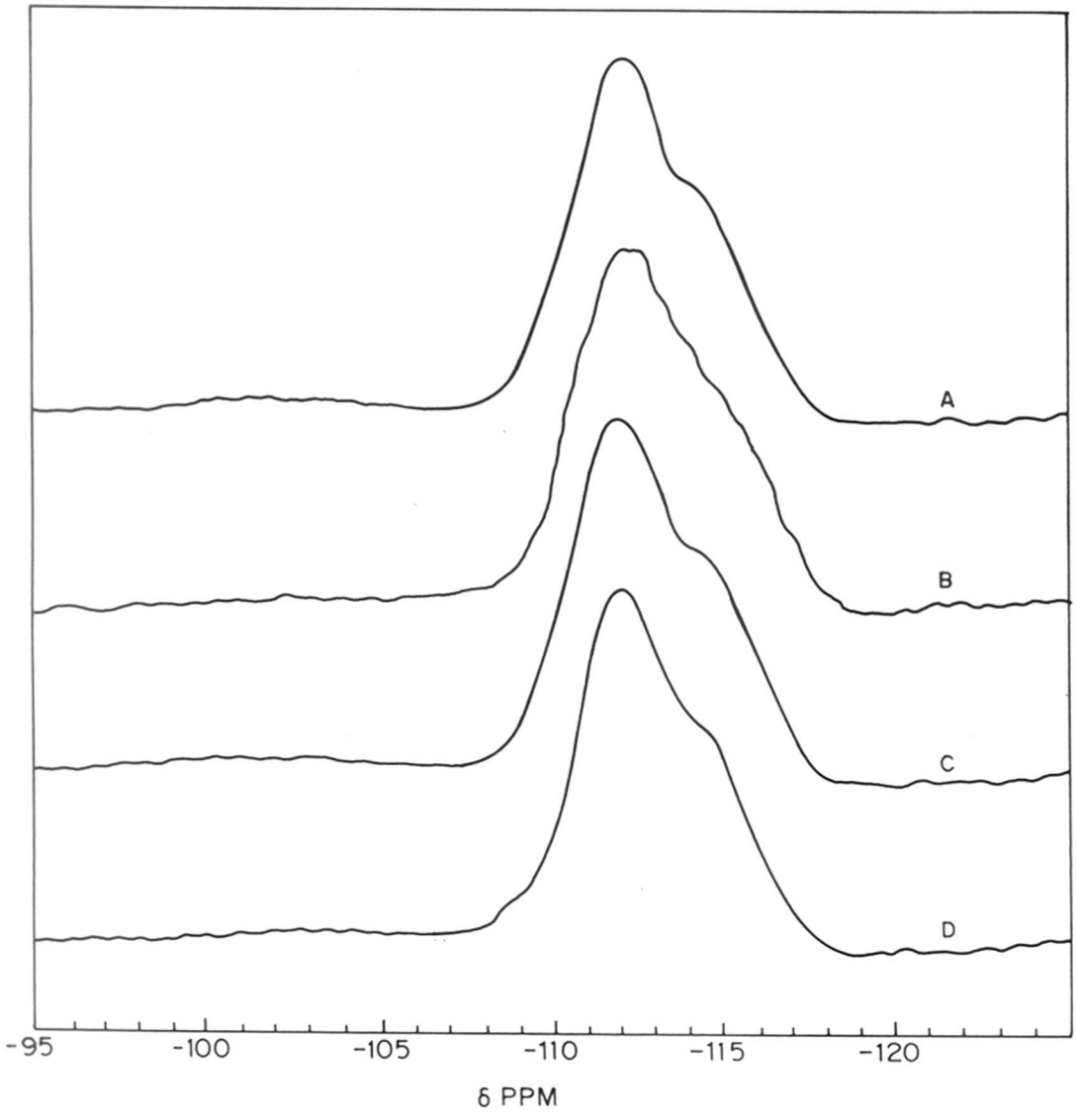

Fig. 4.8 ^{29}Si MAS NMR spectra of TS-1 samples
curves A-D represents samples Ti-MFI-A_2, B, C and D.

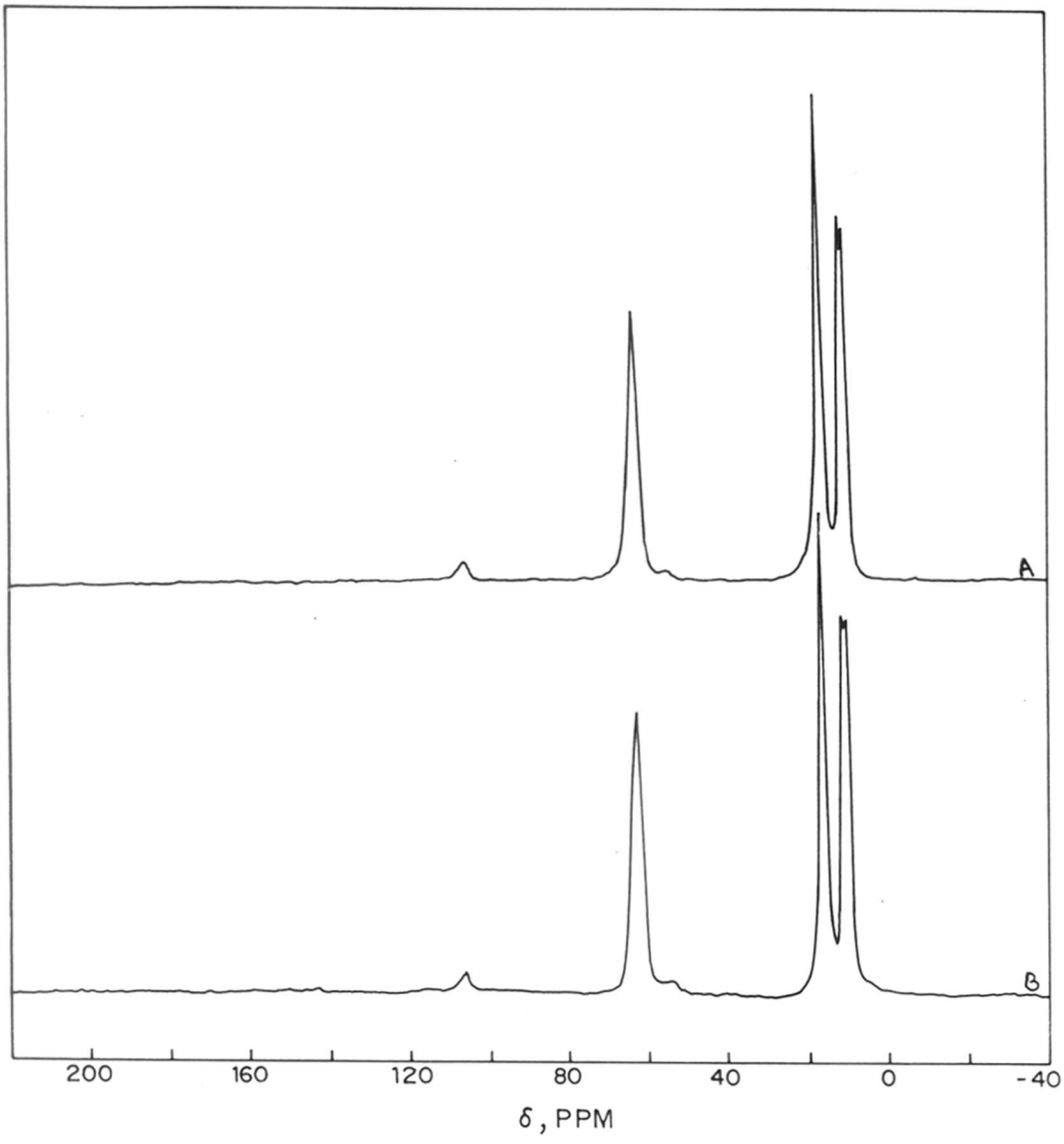

Fig. 4.9 ^{13}C CP MAS NMR spectra of TS-1 samples.
curve A : sample Ti-MFI-A_2 and B: sample Ti-MFI-C.

Table 4.3 summarizes the XPS data for various titanium silicates. The binding energy for $Ti_{2P1/2}$ and $Ti_{2P3/2}$ for sample-Ti-MFI-A_1, A_2, B and D are given. The sample Ti-MFI-A_1 shows a doublet for Ti_{2P}, the peak at lower binding energy value corresponds to TiO_2 as mentioned above.

4.3.1.2.8 Scanning electron microscopy

Fig.4.10 A, B and C correspond to the scanning electron micrographs of the samples Ti-MFI-A, C and D. The micrographs of the samples indicate that these samples are highly crystalline and free from amorphous material. The samples prepared by complexing titanium Ti-MFI-A (*ca.* 0.5-1μm) and D (ca. 0.8-1.2 μm) have crystal sizes larger than that of the reference sample, Ti-MFI-C (*ca.*0.2-0.5 μm).

4.3.1.2.9 Thermal analysis

DTA-TG curves exhibited by as-synthesized samples Ti-MFI-A_2 and Ti-MFI-C (Table 4.4) show similar weight loss due to organic and TPA per UC (11.2 and 11.4 wt% and 3.5 and 3.6 for samples Ti-MFI-A_2 and C, respectively). Rollman and Valyocsik *[23]* have reported a saturation value of 0.05 for the TPA/SiO_2 molar ratio, in the case of Al-ZSM-5 synthesis, which corresponds to approximately 3-4 TPA molecules per unit cell. Boxhoorn et al. *[24]* have reported 3.3-3.8 molecules of TPA^+ cations per unit cell in ZSM-5 samples. The values of TPA/UC for samples Ti-MFI-A (3.5) and Ti-MFI-C (3.6) match very well with reported literature. While the Ti-MFI-B sample shows lower TPA/UC (3.0). Since this sample possesses good XRD crystallinity, the extraframework TiO_2 present in the pores may reduce the overall concentration of TPA^+ in the solid.

4.3.1.2.10 Catalytic studies

The titanium silicate samples synthesized by various methods were also characterized through catalytic tests in oxyfunctionalization of n-hexane and hydroxylation of phenol.

Table 4.3 : XPS data for titanium silicates

Sample	Binding Energy (e.v.)			
	O1s	Si2p	Ti2p1/2	Ti2P3/2
Ti-MFI-A_1	539.0	109.0	456.44 457.16	462.08 464.64
Ti-MFI-A_2	540.0	111.0	459.04	464.60
Ti-MFI-B	539.2	110.4	-	-
Ti-MFI-C	539.44	109.6	459.4	464.96
Ti-MFI-D	540.52	111.0	458.2	464.48

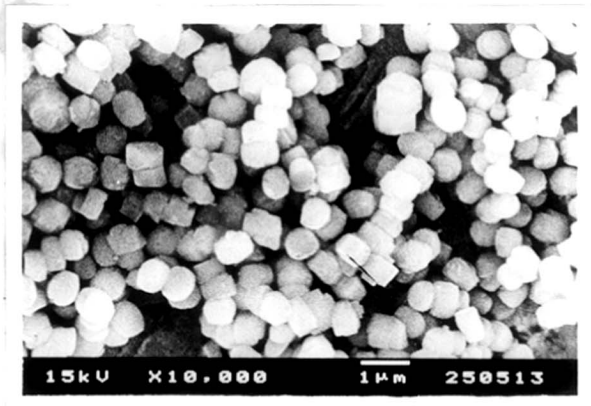

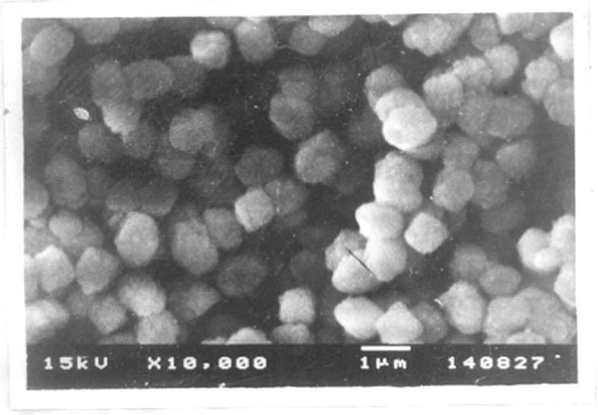

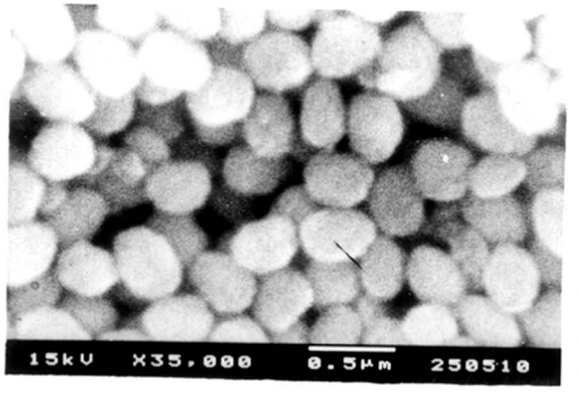

Fig. 4.10 Scanning electron micrographs of samples Ti-MFI-A_2 (A), Ti-MFI-D (B) and Ti-MFI-C (C).

Table 4.4 : Thermal Analysis for samples prepared by different methods.

Sample	organic weight loss	No. of template molecules per unit cell
Ti-MFI-A_2	11.2	3.5
Ti-MFI-B	9.6	3.0
Ti-MFI-C	11.4	3.6

Recentiy, Tatsumi *et al.[25]* and Huybrechts *et al. [26]* have shown that the titanium silicate molecular sieves TS-1 are able to catalyze selectively the oxidation of alkanes in the presence of H_2O_2 with good selectivities to monooxygenates. The results of oxyfunctionalization of n-hexane for samples A_1 to A_4 B, C and D are given in Table 4.5. Ti-MFI-A_2 sample prepared by complexing titanium with acetylacetone gives high selectivities for H_2O_2. The activities and selectivities are comparable to the reference sample Ti-MFI-C. While the sample Ti-MFI-B (prepared by method B, similar to method A without using acetylacetone) gives lower selectivity for oxidation. It is known that the high selectivities for oxidation are observed when titanium is in the framework, whereas the presence of precipitated oxide or titanate phase lowers the selectivity for oxygenated products *[25]*. The sample synthesized using fumed silica and acetylacetone (Ti-MFI-D) was also found to be comparable in activity and selectivity to the reference sample.

The results of hydroxylation of phenol are given in Table 4.6. The activity of samples Ti-MFI-A_2 and D were similar to the sample Ti-MFI-C (reference sample). The sample Ti-MFI-B once again shows poor activity which seems to be due to the presence of extralattice titanium. In this sample the selectivity for parabenzoquinone is high which is formed by the further oxidation of hydroquinone. Lower selectivity for hydrogen peroxide was observed for samples with lower titanium contents (samples Ti-MFI-A_3 and A_4).

4.3.2 Ferrisilicate Molecular Sieves

4.3.2.1 Hydrothermal Synthesis

In the synthesis of ferrisilicate molecular sieves, the formation of iron oxides/hydroxides hinders the incorporation of iron into the framework of zeolite during the gel preparation. The hexaaquo iron ions are present in solutions at a pH < 1. Between pH 1-2, the most predominant species is $[Fe(H_2O)_5OH]^{2+}$ *[27]*. When the

Table 4.5 : Oxyfunctionalization of n-hexane over TS-1 catalysts.

Reaction conditions : Catalyst : 0.2 g; n-hexane : 10 g; Solvent (acetone) : 20 g; reaction temperature : 353K; Time-on-stream : 10 hrs

catalyst	n-hexane conversion	Product distribution (%)			
		3-one	2-one	3-ol	2-ol
Ti-MFI-A_1	17.4	16.0	30.74	41.20	12.04
Ti-MFI-A_2	24.2	19.67	17.27	42.77	20.25
Ti-MFI-A_3	20.4	17.37	30.74	41.2	12.04
Ti-MFI-A_4	18.3	22.64	23.33	38.35	15.66
Ti-MFI-B	8.5	18.82	27.64	35.29	22.94
Ti-MFI-C	25.2	23.8	21.27	27.81	27.10
Ti-MFI-D	22.7	20.5	33.2	32.0	14.3

Table 4.6 : Phenol hydroxylation over TS-1 catalysts

Reaction conditions : Catalyst 0.2 g; Phenol : 1 g; Solvent (acetone) : 8 g; temperature : 353K, reaction time : 10 h, Phenol/ H_2O_2 (molar) : 3

Catalyst	Conversion (wt%)	Product distribution (%)[a]				*p/o*[b]
		OBQ	PBQ	CAT	HQ	
Ti-MFI-A_1	9.90	1.6	2.2	50.0	46.8	1.1
Ti-MFI-A_2	20.99	1.5	2.8	51.7	45.0	1.1
Ti-MFI-A_3	15.84	1.4	3.5	50.8	40.8	1.1
Ti-MFI-A_4	11.87	3.9	4.7	51.28	40.1	1.2
Ti-MFI-B	8.32	10.0	22.8	41.8	25.4	1.1
Ti-MFI-C	2 1.42	1.4	2.9	48.3	47.5	1.1
Ti-MFI-D	19.93	1.5	2.8	48.0	47.7	1.1

[a] : wt% of the product/conversion; CAT : catechol; HQ : hydroquinone; PBQ : paraben-zoquinone

[b] : HQ + PBQ/CAT

[c] : HQ + CAT/conversion

pH is raised above 2, the formation of hydroxo bridged species takes place which, upon further addition of base, become larger and larger eventually resulting in colloidal gels. Eventaullty iron hydroxide precipitates. The formation of iron hydroxide is a major hurdle in the preparation of a good ferrisilicate from alkaline gels required in conventional synthesis of zeolites. Oxygen donor ligands like oxalates, tartarates, citrates form stable complexes at low pH ranges but slowly dissociate in basic medium liberating the metal ions. The dissociation of the complex takes place in steps, through gradual breakage of bonds *[4]*. During such dissociation, silica can bind to form ferrisilicate gel thus avoiding the precipitation of iron as oxides or hydroxides. Once the ferrisilicate gel is formed, the precipitation of iron is avoided even at a higher pH.

Beta is crystallized from highly alkaline gels. The main source of OH^- ions is the basic template (TEAOH) as the alkali content required in its synthesis is low. Fe-Beta has been synthesized by Kumar *et al.* using TEOS *[28]*. Alternatively, silica gel can also be used as a source of silica for Beta synthesis *[29]*. The polymeric species in silica gel require depolymerization at high pH before addition of the silicate to iron. When highly basic silicate is added to the ferric salt solution, the precipitation of iron usually occurs unless a very careful and slow addition of dilute Fe^{3+} salt solution is carried out. Once the precipitation of iron takes place the gel does not form Beta structure even after crystallization for long time. Further, the ethanol formed during hydrolysis of TEOS also retards the formation of Beta *[30]* unless distilled off completely. To avoid such consequences the iron was complexed as oxalate before adding to the basic silicate solution. This resulted in the formation of good ferrisilicate gel leading to the formation of Beta.

The results of the chemical analysis of the ferrisilicates synthesized by different methods A - C are given in the Table 4.8. Sample Fe-MFI-A_2 was synthesized by complexing iron as oxalate before adding it to basic silicate solution. Sample Fe-MFI-B

Table 4.8 : Physico-chemical characterization of ferrsilicates prepared by complex method.

Catalyst	SiO_2/Fe_2O_3 molar ratio		colour		K^+/MO_2^-	ESR intensity of g=4.3 peak	Magnetic moment		Mössbauer isomer shift	Unit cell volumes
	gel	product	C/N form	calcined		AU(X1E5)	RT	LNT	δmm/sec	Å
Fe-MFI-A	45	32	White	Offwhite	0.86	37	5.6	5.9	0.24	5389.5
Fe-MFI-B	45	42	Offwhite	Brown	0.38	11	5.8	5.8	0.22 0.32	5355.3
Fe-MFI-C	45	26	White	Offwhite	0.84	32	5.6	5.7	0.23	5387.2
Fe-BEA-A	60	55	White	Offwhite	0.87	22	5.7	5.7	0.25	-
Fe-BEA-B	60	-	-	-	-	nd	nd	nd	nd	-
Fe-BEA-C	60	52	white	offwhite	0.85	24	5.6	5.7	0.25	-

were obtained in a similar way as sample Fe-MFI-A except that no complexing agent like oxalic acid was added. Sample Fe-MFI-C was obtained using conventional method *[31]*. The chemical analysis suggests that the gels and product had similar SiO_2/Fe_2O_3 ratios indicating that oxalic acid helps to avoid precipitation.

4.3.2.2 Characterization

4.3.2.2.1 Color

In ferrisilicate molecular sieves color is one of the important qualitative tests for the presence of extraframework iron *[2]*. The presence of iron oxide/hydroxide phases imparts a rust color to the gel or sample. The gels of samples Fe-MFI-A and C were pale yellow in color indicating the absence of iron oxide, whereas the gel of Fe-MFI-B sample was light brown suggesting the presence of significant amount of iron oxide (Table 4.8). The color of the final crystalline sample Fe-MFI-A and C was white (as-synthesized form) or offwhite (calcined form) indicating the absence of colored, condensed iron oxide phase in these samples. While the Fe-MFI-B gave an off-white product in the as-synthesized form it became brown in color on calcination suggesting the formation of iron oxide phases.

4.3.2.2.2 Ion-exchange capacity

The ion-exchange capacity (K^+/MO_2^-) exhibited by samples Fe-MFI and Fe-BEA are reported in Table 4.8. The high ion-exchange capacities for sample Fe-MFI-A and C and Fe-BEA-A and C show that most of the iron is incorporated into the framework sites in these zeolites. The low value of ion-exchange capacity for Fe-MFI-B indicates a poor incorporation.

4.3.2.2.3 Powder X-ray diffraction

The powder X-ray patterns suggest the presence of pure ZSM-5 phase without any other crystalline impurities (Fig.4.11) for samples Fe-MFI-A through Fe-MFI-C.

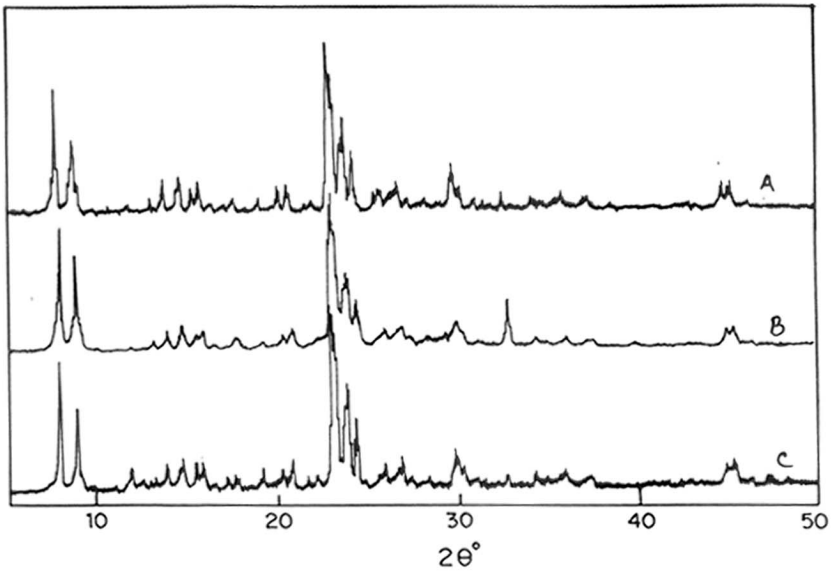

Fig. 4.11 X-ray diffraction patterns for ferrisilicate MFI samples
curves A-C represent samples Fe-MFI-A, Fe-MFI-B and Fe-MFI-C, respectively.

All the samples possessed orthorhombic symmetry, indicating the incorporation of iron into the framework. Silicalite-1 shows monoclinic symmetry (Fig. 4.2A). The samples Fe-BEA-A and Fe-BEA-C exhibited structure similar to Beta (Fig.4.12). However, the sample Fe-BEA-B remained X-ray amorphous even after prolonged crystallization.

4.3.2.2.4 ESR spectroscopy

The ESR spectra of Fe-MFI and Fe-BEA samples are given in Fig.4.13 to 4.17. These spectra reveal two signals a signal at g = 4.3 and another at g = 2.0 characteristic of ferrisilicate zeolites (for discussion see chapter 2). Table 4.8 gives the relative intensity of the samples. It can be seen from the values that the esr intensity for sample Fe-MFI-B is very low compared to the both Fe-MFI-A and Fe-MFI-C samples. This indicates better incorporation of iron in the samples Fe-MFI-A and Fe-MFI-C. In Fe-BEA-A and C the samples also exhibit similar ESR spectra (Fig. 4.16 and 4.17). Here it is important to mention that the gel of sample Fe-BEA (precipitated iron oxide) did not crystallize at all under similar conditions even after 20 days.

4.3.2.2.6 Mössbauer spectroscopy

Mössbauer spectra of the as-synthesized form of Fe-MFI-A to C are given in Fig. 4.18. These spectra exhibit a peak at δ = 0.2 - 0.3 mm/sec (Table 4.8) assigned to tetrahedral framework Fe^{3+} ions. Further, the absence of octahedral component for samples Fe-MFI-A and C indicate the presence of most of the iron in the tetrahedral framework positions. The presence of a large octahedral component in sample Fe-MFI-B indicates the presence of extraframework octahedral Fe^{3+} ions and consequently low incorporation of iron. Beta samples (Fig.4.19) also exhibits an isomer shift at δ = 0.24 mm/sec showing the presence of almost all iron in the framework.

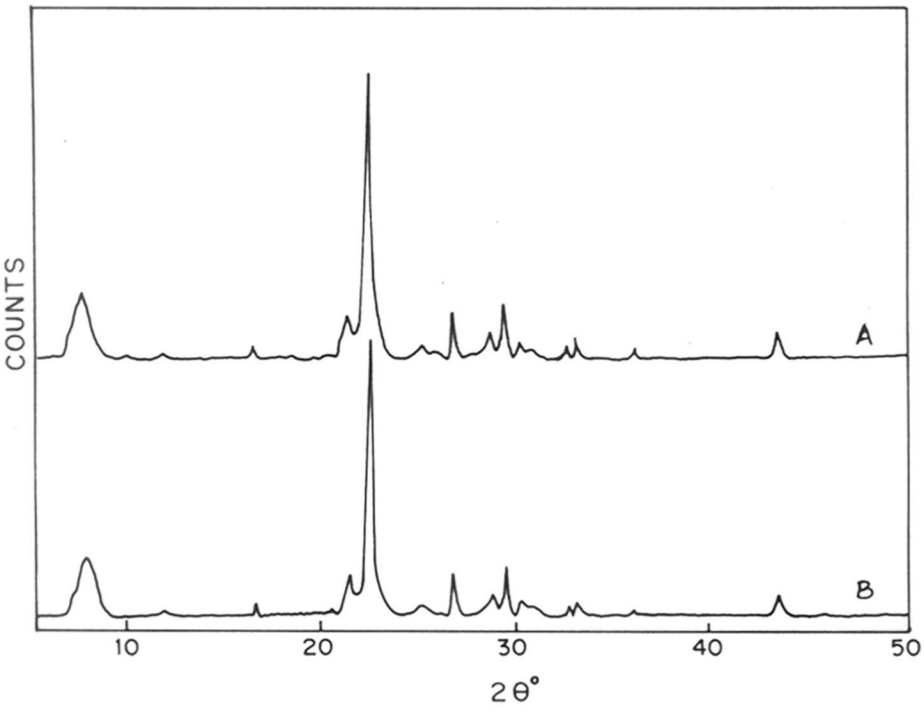

Fig. 4.12 X-ray diffraction patterns for ferrisilicate BEA samples
curves A-C represent samples Fe-BEA-A, Fe-BEA-B and Fe-BEA-C, respectively.

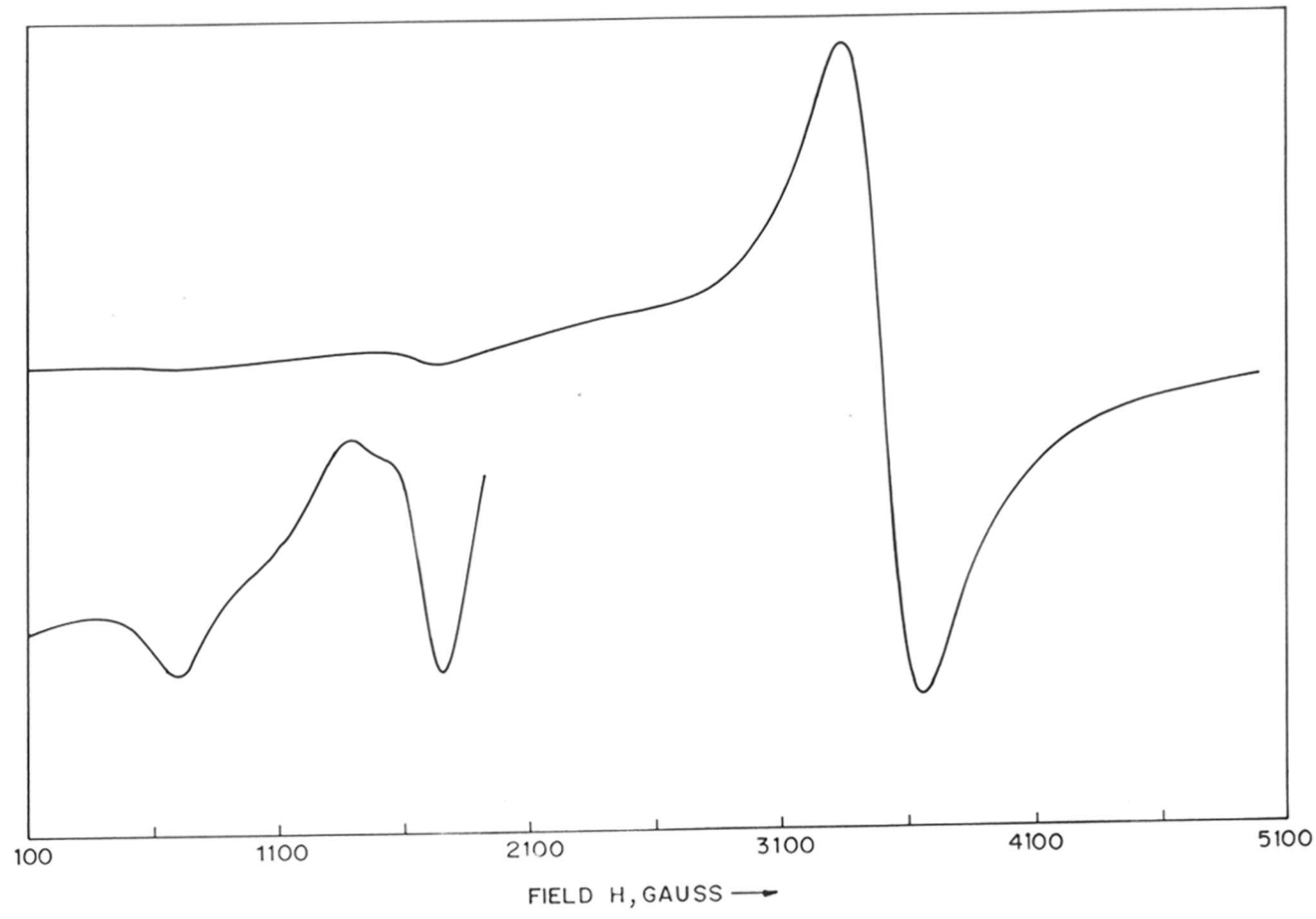

Fig. 4.13 Electron spin resonance spectrum of sample Fe-MFI-A inset expanded portion of g=4.3 peak.

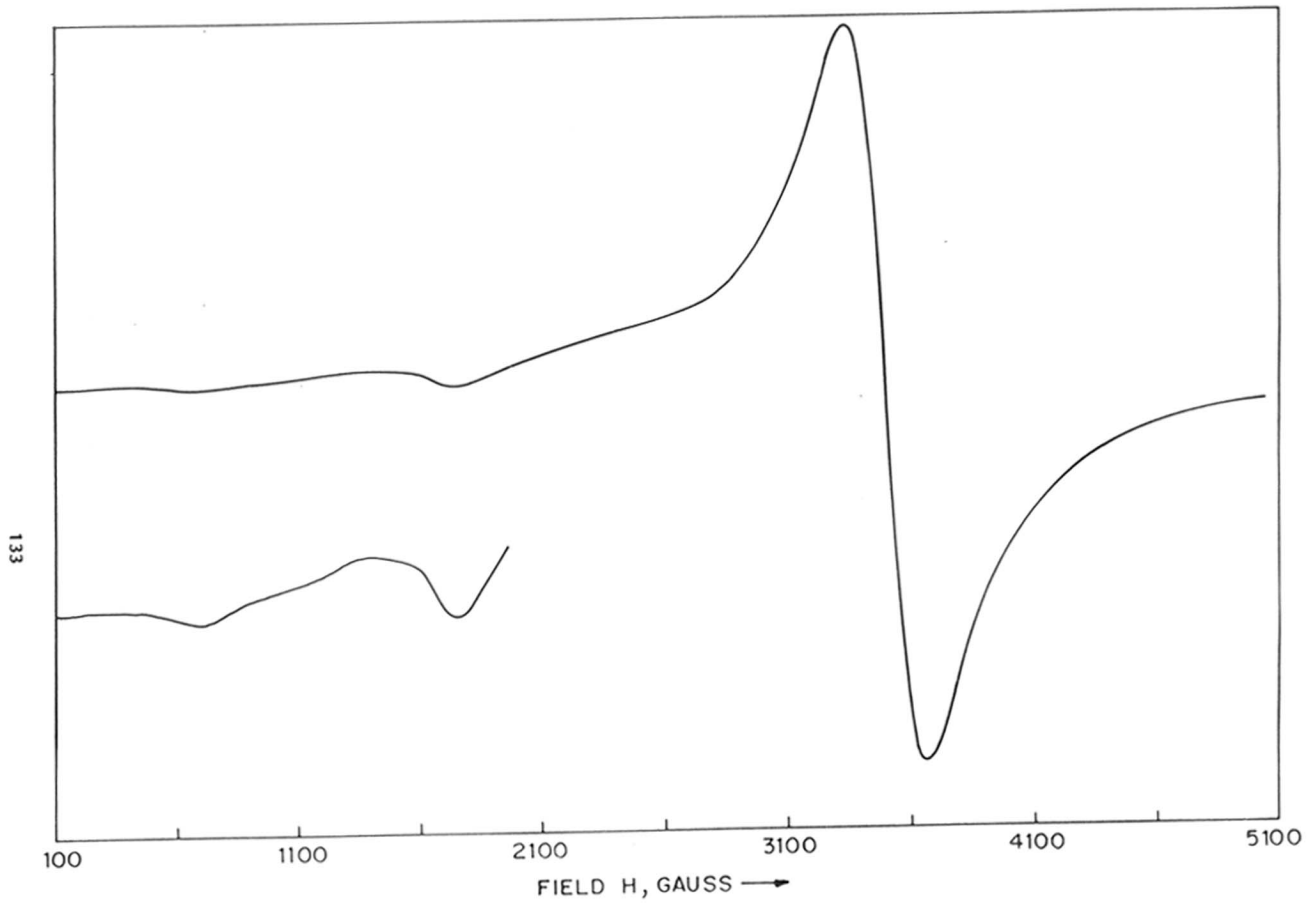

Fig. 4.14 Electron spin resonance spectrum of sample Fe-MFI-B inset expanded portion of g=4.3 peak.

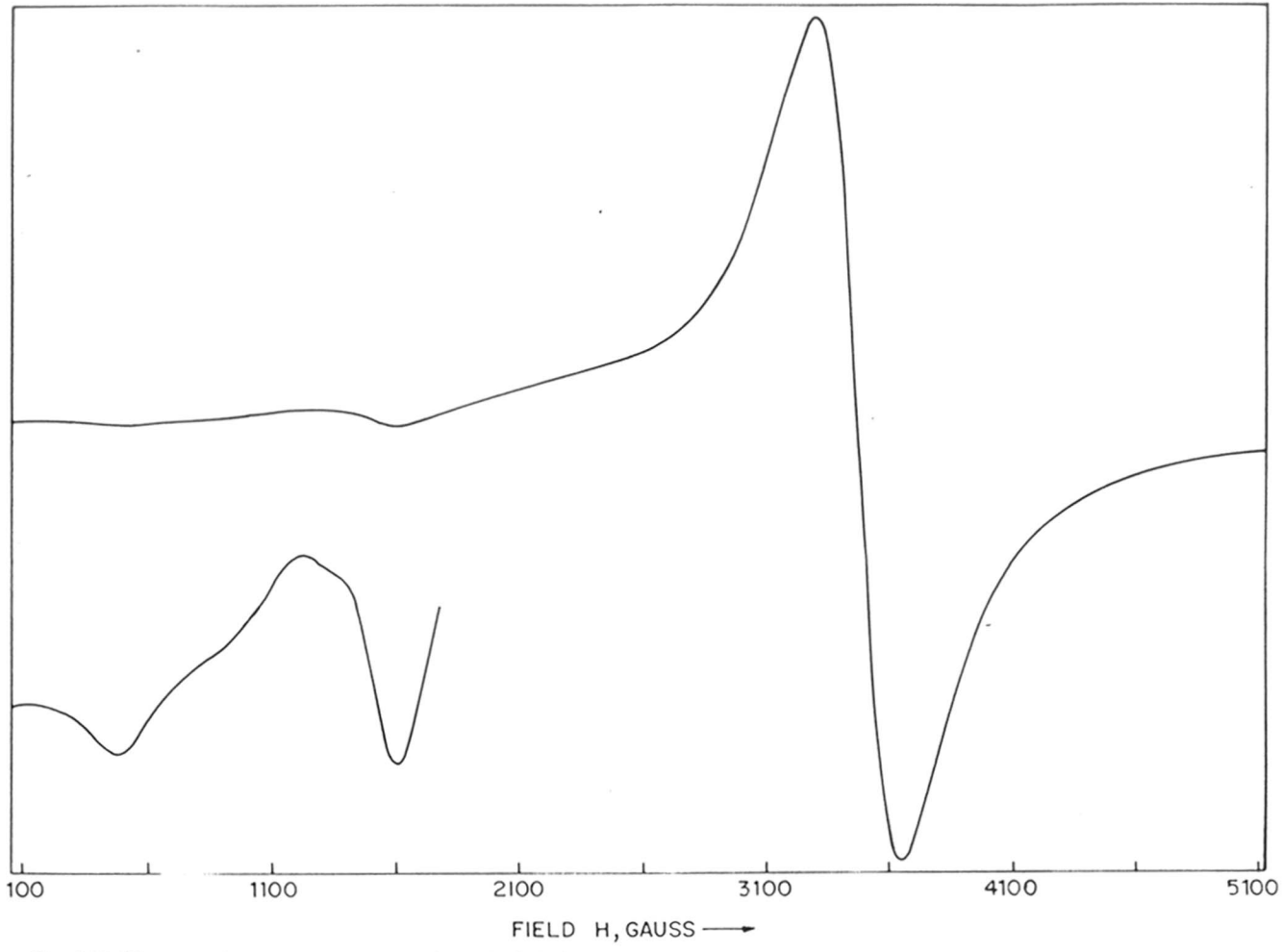

Fig. 4.15 Electron spin resonance spectrum of sample Fe-MFI-C inset expanded portion of g=4.3 peak.

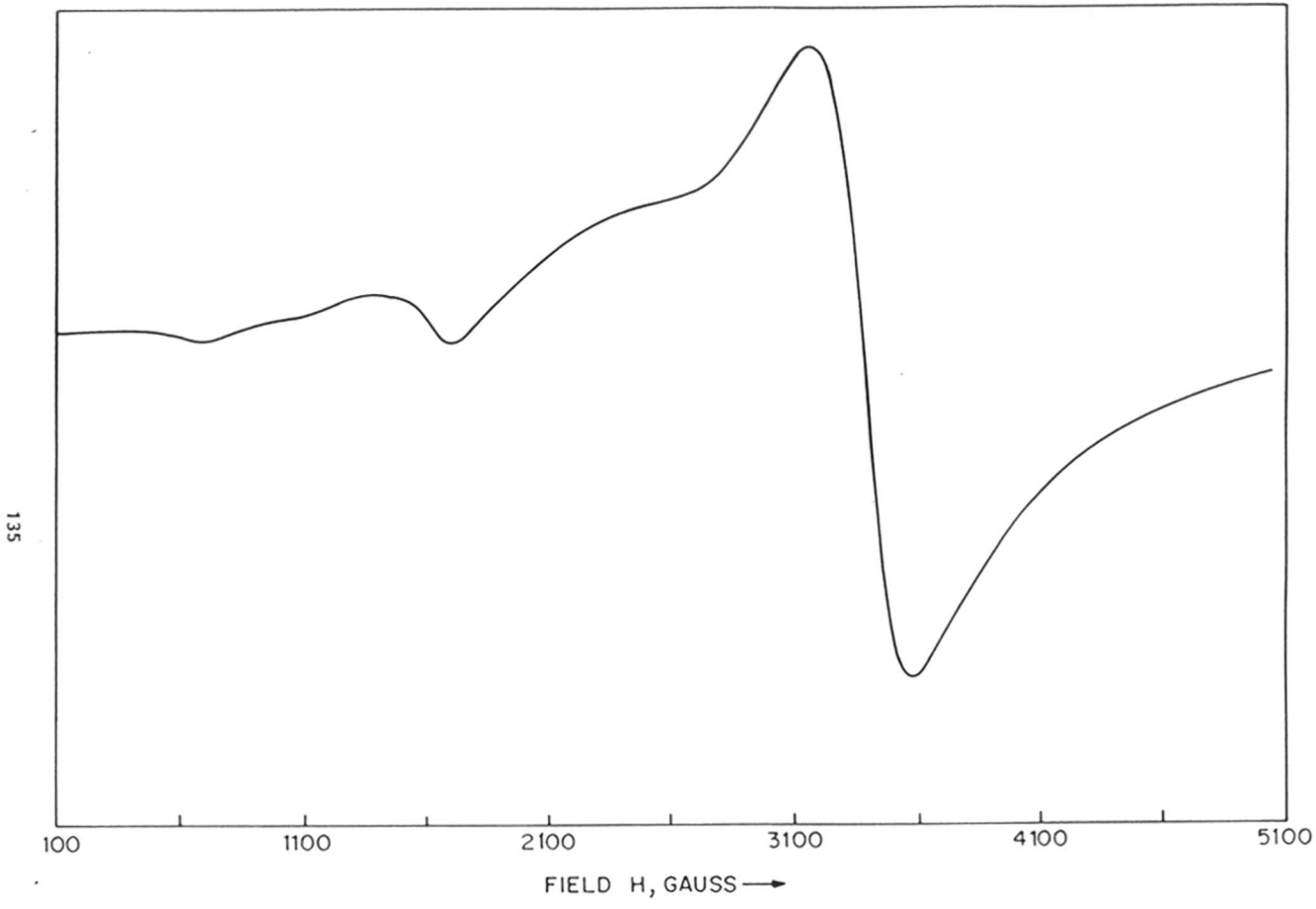

Fig. 4.16 Electron spin resonance spectrum of sample Fe-BEA-A.

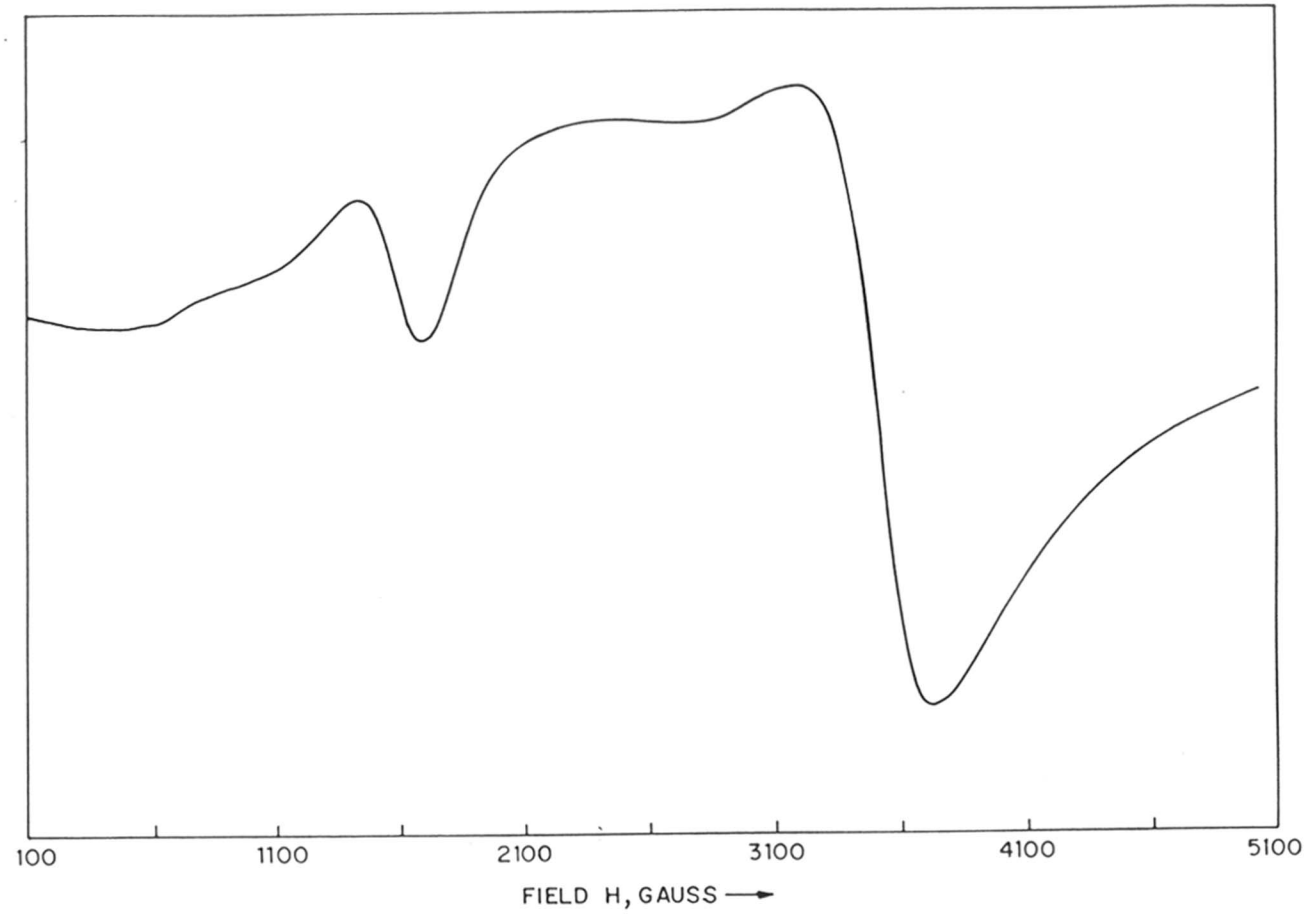

Fig. 4.17 Electron spin resonance spectrum of sample Fe-BEA-C.

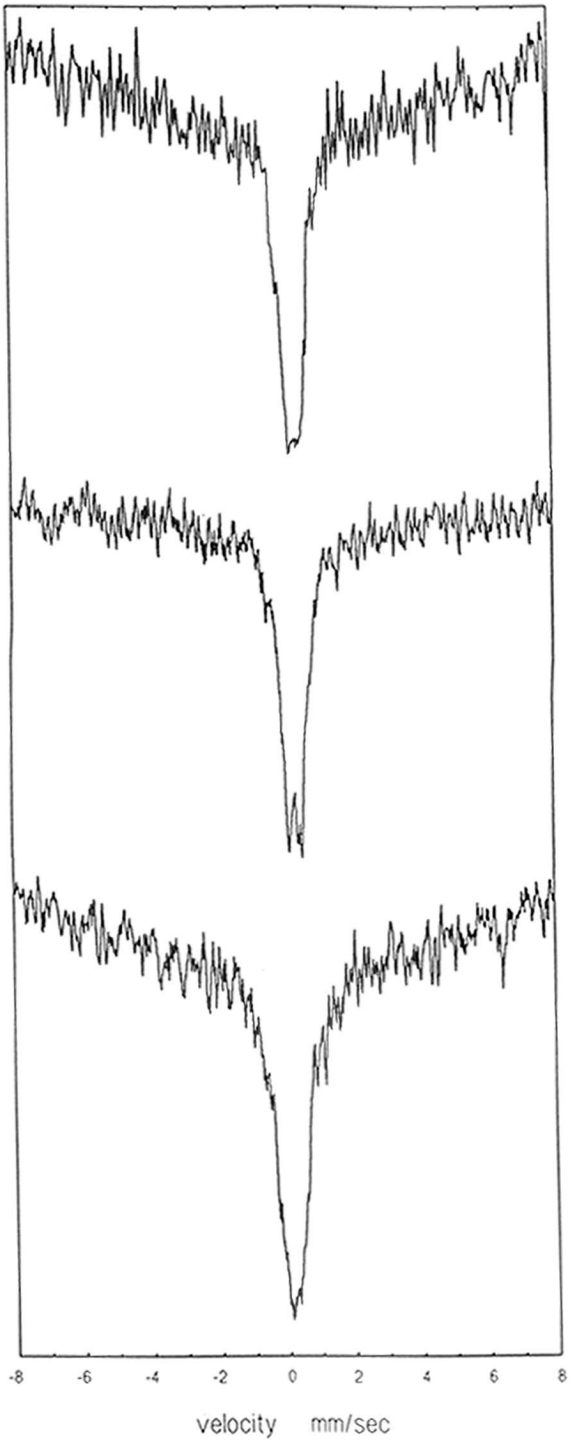

Fig. 4.18 Mössbauer spectra of Fe-MFI- A to C, top to bottom respectively

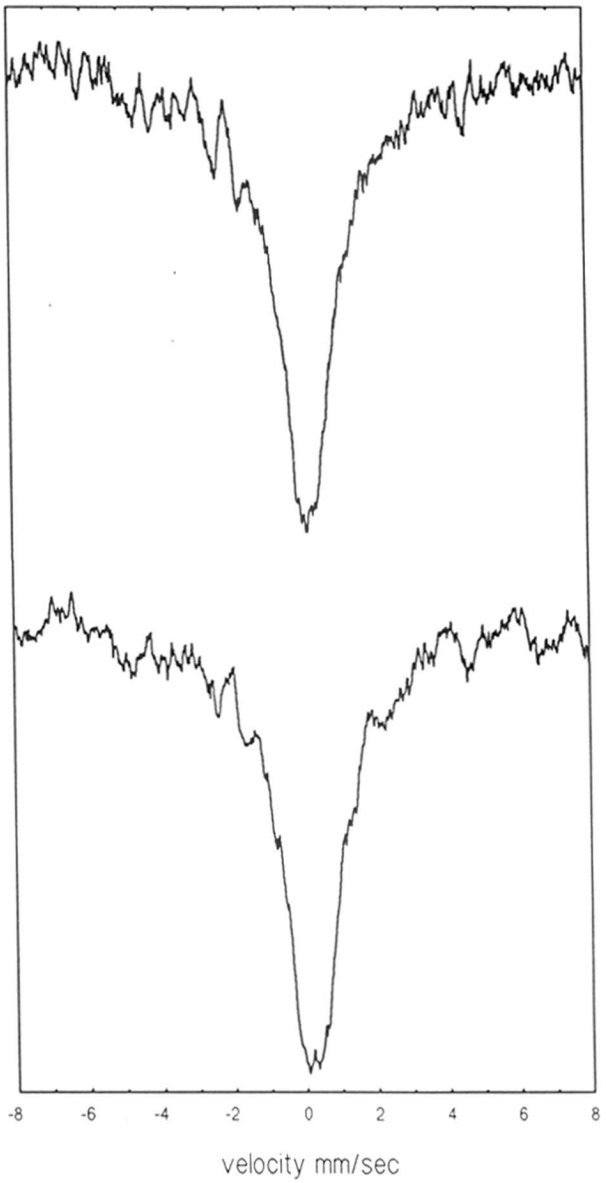

Fig 4.19 Mössbauer spectra of Fe-BEA-A and C, top and bottom respectivel

4.3.2.2.7 Scanning electron microscopy

The scanning electron micrographs of the samples for Fe-BEA are presented in Fig.4.20. The micrographs for Fe-BEA-A (using oxalic acid) were larger (≈1.0 μm) compared to Fe-BEA-C (≈0.8μm). The Fe-MFI micrographs contained agglomerated bundles of crystals in both the cases.

4.4 CONCLUSIONS

Titanium- and Ferrisilicate molecular sieves have been synthesized using acetylacetone and oxalic acid as complexing agents, respectively. This methods simplifies the synthesis procedures significantly. The catalytic activity for zeolites synthesized by this method are comparable to those of a reference sample synthesized by conventional routes.

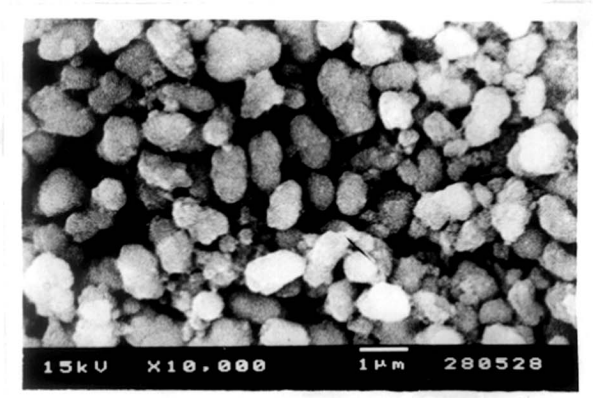

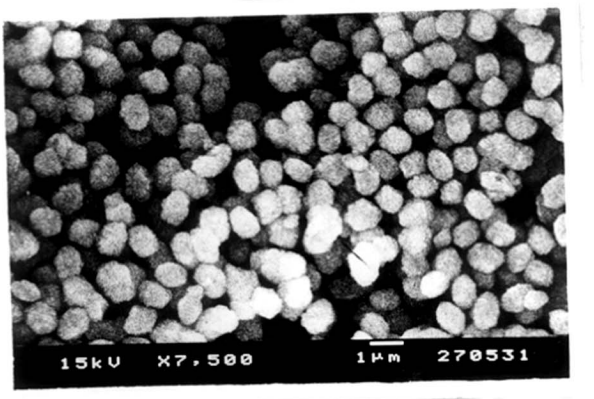

Fig. 4.20 Scanning electron micrographs of Fe-BEA-A (A) and Fe-BEA-B (B) samples.

4.5 REFERENCES

1. A. Thangaraj, R. Kumar, P. Ratnasamy, *Appl. Catal.* **51**, L1 (1990).
2. R. Szostak and T.L. Thomas, *J. Catal.*, **100**, 555 (1984).
3. J.A. Martens, Ph. Buskens, P.A. Jacobs, A. Vander Pol. J.H.C. van Hoof, and P.J. Kooyman and H. van Bekkum, *Appl. Catal. A*, **99**, 71 (1993).
4. A.E. Martell, "*Coordination chemistry" vol.1 ACS Monograph 168*, Van-Nostrand Reinhold, New York, 1971 p.453.
5. A. Ringbom in "*Complexation in Analytical Chemistry*", Chemical Analysis vol. 16, Interscience Publ., New York, 1963
6. G. Schwarzenback, "*Die Komplexometric Titration*" Ferd. Euke. verlag, stuttgart, 1965.
7. M. Taramasso, G. Perego and B. Notari, UK Pat. 80 73 252 (1980); US Pat. 4,410,501 (1983)
8. B. Kraushaar-Czarnetzki, *Ph.D. Thesis, "Characterization and Modification of Zeolites and Related Materials"*, The Technical University of Eindhoven, Eindhoven, The Netherlands, 1989.
9. D.L. Kelpert, "*The Early Transition Metals*", Academic Press, London/New York, 1992 p.104.
10. B. Kraushaar-Czarnetszki and J.H.C. van Hoof, *Catal. Lett.* **1**, 81 (1988).
11. G. Perego, G. Bellusi, C. Corno, M. Taramasso, F. Buomono and A. Eposito, *Stud. Surf. Sci. Catal.* **28**, 129 (1990).
12. A.Carati, S. Contrani, R. Milini and G. Bellusi, *ACS Symp. on Synthesis and Properties of New Catalysts, Boston, Mater. Res. Soc.*, Ext. Abstract (EA-24), **47** (1990).
13. M.R. Boccuti, K.M. Rao, A. Zecchina, G. Leofanti and G. Petrini, *Stud. Surf. Sci. Catal.* **48**, 133 (1989).
14. A. Zecchina, G. Spoto, S. Bordiga, M. Pandovan, G. Leofanti, G. Petrini, *Stud. Surf. Sci. Catal.* **65**, 671 (1991).
15. P.A. Jacobs, *DGMK Tagungsbericht 9204*, (Eds. M. Baerns and J. Weitkamp) DGMK Hamburg, Germany 1992

16. A. Thangaraj, R. Kumar and P. Ratnasamy, *J. Catal.* **130**, 294 (1990).

17. a.J.M. Thomas and J. Klinowski, *in Advances in Catalysis* **33**, 242, 247.
b. J.M. Thomas, *Aust. J. Chem.* **37**,455 (1984).

18. J.B. Nagy, Z. Gabelica and E.G. Derouane, *Zeolites* **3**, 43 (1983).

20. a. S.M. Alexander, D.M. Bibby, R.F. Howe and R.H. Meinhold, *Zeolites* **13**, 441 (1993)

21. J.B. Stothers and J.B. Lauterbur, *Can. J. Chem.* **42**, 1563 (1964).
c. J.B. Stothers, *Carbon 13 NMR Spectroscopy*, Academic Press, New York, 1972, p.214, 288.

22. J.B. Nagy et al., *J. Chem. Soc, Faraday Trans.I*, 2891 (1989).

23. L.D. Rollman and E.W. Valyoscik, EP Pat. 21,674 and 21,675 (1981).

24. G. Boxhoorn, R.A. van Santen, W.A. van Erp, G.R. Hays, R. Huis and A.D.H. Clague, *J. Chem. Commun.*, p.414 (1984)

25. a)T. Tatasumi, M. Nakamura, S. Neigishi and H. Tominaga, *J. Chem. Soc. Chem. Commun.*, p.476 (1990)
b) M. Nakamura, S. Negishi, K. Yuasa and H. Tominaga, *Shokubai*, **32**, 99 (1990).

26. D.R.C. Huybrechts, C.B. de Gruyter, P.A. Jacobs, *Nature* **345** 240 (1990).

27. P. Ratnasamy and R. Kumar, *Catal. Today* **29**, 329 (1991).

28. a. R. Kumar, A. Thangaraj, R.N. Bhat and P. Ratnasamy, *Zeolites*, **10**, (1990).
b. R.N. Bhat and R. Kumar, *J. Chem. Tech. Biotech.***16**,65 (1989)

29. J. Péréz Parianté, J.A. Martens and P.A. Jacobs, *Zeolites* **8**, 46 (1988).

30. R.Szostak and T.L. Thomas, *J. Catal.* **100**, 555 (1984); *J. Catal.* **101**, 549 (1986).

Chapter 5

A STUDY OF THE STABILITY OF IRON IN Fe-BETA

5.1 INTRODUCTION

The stability of iron in the zeolite lattice has been reported to be lower than that of aluminium *[1]*. Identification of various species formed during synthesis, subsequent pretreatments and during reactions are important in analyzing the catalytic data obtained *[2,3]*. ESR spectrum of ferrisilicates gives rise to two signals one at g = 4.3 and another at g = 2.0 *[4]*. However, based on the ESR spectra, it is difficult to assign these signals unambiguously to specific Fe^{3+} species *[4]*. Again, ESR cannot identify species like Fe^{2+} which do not possess unpaired electrons. Thus, Mössbauer spectroscopy which can identify all the forms of iron is best suited to study the Fe-species present in ferrisilicates under different pretreatments *[5-9]*. Though Mössbauer spectroscopy has often been used to characterize ferrisilicates *[10-12]*, in-situ studies on the stability of iron in these systems have been rare *[13]*.

Zeolite Beta was reported by Wadlinger *et al. [14]*. The structure of Beta was reported recently. It was found to be a combination of two types of polymorphs with left and right handed symmetries *[15-17]*. The intersections of both polymorphs are highly faulted and chiral. The ferrisilicate analog of Beta was reported by Kumar *et al.*. They have used Mössbauer spectroscopy to characterize the lattice iron *[10,18]*. In general, a change in the oxidation state of iron from Fe^{3+} to Fe^{2+} lowers the stability of the iron in tetrahedral frameworks *[19]*. In this chapter the stability, of Fe^{3+} in Beta towards reduction in hydrogen will be studied and the different specie formed will be characterized using in-situ Mössbauer spectroscopy, XRD, ion-exchange, and catalytic activity tests.

5.2 EXPERIMENTAL

Details regarding the synthesis of the ferrisilicate analog of Beta have been reported in chapter 2 section 2.2.1. The experimental techniques involved in the characterization have been described in section 2.2.2. Some more techniques used are here described below.

The Mössbauer measurements have been described in section 2.2.2.6. In-situ Mössbauer measurements were carried out in a special cell given in Fig. 5.1 *[20]*. The spectra were collected in 512 channels. The estimated accuracy of the positional data is $\delta = \pm 0.03$ mm/s. All spectra were recorded at room temperature following the different treatments. In-situ evacuation was carried out at 0.02 Pa in the Mössbauer cell, while hydrogen reductions were performed under continuous flow (ca. 0.3 l h^{-1}, 100 kPa) of purified hydrogen.

Catalytic cracking of n-hexane and disproportionation of ethylbenzene (EB) were carried out on samples B-E (Table 5.1) in a fixed bed down flow reactor (Chapter 3, Fig. 3.1) in a flow of purified nitrogen gas. During n-hexane cracking the molar ratio of nitrogen to hexane (Aldrich >99%) was 6. For ethylbenzene disproportionation, the molar ratio was 2. The weight hourly space velocity (WHSV) was kept at 1.76 h^{-1} and 1.73 h^{-1} for n-hexane and EB, respectively. The samples were analyzed in a HP1 (50m X 0.2 mm X 0.5 μm film thickness, crosslinked methylsilicone gum) column in a gas chromatograph (Hewlett Packard; 5880 A) equipped with a flame ionization detector.

5.3 RESULTS

The as-synthesized (Si/Fe = 26) form of the sample shows a broad single line spectrum with IS = 0.22; Γ = 1.74 mm/sec (Fig. 5.1). Attempts to fit this to two or more mutually consistent Lorentzian lines failed. This conforms with the results

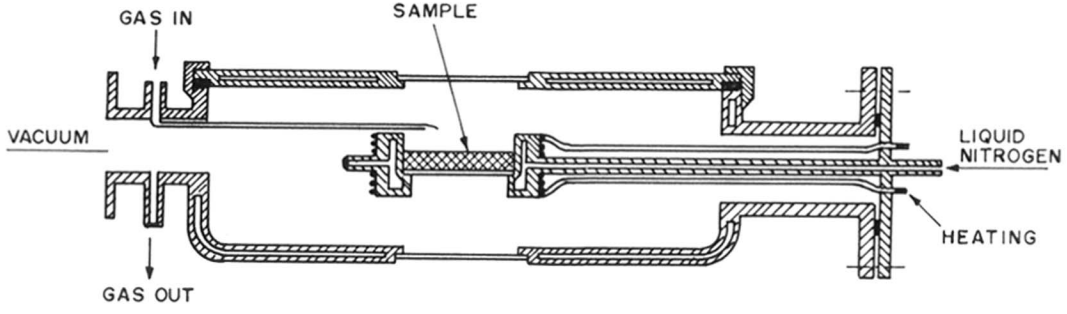

Fig. 5.1Mössbauer cell used for in-situ measurements *[20]*.

Table 5.1 Results of the in-situ Mössbauer measurements over Fe-Beta

Sample		Mössbauer parameters		Nature of Fe		Relative* spectral
code	pretreatment	IS (mm	QS Sec^{-1})	oxidation state	coordination	intensity (%)
A	C/N form	0.22	-	3+	Td	100
B	NH_4 form	0.21 0.29	- 0.76	3+ 3+	Td Oh	79 21
C	**B** calcined at 723 K (12 h) (H-form)	0.15 0.33 0.37	0.56 1.32 0.68	3+ 3+ 3+	Td Oh(1) Oh(2)	27 50 23
Series I						
D′	**C** evacuated (0.02Pa) at 723 K	0.22 0.63 0.85	1.93 0.89 2.48	3+ 2+ 2+	Td Td Oh	51 42 7
E′	**D′** reduced in H_2 at 623 K (3h)	0.19 0.70 1.02	1.46 0.77 1.94	3+ 2+ 2+	Td Td Oh	41 9 50
F′	**E′′** reduced in H_2 at 723 K (3h)	0.14 0.68 0.97 1.08	1.25 0.65 1.63 2.14	3+ 2+ 2+ 2+	Td Td Oh Oh	18 8 42 32
Series II						
D	**C** reduced in H_2 at 523 K (3h)	0.17 0.51 1.02	1.13 0.91 2.47	3+ 2+ 2+	Td Td Oh	64 19 17
E	**D** reduced in H_2 at 623 K (3h)	0.18 0.68 0.92 1.22	1.28 0.62 1.89 2.14	3+ 2+ 2+ 2+	Td Td Oh Oh	40 8 35 16
F	**E** reduced in H_2 at 723 K (3h)	0.16 0.67 0.99 1.12	1.23 0.57 1.71 2.21	3+ 2+ 2+ 2+	Td Td Oh Oh	14 8 45 33

*parameter strongly related to concentration of the ions. Differences in Mössbauer-Lamb factors among the different species could influence the estimation of the concentrations based on the relative spectral intensities.

Table 5.2 : Physico-chemical characterization of the zeolites used in the study.

Sample (code)	colour	d(A°) of 22.4° peak in XRD	ion exchange capacity* (K/Fe)	Fe^{3+}-Td (Mössbauer) (%)
NH_4-form(B)	white	3.952	0.96	79
H-form (C)	white	3.948	0.89	27 (50)
Evac. 723K (D')	yellowish brown	3.938	0.57	51
Red. 523K (D)	light brown	3.940	0.69	64
Red. 623K (E)	light brown	3.935	0.45	41
Red. 723K (F)	dark brown	3.924	0.31	18

* values in brackets refer to Fe^{3+}(Oh1); these species also possess ion-exchange capacity.

reported earlier (IS = 0.22; Γ = 2.23) by Kumar *et al. [10,18]*. The magnetic moment 5.6 BM (see chapter 2 for details of magnetic measurements) are characteristic of finely dispersed paramagnetic iron in ferrisilicates. The white color of the sample indicates that it is relatively free of any oxide/hydroxide phases *[12,7]*.

After calcination and ammonium exchange (sample B), the sample was white in color and found to contain two different type of tetrahedral iron species. Meagher *et al.* found that in the case of Fe-ZSM-5 of similar ratio (Si/Fe = 27.5), calcination at 773 K resulted in a large fraction of extra lattice iron, besides a significant amount of tetrahedral iron *[21]*. They also observed a change in color of the sample (to light brown) after calcination.

On calcination of the NH_4^+-form at 723 K, the sample (H-form, Sample C) contains, 27% tetrahedral and 73% octahedral Fe^{3+}. The latter component of iron could be resolved into two types; i) species designated Oh1 (Table 5.1) which have an isomer shift that falling in the range of octahedral Fe^{3+} and those be due to Fe^{3+}Oh species, and ii) Oh2 species attributable to Fe^{3+} in iron exchange sites or to an oxide/hydroxide phase. The nearly white color of the sample suggests that these are probably finely dispersed in the lattice. The magnetic moment of the sample (5.8 BM) suggests little or no occluded iron oxide phases. The high values of ion-exchange suggests that most of the iron possessed ion-exchange capacity. The total amount of the Oh1 species and the Fe^{3+}Td species present in the sample correlate well with the ion-exchange capacity and the interplanar spacing (XRD, 2θ = 22.4° line; Fig. 5.6).

5.3.1 In-situ experiments

Two series of in-situ experiments were performed on the H-form of the catalyst. In the first set of experiments evacuation was followed by reduction at 623 and 723 K. In the second set of experiments direct reduction at 523, 623 and 723 K was performed. All operations carried out are schematically shown in Scheme 1.

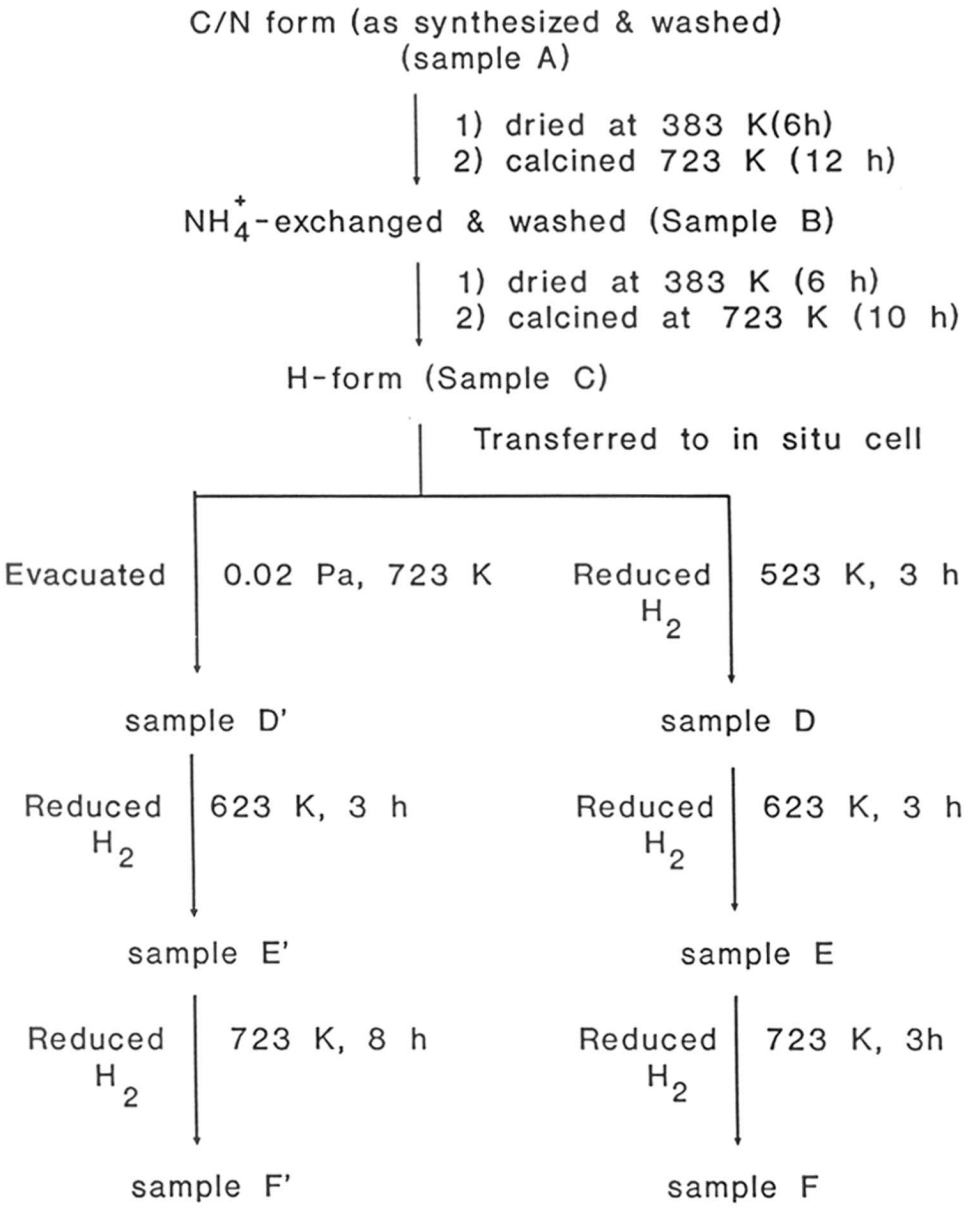
C/N form (as synthesized & washed)
(sample A)
1) dried at 383 K(6h)
2) calcined 723 K (12 h)
NH_4^+-exchanged & washed (Sample B)
1) dried at 383 K (6 h)
2) calcined at 723 K (10 h)
H-form (Sample C)
Transferred to in situ cell
Evacuated
0.02 Pa, 723 K
Reduced H_2
523 K, 3 h
sample D'
sample D
Reduced H_2
623 K, 3 h
Reduced H_2
623 K, 3 h
sample E'
sample E
Reduced H_2
723 K, 8 h
Reduced H_2
723 K, 3h
sample F'
sample F

SCHEME 1

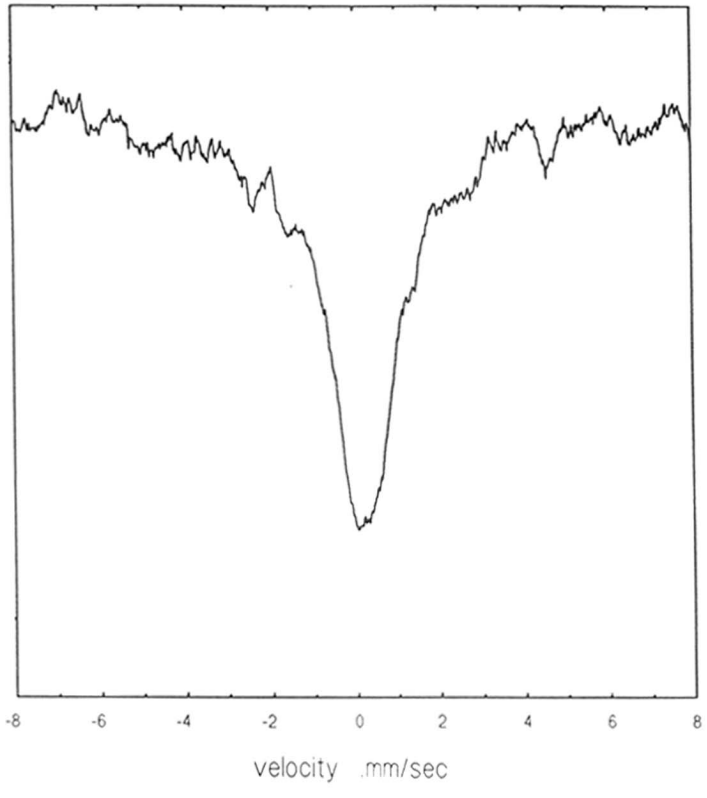

Fig. 5.2Mössbauer spectra of sample A.

5.3.1.1 Series I

The Mössbauer spectrum of the sample C evacuated to 0.02 Pa at 723 K is given in Fig. 5.3 D'. On evacuation a major part of the Oh iron undergoes autoreduction to Fe^{2+} state (Table 5.1, sample D'). Simultaneously, an increase in the Fe^{3+}Td species is also noticed (Table 5.3). The autoreduction of iron has been observed earlier for Fe^{3+} exchanged Y *[25]* and ferrisilicate ZSM-5 *[17]* zeolites. In the former case complete reduction to Fe^{2+} is reported. In the latter case ≈ 40% was reduced. A similar amount of reduced iron was observed for Fe-beta samples in our experiment (Table 5.3). a very small component of octahedral iron was also observed that was observed earlier *[25]* for samples evacuated at high temperature (773 K).

Further, the reduction of this sample at 523 K led to a decrease in the tetrahedral Fe^{3+} species corresponding to the framework iron (according to the isomer shift) and an increase in the Fe^{2+} species. A significant amount of the Fe^{2+}Td transformed in to Fe^{2+}Oh. It appears that the Fe^{2+} species are dislodged from the framework and do not possess any ion-exchange capacity (Table 5.2).

On increasing the severity of reduction (723 K) most of the iron is reduced to Fe^{2+} (Table 5.1). Simultaneously, and additional octahedral Fe^{2+}Oh2 is also noticed. This additional octahedral component is probably due to a bulk iron phase.

5.3.1.2 Series II

In the series II experiments direct reduction of the sample C in H_2 was carried out. Fig. 5.4 D shows the spectrum of Fe-Beta reduced at 523 K. Direct reduction also caused an increase in Fe^{3+}Td species as observed in series I experiments (Table 5.1). Direct H_2-reduction at 523 K appears to be more severe than autoreduction as seen by the amount of Fe^{2+}Oh species formed. However, larger amounts of Fe^{3+}Td species are observed during direct reduction. Further reduction of sample D at 623

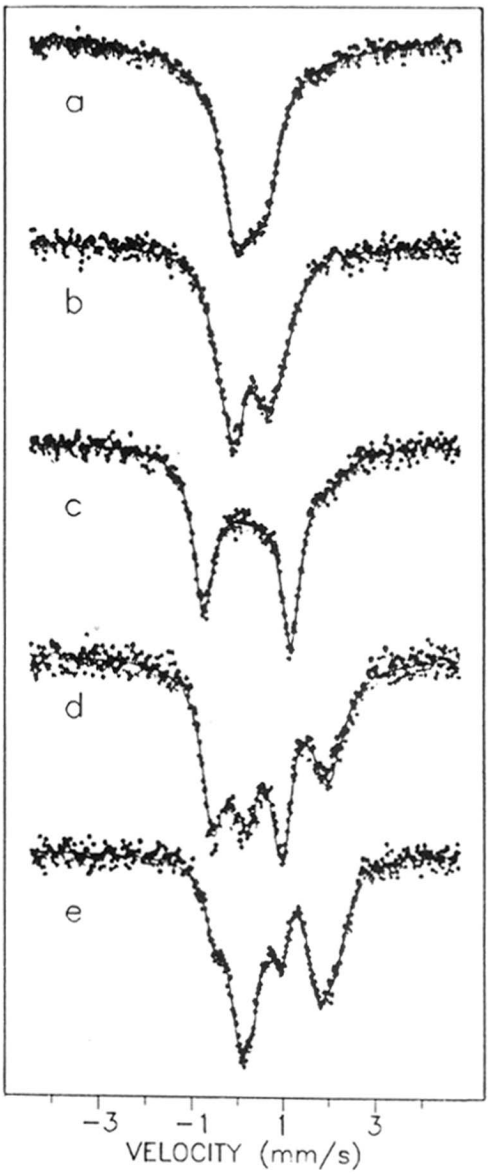

Fig. 5.3Series I in-situ measurements.

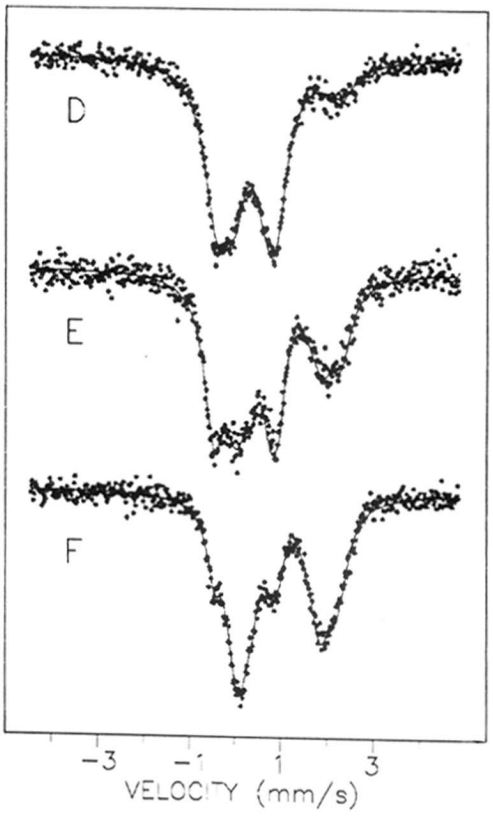

Fig. 5.4Series II in-situ measurements.

and 723 K yielded samples E and F. The Mössbauer spectra (Fig. 5.4 E and F) of these are similar to the corresponding samples E′ and F′ of series I experiments (Fig. 5.3). Only a marginal change in the intensities of different species is observed.

The changes occuring in the iron species through different samples (sample A - F) are plotted in Fig. 5.5.

5.4 DISCUSSION

Starting from all of the iron in the framework (sample A, C/N form), calcination at 753 K followed by ammonium exchange (sample B) leads to the presence of two different forms of iron. The major component consists of iron in framework lattice positions (IS = 0.21 mm/sec.). The second component (0.29 mm/sec.) is not exactly assignable to an octahedral species as the isomer shift is 'intermediate' between Td and Oh and is tentatively assigned to iron in defect sites formed during calcination.

On calcination at 723 K for 5 h, three different species, viz., Fe^{3+}(Td) (IS = 0.15 mm/sec), Fe^{3+}Oh1 (δ= 0.33 mm/sec) and Fe^{3+}Oh2 (δ = 0.37 mm/sec) can be identified based on the isomer shift values. Apparently, some Fe^{3+}Td ions transformed into Fe^{3+}Oh ions on calcination of the NH_4^+-form. While Oh2 species can be attributed easily to extra lattice iron species, the Oh1 species are similar to the defect species in the ammonium form. The isomer shift (0.33 ± 0.03 mm/sec) value is closer to Oh coordination but the quadrupole splitting (QS) value is too large for Fe^{3+}Oh. The QS values are also characteristic, though the limits for distinction of various components are less strict. In general, an increasing symmetry of coordination of Fe(III) ions decreases QS, while the reverse holds good for Fe(II) ions *[23]*. The above information and no noticeable color change suggest that the Oh1 species are not extra lattice bulk iron oxide species.

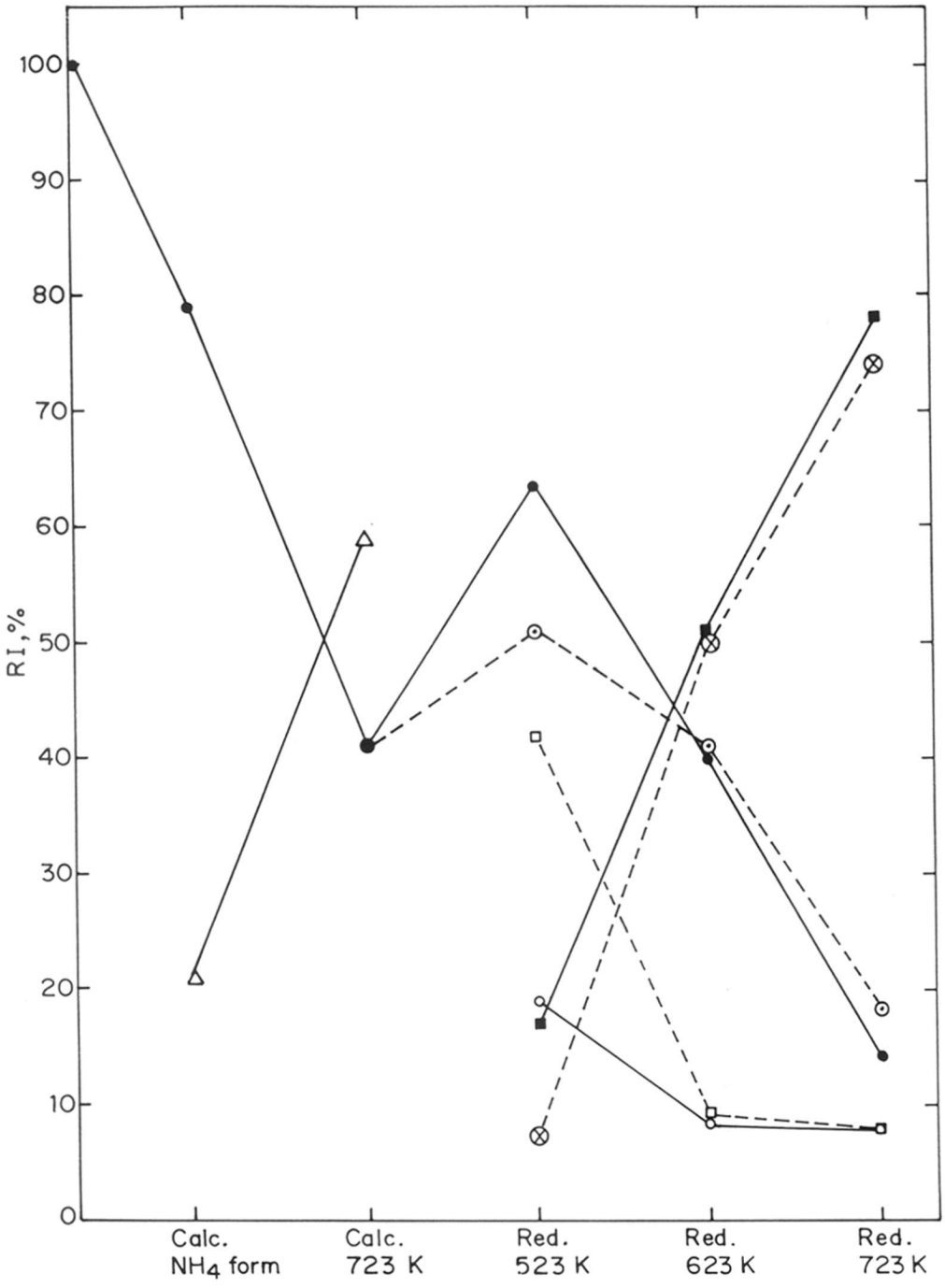

Fig. 5.5 Changes observed during various treatments A-F corresponds to sample names. Solid lines (-) indicate series I, dashed lines (--) indicate series II experiments (•) Fe^{3+} Td; ▲ Fe^{3+} Oh; ⊙ Fe^{2+} Td; ⊗ Fe^{2+} Oh.

On evacuation of the sample C at 723 K, two processes are observed (i) auto-reduction, (ii) increase in Fe^{3+}Td iron accompanied by disappearance of Fe^{3+}Oh. Since the latter species are not reduced during autoreduction and show ion exchange capacity and catalytic activity, they may correspond to the iron in framework defect sites. Similar result is obtained when the H-form is reduced directly with H_2 at a lower temperature (523 K). Under both the conditions, a significant amount of Fe^{3+}Td reappears upon reduction. However, the exact location of this species could not be identified. The tetrahedral Fe^{2+} component has been assigned earlier to the iron located in the S_I sites of zeolite Y *[23]*. In our case, they (Fe^{2+}Td species) may be located as single ions outside lattice positions in the center of secondary building units as suggested by earlier workers *[23]*. Increase in temperature of H_2 reduction increases the amount of Fe^{2+} species at the cost of Fe^{3+} species. At 623 K the conversion of Fe^{3+} to Fe^{2+} is not total ($\approx$ 40 wt.% Fe^{3+}Td remains in framework). The stability of iron to direct reduction indicates its probable presence in the metallosilicate framework. Finally, the reduction at 723 K is severe enough to reduce most of the Fe^{3+} species to Fe^{2+}. Further, an increase in temperature from 623 to 723 K transforms the Fe^{2+} Td species to Fe^{2+} Oh species. This may be due to the migration of Fe^{2+} from defect sites to channels or to the external surface.

A plot of interplanar spacing (d at 2θ = 22.4) versus Fe^{3+}Td Mössbauer spectral intensity and ion exchange is given Fig. 5.6. It shows a good linearity for all the samples except the H-form (sample C). The 'fit' is better if the Oh1 contribution is added to it. A similar trend is observed for the catalytic activities of various ferri-Beta samples in the n-hexane cracking and ethylbenzene disproportionation presented in

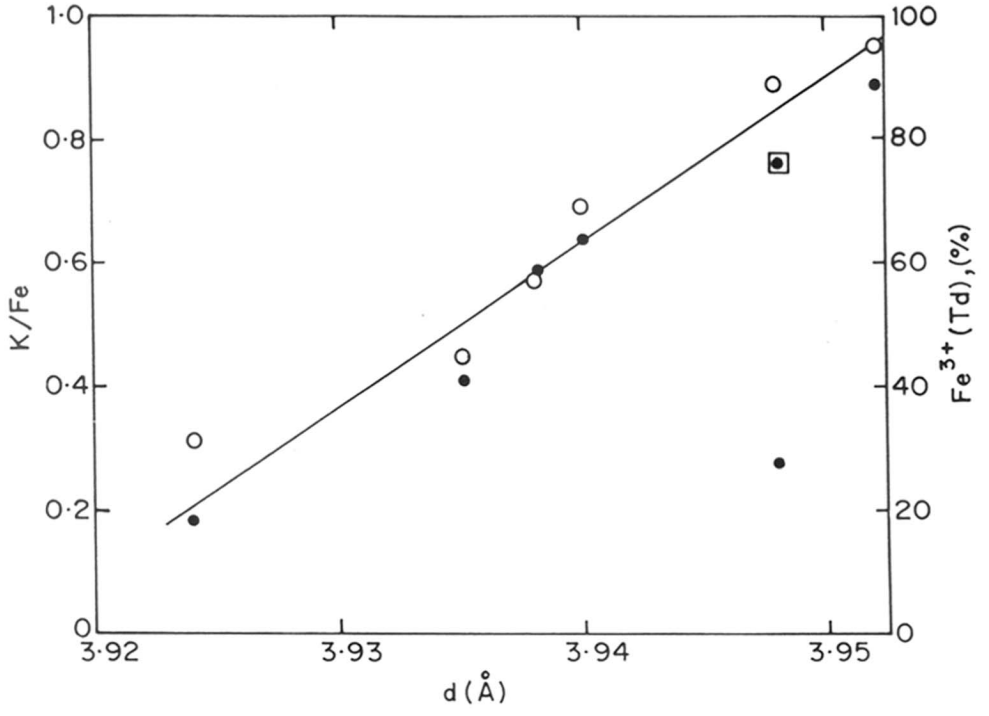

Fig. 5.6 Correlation between interplanar spacing (d value of θ = 22.4° peak, (CuK_α) and Fe^{3+} ions in lattice. ⊙, ion-exchange capacity ($\frac{k}{Fe}$), •, Fe^{3+}Td from Mössbauer spectroscopy, • , calcined sample C (Fe^{3+}Oh1).

Table 5.3 Catalytic studies over Fe-Beta zeolites.

Temperature = 723 K; WHSV(h^{-1}) = 1.76 and 1.73 for n-C_6 and EB; N_2/HC (mole) = 6 and 3 for n-hexane and EB.

Sample code	n-hexane cracking				EB transformation				
	Conv.	C_6^-	iso-C_6	others	conv.	C_5^- gases	Bz[1]	DEB[2]	other Aromatics[3]
	wt(%)				(wt%)				
C	16.88	14.26	0.82	1.40	29.97	1.37	21.90	0.83	5.87
D	13.05	10.69	0.57	1.59	26.78	1.57	18.73	0.79	5.69
E	6.08	4.29	0.45	1.39	18.0	1.43	11.75	0.76	4.06
F	2.96	1.45	0.46	1.05	10.87	0.92	6.60	0.77	2.58

[1] Bz : Benzene
[2] DEB : Diethylbenzenes
[3] Mostly ethyl toluenes, cumene and styrene

Table 5.3. In ethylbenzene disproportionation the amount of DEB does not vary much, but a correlation between the amount of benzene produced and the ion-exchange capacity is observed.

5.5 CONCLUSIONS

1. Some Fe^{3+} framework ions loose their identity on calcination. They are tentatively assigned to the defect sites formed during thermal treatment.
2. Upon evacuation of the sample at 723K an increase in the tetrahedral component is observed.
3. Autoreduction of the Fe^{3+}Oh to Fe^{2+} takes place on evacuation.
4. Reduction at higher temperature increases the Fe^{2+} components while a corresponding decrease in Fe^{3+} is observed.
5. Strong correlation is demonstrated between cracking activity and the amount of exchange sites in the sample.

5.6 REFERENCES

1. R. Szostak and T.L. Thomas, *J. Catal.* **100**, 555 (1986).

2. G. Doppler, R. Lehnert, L. Marosi and A.X. Trautwein, *Stud. Surf. Sci. Catal.* **37**, 215 (1988).

3. A. Brückner, R. Lück, Wieker, B. Fahlke and H. Mehner, *Zeolites* **12**, 380 (1992)

4. N.P. Evmiridis, *Inorg. Chem.* **25**, 4362 (1986).

5. R. Schmidt, M.D. Amiridis, J.A. Dumesic, L.M. Zelewski and W.S. Millman, *J. Phys. Chem.* **96**, 8142 (1992).

6. K. Lázár, *Struct. Chem.* **2**, 245 (1991).

7. F.J. Berry, S. Jobson, T. Zhang and J.F. Marco, *Catal. Today* **9**, 137 (1991).

8. C.N.R. Rao, G.U. Kulkarni, K.R. Kannan and S. Chaturvedi, *J. Phys. Chem.* **96**, 7379 (1992).

9. F.J. Berry, *Stud. Surf. Sci. Catal.* 57A, 229 (1991).

10. R. Kumar, S.K. Date, E. Bill and A. Trautwein, *Zeolites* **11**, 211 (1991).

11. A.J. Chandwadkar, S.K. Date, E. Bill and A. Trautwein, *Zeolites* **12**, 180 (1992).

12. R. Szostak, V. Nair, D.K. Simmons, T.L. Thomas, R. Kuvadia, B. Dunson and D.C. Shieh, *Stud. Surf. Sci. Catal.* **37**, 403 (1988).

13. K. Lázár, G. Borbely and H. Beyer, *Zeolites* **11**, 214 (1991).

14. R.L. Wadlinger, G.T. Kerr and E.J. Rosinski, US Pat. 3308069 (1967).

15. M.M.J. Treacy and M. Newsam, *Nature* **332**, 249 (1988).

16. J.M. Newsam, M.M.J. Treacy, W.T. Koetsier and C.B. de Gruyter, *Proc. Royal Soc. London* **A420**, 375 (1988).

17. J.B. Higgins, R.B. La Pierre, J.L. Schlenker, J.D. Wood, G.T. Kerr and W.J. Rohrbaugh, *Zeolites* **8**, 446 (1988).

18. R.Kumar, A. Thangaraj, R.N. Bhat and P.Ratnasamy, *Zeolites* **10**, 85 (1990).

19. B. Wichterlowa, L. Kubelkova, P. Jiru and Kolihova, *D. Coll. Czech. chem. commun.* **45**, 2143 (1980).

20. K. Lázár, K. Matusek, J. Mink, S. Dobos, L. Guczi, A. Vizi-Orosz, L. Marko and W.M. Reiff, *J. Catal.* **87**, 163 (1984).

21. A. Meagher, V. Nair and R. Szostak, *Zeolites* **8**, 3 (1988).

22. P.A. Jacobs, *Stud. Surf. Sci. Catal.* **29**, 357 (1988).

23. M. Petrera, A. Gennaro, P. Gherardi, G. Gubitosa and N. Pernicone, *J. Chem. Soc. Faraday Trans.I* **80**, 709 (1984).

24. D.G. Rethwisch and J.A. Dumesic, *J. Phys. Chem.* **90**, 1863 (1986).

25. B. Wichterlowa, *Zeolites* **1**, 181 (1981).

LIST OF PUBLICATIONS

PAPERS

1. Anuj Raj, J.S. Reddy and R. Kumar
   "*Selective formation of 1,2,4-trimethylbenzenes over different MEL metallosilicate Molecular Sieves*"
   J. Catal. **138**, 518 (1992)

2. Anuj Raj, J.S. Reddy and R. Kumar
   "*Catalytic Properties of [Al]-, [Ga]- and [Fe]-silicate Analogs of ZSM-11 in C_7 and C_8 Aromatic Hydrocarbon Reactions: Influence of Isomorphous Substitution*",
   Proc.9th Int. Zeo. Conf. I, Montreal, 1992, R. von Ballmoos, J.B. Higgins and M.M.J. Treacy Eds., Butterworth-Heinmann, USA p. 551.

3. R. Kumar, K.R. Reddy, Anuj Raj and P.Ratnasamy,
   Synthesis and Characterization of a new high silica zeolite, NCL-1, 9th Int. Zeo. Conf., Montreal, 1992, R. von Ballmoos, J.B. Higgins and M.M.J. Treacy Eds., Butterworth-Heinmann, USA, 1993 p.189.

4. Anuj Raj, K.R. Reddy, J.S. Reddy and R. Kumar
   "*Catalytic Properties of Ferrisilicate Analogs of Some Medium Pore Zeolites in C_7 and C_8 Aromatic Hydrocarbon Reactions*"
   Stud. Surf. Sci. Catal. **75B**, 1715 (1993).

5. Anuj Raj, S. Sivasanker and K. Lázár,
   "*Studies on the Stability of Fe^{3+} ions in ferrisilicate molecular sieves : I Ferri-Beta a case study*" J. Catal. (Accepted).

6. A.P. Singh, Sujit B. Kumar and Anuj Raj,
   "*Selective para-chlorination of toluene using zeolite catalysts*",
   J. Catal. (Accepted)

7. R. Kumar, Anuj Raj, S.B. Kumar and P. Ratansamy,
   "*A convenient methdology for the preparation of transition metal silicate molecular sieves*"
   10^{th} International Zeolite Conference
   (communicated)

8. K.R. Reddy, Anuj Raj and R. Kumar,
   "Toluene alkylation over ferrisilicate analog of ZSM-48",
   Appl. Catal. (communicated)

9. K.R. Kamble. Anuj Raj, A.P. Singh and R. Kumar
"Isopropylation of Biphynyl with propane-2-ol over various large pore zeolites"
J. Catal. (communicated).

10. A. Paul, Anuj Raj and A.P. Singh
"*Isomerization of dichlorotoluenes over Zeolites*",
Appl. Catal. (communicated)

11. Anuj Raj, J.S. Reddy and A.P. Singh
"*Hydroxylation of Phenol over Various Metallo- and Metallo-Titanium-Silicate Analogs of MEL*",
Poster presentation, 11th National Symposium on Catalysis, Hyderabad, 1993.

12. Anuj Raj, A.P. Singh and R.Kumar,
A new Route to the synthesis of ferrisilicates using complexing agents.
Poster presentation at 11th National Symposium on Catalysis, Hyderabad, 1993.

13. Anuj Raj, Sujit B. Kumar and R. Kumar,
"A convenient method for the synthesis of titanium silicate molecular sieves (TS-1 and TS-2)"
J. Chem. Soc. Chem. Commun. (targetted).

14. Anuj Raj, D. Bhattacharya and S. Sivasanker,
Aromatization of n-hexane Over metallosilicates of MEL and EUO (in preparation)

15. Anuj Raj and A.P. Singh,
Reductive Hydrolysis of Nitriles to Aldehydes over Bifunctional Zeolites (in preparation.)

16. R.B. Tejwani, Anuj Raj, and R.B. Mitra,
Baeyer-Villager oxidation over zeolites (in preparation)

PATENTS

1. Anuj Raj, J.S. Reddy, R. Kumar and P. Ratnasamy "A Process for the Production of 1,2,4 Trimethylbenzene" - (Applied).
2. A.Paul, Anuj Raj, A.P. Singh and P. Ratnasamy " A process for the production of dichlorobrnzenes (applied)